Integration between the mosquito immune and circulatory systems: from genetic mechanisms to evolutionary conservation

By

Yan Yan

Dissertation

Submitted to the Faculty of the

Graduate School of Vanderbilt University

in partial fulfillment of the requirements

for the degree of

DOCTOR OF PHILOSOPHY

in

Biological Sciences

May 31, 2021

Nashville, Tennessee

Approved:

Kenneth C. Catania, Ph.D.

John A. Capra, Ph.D.

Ann T. Tate, Ph.D.

Andrea Page-McCaw, Ph.D.

Julián F. Hillyer, Ph.D.

Dedication

To my parents, YuLong Yan and LiYing Bai, for their endless encouragements

and

To my partner, Dr. Scott B. Williams, for his infinite support

ACKNOWLEDGEMENTS

For the past five years, I have been surrounded by all the kindness and wisdom of an amazing group of people. I would like to thank my advisor, Dr. Julián Hillyer, for always considering what was best for me, both science- and career-wise. His guidance has helped me become a better critical-thinker, a diligent researcher, and a far better writer than I was years ago. He has always challenged me to do better, but never missed an opportunity to make sure I was recognized for my efforts; selflessly nominating me for many awards. I am extremely lucky to have him as my advisor.

I would like to thank my committee: Drs. Kenneth Catania, John (Tony) Capra, Andrea Page-McCaw and Ann Tate. Their advice made my research better and shaped this dissertation. Thanks to Dr. Capra's postdoctoral researcher, Dr. David Rinker, for helping us map the reads for the RNAseq analysis in chapter III of this dissertation. To my previous advisors, Drs. Larry Murdock and Dieudonné Baributsa (Purdue University), and Ding Yang (China Agricultural University) thank you for giving me opportunities to grow as a scientist and laying the foundations for later success. I am especially grateful to Larry, who tells me that the ultimate goal of research should be to help people and this started my path of studying the malaria-carrying mosquitoes.

I would like to thank everyone from the Hillyer lab, past and present: Tania Estévez-Lao, Dr. Jonas King, Dr. Garrett League, Dr. Leah Sigle, Dr. Lisa Brown, Dr. Lillian Shapiro, Bryan Joosse, Abinaya Ramakrishnan, Carter Powers, Raymar Turangan, Cole Meier, Jordyn Sanner, and Lindsay Martin. I thoroughly enjoy the kind and friendly work environment you created. To my colleagues, Jacob Steenwyk, Justin Critchlow,

Destane Garrett, Parker Rundstrom, Dr. Michael Tackenberg, Dr. Manuel Giannoni Guzman, Dr. Emily Hudson, Dr. Matt Wilkins, and Dr. Grzegorz Buczkowski, thank you for helping me collect various insects used in chapter V of this dissertation.

Additional thanks to my fellow graduate student and my best friend, Luísa Jabbur. She is smart, generous and funny. I am constantly amazed at the way she thinks and the projects she conceptualizes. She has endless personal drive and has provided me with countless support with my work and a seemingly infinite supply of cakes. I am extremely lucky to have such a friend.

I would like to thank my parents, YuLong Yan and LiYing Bai, for their endless support. They valued education and encouraged me to pursue my own dreams, even when it meant sending their only child abroad. They celebrate every tiny bit of my achievements and I am grateful for their unconditional love.

Finally, I would like to thank my partner, Dr. Scott B. Williams. Since we met, he has been a constant in my life. He always believes in me, giving me freedom and respecting my choices, supporting me in every way he can. He celebrates my every small achievement and comforts me whenever graduate school life gets too hard. He is also the first person to challenge me to be a better scientist. I am thankful for him standing his ground all those years ago and demanding that I have proper control groups for my very first experimental design. Thank you for your love and support. I am excited for our future together.

Table of Contents

List of Figures

CHAPTER I

CHAPTER II

CHAPTER III

CHAPTER IV

CHAPTER V

CHAPTER VI

List of Tables

CHAPTER III

CHAPTER I

Introduction

Overview

Mosquitoes are considered the deadliest animals on earth because they transfer pathogens that cause malaria, dengue, chikungunya, zika, lymphatic filariasis, etc (1). The *Anopheles gambiae* mosquito – the organism this dissertation primarily focused on – transmits malaria, which causes more than 200 million cases worldwide and 400,000 deaths each year (2). More than two thirds of these deaths are children under the age of 5, taking the life of a child every two minutes. Malaria cases have declined over the last decade, because of the employment of insecticide-treated bed nets and indoor residual spraying (3). However, pesticide resistance is evolving rapidly and spreading in mosquitoes, diminishing the effectiveness of these tactics (4). Moreover, other mosquito-borne diseases – like dengue and the recent outbreaks of Zika – are on the rise, but no medicines are currently available to treat them (5-7). As global warming expands the geographic range of mosquitoes and global travel provides more opportunities for the spread of invasive mosquito species and pathogens, mosquito-borne diseases will become more severe in already endemic countries and invade quickly into new countries, threatening people's health (6, 8, 9). Therefore, developing new tools and strategies for controlling and treating mosquito-borne diseases is a pressing issue worldwide.

The ability of mosquitoes to transmit pathogens depends on factors such as longevity, blood feeding preferences and immune responses. Therefore, altering any of these factors may reduce disease transmission (10-13). Indeed, manipulating the immune responses of mosquitoes has been proposed as a strategy to control mosquito-borne diseases (14-20). Therefore, a better understanding of how the immune system destroys pathogens will contribute to the development of novel vector control strategies.

Mosquitoes are exposed to pathogens throughout their life. Mosquito larvae live in an aquatic environment and the microbes within this environment can breach though the larval cuticle and enter the hemocoel (21). Mosquito adults are terrestrial, but many vector species take blood meals which may contain pathogens. Indeed, the malaria parasites *Plasmodium* enter the mosquito via feeding, but must traverse the hemocoel before reaching the salivary glands and transmitting to the next host (2). Therefore, understanding the hemocoelic immunity is important and can contribute to novel strategies to control mosquito-borne diseases. This dissertation mainly focuses on how the immune system kills pathogens in the hemocoel.

The hemocoel is a dynamic environment where the flow of hemolymph rapidly disperses pathogens, as well as immune cells called hemocytes, to all regions of the body (22). However, the distribution of the pathogens and hemocytes is not homogeneous; hemocytes preferentially aggregate on the areas of highest hemolymph flow, especially near the valves of the heart. These heart-associated hemocytes further sequester more pathogens (23), showing the circulatory system plays a major role in how and where the immune system kills pathogens. In the next three sections, I will focus on mosquitoes to introduce the circulatory system, the immune system and how the two systems are

functionally integrated to maximize immune surveillance and pathogen killing. The last section of this chapter will give an overview of my dissertation research.

The circulatory system

The insect circulatory system is essential for multiple physiological processes, such as transporting nutrients, hormones and signaling molecules, regulating homeostasis, gas and temperature, and mediating immune defense, wound healing, and molting (22, 24). Despite its central roles in various physiological tasks, the insect circulatory system is largely understudied. Our knowledge of the insect circulatory system mainly comes from the tobacco hornworm *Manduca sexta* (25, 26), the model organism *Drosophila melanogaster* (27-29) and the disease vector *A. gambiae* mosquitoes (30-33).

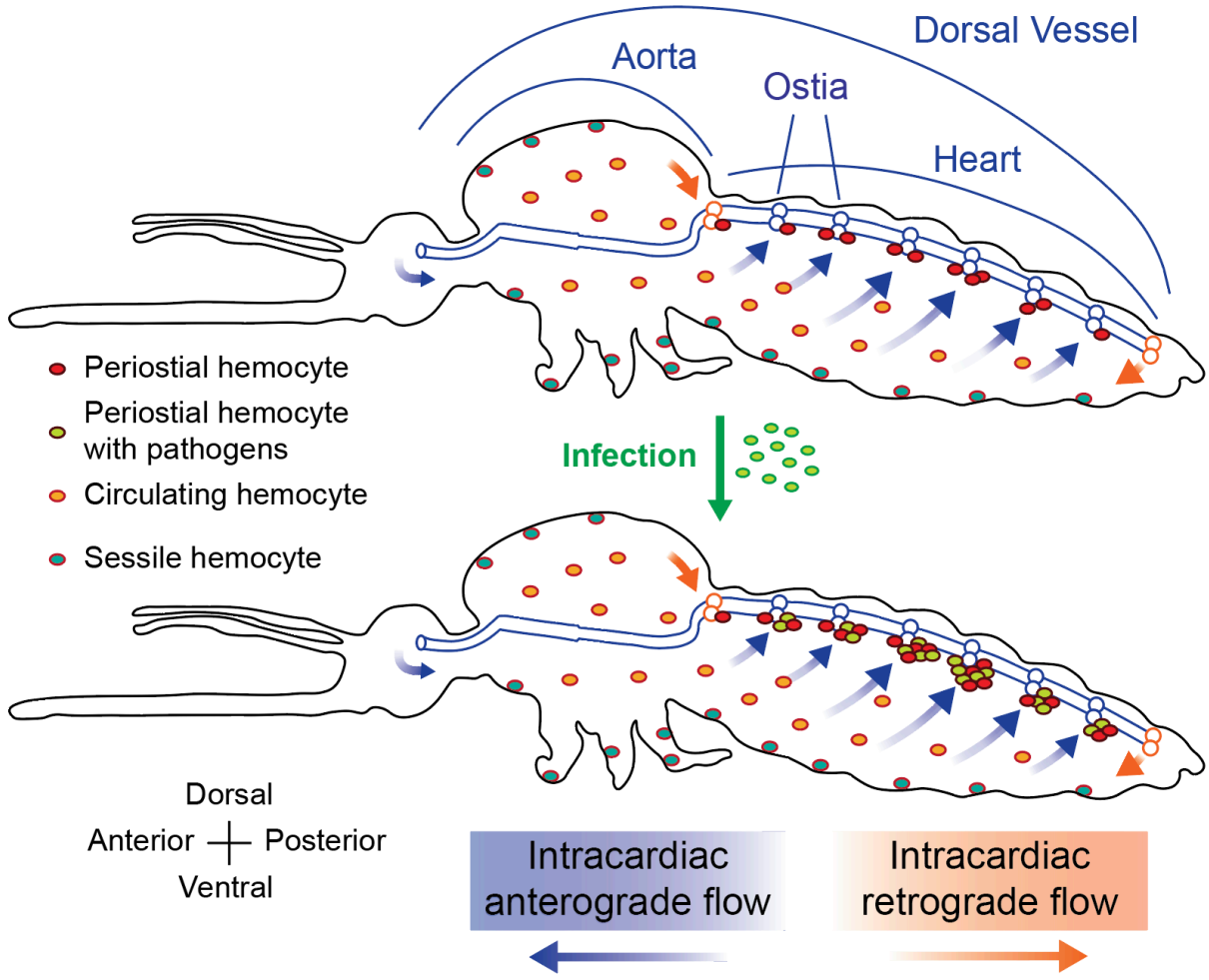

Figure 1 Schematic illustration shows the interaction between the immune and circulatory systems in mosquitoes.
Upper panel details the internal morphology of the mosquito heart, pattern of hemolymph movement, and its integration with the immune system. Lower panel shows that infection induces periostial hemocyte aggregation.

Contrary to the closed circulatory system in mammals, mosquitoes and other insects have an open circulatory system, but its hemolymph still moves in an organized and dynamic fashion. The dorsal vessel is the main pumping organ that propels hemolymph circulation (Figure 1). It is a cylindrical structure that extends the entire length of the dorsal midline of the mosquito and is subdivided into a thoracic aorta and an abdominal heart (30, 33). The aorta is located in the head and thorax and simply conducts

hemolymph from the heart to the head (33). The heart is located in the abdomen, tethered by alary muscles to the dorsal midline, and flanked by pericardial cells that filter the hemolymph (23, 30). Unlike the aorta, the heart contracts myogenically in a wave-like manner and alternates between anterograde (toward the head) and retrograde (towards the posterior end of abdomen) directions (30). When contracting anterograde, the heart relaxes and aspirates hemolymph via six pairs of abdominal ostia – the valves of the heart – then closes the ostia, contracts, and pumps the hemolymph through the aorta towards the head and releases the hemolymph there (30). This hemolymph then moves slowly in the posterior direction within the hemocoel, but outside of the heart (31). When the heart contracts in the retrograde direction, all the abdominal ostia close, but a single pair of thoraco-abdominal ostia open and aspirates hemolymph into the relaxed heart. Then, the heart contracts and propels hemolymph towards the abdominal end of the heart and exits there (30, 34). In addition to the heart, insects also utilize accessory pulsatile organs – auxiliary hearts – to circulate hemolymph in the antennae, wings and legs (35-39).

While the heart of most adult holometabolous insects contracts this way, variations exist in the general plan. For example, the circulatory system in mosquito larvae is different from the adults (32). The larval heart only contracts in the anterograde direction, and it lacks mature abdominal ostia. Instead, the hemolymph enters through an incurrent opening at the posterior end of the heart. Beyond holometabolous insects, the heart of some – if not all – hemimetabolous insects only contracts in the anterograde direction (40, 41). Furthermore, the heart of most apterygotes and mayflies contracts in a bidirectional flow, whereby a valve located near the posterior region of the heart splits the flow direction and the hemolymph anterior to this valve flows towards the head whereas the hemolymph

posterior to this valve flows towards posterior appendages (42, 43). Despite these variations of the circulatory system, the incurrent ostia perform similar roles as the heart valves that permit hemolymph into the heart and are the locations that experience the swiftest hemolymph flow (44).

The immune system

Mosquitoes lack an adaptive immune response, but utilize a strong innate immune system to combat infections (45-47). The immune system – primarily mediated by hemocytes – first recognizes invading pathogens with host-derived pattern recognition receptors, which then activates immune signaling pathways, and finally kills the pathogens with effector mechanisms, like phagocytosis, melanization and lysis (48).

Hemocytes are among the first responders of the immune system as they phagocytose pathogens within minutes of infection (49, 50). Around three quarters of hemocytes circulate with the hemolymph and are called circulating hemocytes, while one quarter attaches to tissues and are called sessile hemocytes (51, 52). Within the hemocoel, circulating hemocytes can attach to tissues and become sessile, whereas sessile hemocytes can release from their attachment and enter circulation (34, 53-55). Regardless of their spatial locations, from a functional perspective hemocytes can also be classified into granulocytes, oenocytoids, and prohemocytes (45, 51). Granulocytes represent 90% of hemocytes and fight infections primarily through phagocytosis (49, 50, 56). Oenocytoids primarily produce phenoloxidase and mediate melanization (57). Prohemocytes represent small granulocytes that have recently undergone asymmetric

cell division (52). Recent advancements of single cell RNA sequencing and fluorescence imaging propose a new facet of hemocyte classification based on its size and heterogeneity (58-60).

The onset of immune activation requires host-derived pattern recognition receptors bind to pathogen-associated molecular patterns (48). These pattern recognition receptors include members of gene families like peptidoglycan recognition proteins (PGRP), fibrinogen-related proteins (FREP), C-type lectins, leucine-rich repeat containing proteins and thioester-containing proteins (TEP) (61). Most of these gene families diversify within each taxon, likely due to different pathogens experienced by various insects (48, 62). Accurately recognizing pathogens helps insects combat infection. For example, TEP proteins – especially TEP1 and to a lesser extent TEP3 – recognize malaria parasites during their midgut invasion and mediate their lysis and melanization (63-69). Failure to recognize pathogens leads to uncontrolled pathogen replication and eventual host death (69-74). Because of the significance of pattern recognition receptors in limiting pathogens, many transgenic mosquitoes were produced with alternated expression of these receptors – e.g. TEP, FREP, C-type lectins – with the hope that they can be used as vector-control strategies (75-77).

After the recognition of pathogens, immune signaling pathways activate and amplify immune responses, induce the production of antimicrobial peptides and the activation of effector mechanisms (48). Mosquitoes have the three well-characterized immune signaling pathways: IMD, TOLL and JAK/STAT pathways (78, 79). The IMD pathway is primarily activated when a mosquito is infected with Gram negative bacteria, viruses, fungi, and malaria parasites *Plasmodium falciparum* (80-85). The IMD pathway

typically begins when transmembrane receptor PGRP-LC recognizes a pathogen and signals to intracellular molecules like Imd, Fadd, Dredd. This leads to the nuclear translocation of the transcription factor Rel2 and the expression of genes encoding antimicrobial peptides and other immune mechanisms (86). The TOLL pathway is primarily activated when a mosquito is infected with Gram positive bacteria, viruses, fungi, filarial worms, and malaria parasites *P. berghei* (78, 87-94). The TOLL pathway typically begins when an extracellular cytokine binds to Spätzle, which then binds to a Toll receptor. This activates intracellular signaling molecules like Tube and Pelle, which leads to the nuclear translocation of the transcription factor Rel1 and the expression of effector genes. The JAK/STAT pathway is primarily activated by viral infection, but sometimes by fungi and malaria parasites (17, 81, 90, 91, 95, 96). Other signaling pathways – like the JNK pathway – also play a role in immunity; the JNK pathway is involved in anti-malarial and antiviral immunity as well as mosquito longevity and reproduction (97-102). Although each pathway has its specialty, many work together or even share signaling components during its transduction (90, 103). The best understood example is the IMD pathway and the JNK pathway where they share the upstream receptor and intracellular signaling molecules, but then the JNK pathway bifurcates from the Imd pathway and induces the expression of other immune genes, like *TEP1* (98). All these immune pathways are tightly regulated; Caspar, Cactus, Socs/Pias, and Puckered are the negative regulators for the IMD, TOLL, JAK/STAT, and JNK pathways, respectively (80, 82, 87, 95, 104).

The pathogens are eventually killed by multiple effector mechanisms, including phagocytosis, melanization and lysis (48). Phagocytosis happens when a hemocyte – either circulating or sessile – uses its membrane to internalize a foreign object (87, 105-

108). Melanization has multiple functions, such as cuticle tanning and wound healing, but also plays a major role in immune response against infections like bacteria, fungi, malaria parasites and nematodes (48, 57, 109, 110). Melanization is manifested as black deposits of melanin on the surface of the pathogens and eventually kills pathogens via oxidative damage or starvation (110). Unlike phagocytosis and melanization, lysis is hard to directly visualize but it happens when the membrane of a pathogen is disrupted by host molecules, such as lysozymes, reactive oxygen species and different classes of antimicrobial peptides, like Defensin, Cecropin, Attacin, and Gambicin (48).

The functional integration of the immune and circulatory systems

In mammals, the immune and circulatory systems are functionally integrated as exemplified by the immune functions of the spleen and lymph nodes (111). A similar functional integration between the two systems also presents in *A. gambiae* mosquitoes, as exemplified by the infection-induced aggregation of hemocytes on the heart valves (Figure 1) (23). In naïve mosquitoes most circulating hemocytes pass through the abdominal ostia freely, while only a few hemocytes reside on the surface of the heart near the abdominal ostia – locations called the periostial regions (23, 30). Within seconds of infection, these heart-associated hemocytes – called periostial hemocytes – phagocytose circulating pathogens, and soon thereafter, additional hemocytes migrate to the periostial regions and amplify this phagocytosis response and mediate the melanization cascade (23, 112). The periostial regions account for less than 5% of the surface area in the abdomen, yet it comprises the most concentrated population of hemocytes (34). Periostial

immune responses are advantageous because they occur in areas of high hemolymph flow, placing hemocytes where they are most likely to encounter and destroy pathogens (23, 112). Interestingly, even among the six pairs of the abdominal ostia, the strength of hemocyte aggregation varies; periostial hemocytes preferentially aggregate around the middle pairs of abdominal ostia because they receive more hemolymph circulation than the other pairs of ostia (112). This again, strengthens the fact that the immune and circulatory systems are functionally integrated in mosquitoes.

The heart of mosquitoes also contracts in a retrograde direction, during which hemocytes and pathogens enter the heart via a single pair of thoraco-abdominal ostia (30, 33, 34). However, hemocytes do not aggregate near the thoraco-abdominal ostia. This could be because the circulation near this pair of ostia is too fast for hemocytes to firmly adhere, or because the substrates near the thoraco-abdominal ostia lack the necessary ligands for the receptors of aggregating hemocytes (34).

Hemolymph circulation is different in mosquito larvae where both hemocytes and pathogens only enter the heart via a posterior opening (32). As a result, hemocytes only concentrate near the posterior end of the larval heart and specifically on the nearby tracheal tufts, and phagocytose pathogens and mediate melanization response (113, 114). This reiterates that no matter the direction of the circulatory current, hemocytes always aggregate at the location where there is high hemolymph flow.

Beyond mosquitoes, hemocytes surround the heart of *Drosophila melanogaster*, another member of Diptera, and function both as immunologically active cells and a hematopoiesis organ (115-119). At the onset of this dissertation, very little was known about whether hemocyte aggregation happens in other insect species. In fact, few studies

have focused on the immune system of insects outside of members of Diptera, Coleoptera, Lepidoptera and Hymenoptera, and even fewer work has studied the circulatory system of insects (48). However, hemocytes have been observed on or in the heart of silkworms and stick insects, and pathogens have been observed on the heart of Lepidoptera (120-122).

Summary and preview of subsequent chapters

The mosquito immune and circulatory systems are functionally integrated, as exemplified by the aggregation of hemocytes on the heart during an infection (23). Periostial hemocytes efficiently kill gram-positive and gram-negative bacteria and malaria parasites (23, 112), highlighting their significance in combating a broad range of infections. At the onset of this dissertation, we had already gained an understanding of the structural mechanics of periostial hemocyte aggregation; however, the genetic mechanisms that drive this process remained largely unknown. A recent study showed that Eater and Draper – members of the Nimrod protein family – positively regulate periostial hemocyte aggregation (123). Since the Nimrod protein family is involved in phagocytosis (54, 124-126), Eater and Draper likely function as effector molecules that mediate adhesion and phagocytosis in periostial hemocytes. However, the molecular drivers of periostial hemocyte aggregation undoubtedly extend beyond the Nimrod protein family. This dissertation dissects the genetic mechanisms that drive periostial hemocyte aggregation. Chapter II determined that Thioester-containing proteins – a family of the pattern recognition receptors – positively regulate periostial hemocyte aggregation. Chapter III

utilized a combination of RNA sequencing and RNA interference to uncover that the IMD and JNK pathways drive periostial hemocyte aggregation. Chapter IV extended beyond the canonical immune genes/pathways and investigated the roles of transglutaminases – a protein family that regulates peptide cross-linking – in periostial hemocyte aggregation. After uncovering the genetic mechanisms of periostial hemocyte aggregation, chapter V explored whether periostial hemocyte aggregation is conserved in class Insecta. After analyzing 68 species of insects across 16 orders spanning the insect tree of life, Chapter V shows that the immune and circulatory systems are functionally integrated throughout insect evolution.

Altogether, this dissertation uncovered the genetic mechanisms and evolutionary conservation of the functional integration between the insect immune and circulatory systems. It details how hemocytes recognize pathogens, activate immune signaling cascades, and attach to the surface of the heart – at the location of highest circulation – and kill pathogens. The genetic factors identified from this dissertation could be used as targets for genetic manipulation, with the aim to create mosquitoes that are refractory to malaria parasites or other mosquito-borne pathogens. Moreover, many of these genetic factors are conserved across insect taxa and the heart-associated immune response is also conserved among insects. Therefore, the genetic mechanisms uncovered in *A. gambiae* mosquitoes likely share similar functions in other insects and contribute to their pathogen killing response. As a result, this research may yield novel insights that can be harnessed to develop strategies to preserve beneficial insects – like honeybees – and kill agricultural and urban pests – like armyworms and bed bugs.

CHAPTER II

Complement-like proteins, TEP1, TEP3 and TEP4, are positive regulators of periostial hemocyte aggregation in the mosquito, *Anopheles gambiae*

Preface

This chapter determined that the pattern recognition receptors – TEP1, TEP3 and TEP4 – positively regulate periostial hemocyte aggregation, highlighting their roles in the interaction between the mosquito immune and circulatory systems. This finding is significant because TEP proteins opsonize pathogens, like malaria parasites, and periostial hemocytes also phagocytose them, indicating that TEP proteins mediate the phagocytosis of malaria parasites by periostial hemocytes. My advisor, Dr. Julián Hillyer, provided the funding and resources for this study. I conducted the experiments presented in this paper. We designed the experiments, analyzed and visualized the data, and wrote the manuscript. I thank Ms. Tania Estévez-Lao and Dr. Scott B. Williams for helpful discussions and feedback on this manuscript. This chapter is adapted from "*Complement-like proteins TEP1, TEP3 and TEP4 are positive regulators of periostial hemocyte aggregation in the mosquito* Anopheles gambiae", published in 2019 in the journal *Insect Biochemistry and Molecular Biology* (127) and has been reproduced with the permission of the publisher and my co-author, Dr. Julián Hillyer.

Abstract

The mosquito immune and circulatory systems are functionally integrated. During an infection, hemocytes aggregate around the ostia (valves) of the dorsal vessel – areas of the heart called the periostial regions – where they phagocytose live and melanized pathogens. Although periostial hemocyte aggregation is an immune response that occurs following infection with bacteria and malaria parasites, the molecular basis of this process remains poorly understood. Here, we show that the thioester-containing proteins, TEP1, TEP3 and TEP4 are positive regulators of periostial hemocyte aggregation in the African malaria mosquito, *Anopheles gambiae*. RNAi-based knockdown of *TEP1*, *TEP3* and *TEP4* resulted in fewer periostial hemocytes following *Escherichia coli* infection, without affecting the adjacent population of non-periostial, sessile hemocytes. Moreover, knockdown of *TEP1*, *TEP3* and *TEP4* expression resulted in reduced bacterial accumulation and melanin deposition at the periostial regions. Finally, this study confirmed the role that TEP1 plays in reducing infection intensity in the hemocoel. Overall, this research shows that the complement-like proteins, TEP1, TEP3 and TEP4, are positive regulators of the functional integration between the immune and circulatory systems of mosquitoes.

Introduction

Bacteria, fungi and malaria parasites invade the mosquito hemocoel (body cavity) where they face immune responses and circulatory currents (21, 48). Immune responses

are primarily mediated by hemocytes (immune cells) that either circulate with the hemolymph (blood) – called circulating hemocytes – or remain attached to tissues – called sessile hemocytes (51). The circulation of hemolymph is maintained by the bidirectional (anterograde and retrograde) contraction of a dorsal vessel that extends the length of the body and is divided into two contiguous segments: a heart in the abdomen and an aorta in the thorax (30, 33). Hemolymph enters the heart though 6 pairs of abdominal ostia (valves) and 1 pair of thoraco-abdominal ostia, and exits back into the hemocoel via excurrent openings located at the anterior and posterior ends of the mosquito (30, 33). When pathogens enter the hemocoel, they circulate with the hemolymph and often become sequestered and killed in the areas surrounding the abdominal ostia – called the periostial regions – with this sequestration being due to phagocytosis by a group of sessile hemocytes called periostial hemocytes (23, 128). During the course of an infection, additional hemocytes exit circulation and aggregate at the periostial regions, thus amplifying this pathogen elimination response.

Periostial hemocyte aggregation preferentially occurs around the ostia that receive the most hemolymph flow, and is induced by Gram(+) and Gram(–) bacteria, malaria parasites, and soluble microbial components (23, 112). Periostial hemocytes occupy less than 5% of the abdominal wall, yet sequester more than 40% of pathogens present on the cuticular integument (34, 52). Periostial hemocytes also phagocytose melanized pathogens, and presumably secrete humoral immune factors (112). Therefore, periostial hemocyte aggregation highlights the functional integration between the immune and circulatory systems of mosquitoes.

The genetic factors that regulate periostial hemocyte aggregation remain largely unknown. Our laboratory recently showed that two immune genes in the Nimrod gene family – *Eater* and *Draper* – influence periostial hemocyte aggregation (123). However, given the modest effects that *Eater* and *Draper* have on this process, we hypothesized that additional genes regulate periostial hemocyte aggregation. Thioester-containing proteins (TEPs) are complement-like opsonins that bind pathogens and promote phagocytosis by hemocytes (106, 107, 129). TEP1, TEP3 and TEP4 regulate the phagocytosis of Gram(+) and/or Gram(–) bacteria, and both TEP1 and TEP3 bind malaria parasites and mediate their lysis and melanization (63, 64, 69, 71, 80, 107, 129). The pleiotropic functions of TEPs led us to hypothesize that they are also involved in periostial hemocyte aggregation. Here, we show that *TEP1*, *TEP3* and *TEP4* are positive regulators of periostial hemocyte aggregation in the African malaria mosquito, *Anopheles gambiae*, and thus, are involved in the functional integration between the immune and circulatory systems.

Materials and Methods

Mosquito colony

Anopheles gambiae, Giles sensu stricto (G3 strain; Diptera: Culicidae), were maintained at 27°C and 75% relative humidity (R.H.) under a 12h:12h light:dark photoperiod, as previously described (30). Larvae were reared in deionized water and fed a mixture of 2.8 parts koi food and 1-part baker's yeast. Adults were maintained in 2.4 L plastic buckets and fed 10% sucrose.

RNA extraction and cDNA synthesis

RNA was extracted and isolated from ~10 whole-body mosquitoes using TRIzol Reagent (Invitrogen, Carlsbad, CA, USA), and purified using the RNeasy Mini Kit (Qiagen, Valencia, CA, USA). The concentration of RNA was quantified using a BioPhotometer Plus spectrophotometer (Eppendorf AG, Hamburg, Germany), and the RNA was treated with RQ1 RNase-free DNase (Promega, Madison, WI, USA). Up to 5 µg of RNA was then used for cDNA synthesis by means of an Oligo$(dT)_{20}$ primer and the SuperScript III First-Strand Synthesis System for RT-PCR (Invitrogen).

Double-stranded RNA (dsRNA) synthesis

Three mosquito-specific dsRNAs were synthesized: ds*TEP1*, ds*TEP3* and ds*TEP4*. One non-mosquito dsRNA – used as a negative control – was synthesized: ds*BLA(Ap^R)* (beta-lactamase) (123, 126). To synthesize the TEP dsRNAs, *A. gambiae* cDNA was subjected to PCR using gene-specific primers with T7 promoter tags (Appendix B). Each amplicon was separated by agarose gel electrophoresis, excised, and purified using Qiagen's QIAquick Gel Extraction kit (Qiagen, Valencia, CA, USA). To increase the amount of template for dsRNA synthesis, each amplicon was then used as template for a second PCR reaction using the same primers. The product was purified using the QIAquick PCR Purification Kit (Qiagen, Valencia, CA, USA), and the concentration was quantified spectrophotometrically. Up to 1 µg of the second PCR product was used as template for dsRNA synthesis using the MEGAscript T7 Kit (Applied Biosystems). The resultant dsRNA was precipitated with ethanol and re-suspended in

phosphate-buffered saline (PBS). The concentration of dsRNA was quantified spectrophotometrically and the integrity of dsRNA was verified by agarose gel electrophoresis. The same procedure was followed for ds*BLA(Ap^R)* synthesis, except that the starting material was DNA extracted from *Escherichia coli* BL21(DE3) containing the pET-46 plasmid (EMD Chemicals, Gibbstown, NJ).

RNA interference (RNAi), mosquito treatments, and bacterial rearing

Two-day-old female mosquitoes were anesthetized briefly by placing them in a Petri dish held over ice, and then injected 300 ng of dsRNA at the thoracic anepisternal cleft using a Nanoject III Programmable Nanoliter Injector (Drummond Scientific Company, Broomall, PA, USA). Four days after dsRNA injection, mosquitoes were divided into two groups: (1) not infected (left unmanipulated and herein termed “naïve”), and (2) infected by injecting 69 nL of tetracycline resistant, GFP-expressing *E. coli* (modified DH5α; GFP-*E. coli*). An injury group (e.g., sham injection) was not assayed because injury does not induce periostial hemocyte aggregation (23, 52, 112). For infections, GFP-*E. coli* were grown overnight in Luria-Bertani’s rich nutrient medium (LB) in a 37°C shaking incubator (New Brunswick Scientific, Edison, NJ, USA). The absorbance of *E. coli* cultures was measured spectrophotometrically and normalized to OD_{600} = 2 prior to injection. Across experimental trials, the infection dose averaged at 38,330 *E. coli* per mosquito.

RNAi knockdown efficiency

RNA was purified from mosquitoes that were either naïve, or had been infected with *E. coli* for 4 h or 24 h. cDNA was synthesized and used as template for real-time quantitative PCR (qPCR) using gene-specific primers (Appendix B) and Power SYBR Green PCR Master Mix (Applied Biosystems, Foster City, CA) on an ABI 7300 Real-Time PCR System. Relative quantification of mRNA levels was conducted using the $2^{-\Delta\Delta C_T}$ method, using the housekeeping gene *RPS7* as the reference gene (130, 131). Three biological replicates were conducted with two technical replicates each. The absence of genomic DNA in the cDNA preparations was confirmed by melting curve analysis at the end of each qPCR run. The data were combined and analyzed by two-way ANOVA, followed by Dunnett's multiple comparison test, with ds*BLA(Ap^R)*-injected mosquitoes as the reference group.

In vivo hemocyte staining and mosquito dissections

Hemocytes were stained *in vivo* using Vybrant CM-DiI Cell-Labeling Solution (Invitrogen) as previously described (23). Briefly, live mosquitoes were anesthetized and injected with 0.4 μl of a solution consisting of 67 μM CM-DiI and 1.08 mM Hoechst 33342 (Invitrogen) in PBS. Mosquitoes were incubated at 27°C and 75% R.H. for 20 min, and then fixed for 10 min by injecting 16% formaldehyde into the hemocoel. The abdomens were immersed in PBS containing 0.1% Triton X-100, bisected along a coronal plane, and the internal organs were removed. The dorsal abdomens – containing the heart and periostial hemocytes – were rinsed briefly in PBS and mounted between a glass slide and a coverslip using Aqua-Poly/Mount (Polysciences; Warrington, PA, USA).

Microscopy and image acquisition

Each dorsal abdomen was imaged under bright-field and fluorescence illumination on a Nikon 90i compound microscope connected to a Nikon Digital Sight DS-Qi1 monochrome digital camera and Nikon's Advanced Research NIS Elements software (Nikon, Tokyo, Japan). Z-stacks were acquired using a linear encoded Z-motor. For image presentation and pixel intensity measurements, all images within a stack were combined into a two-dimensional, focused image using the Extended Depth of Focus (EDF) function in NIS Elements.

Quantification of hemocytes

Hemocytes were counted manually by examining all images within a Z-stack. A cell was counted as a hemocyte if it measured 9-18 μm in diameter and was labeled with both CM-DiI and Hoechst 33342 (112). A cell was counted as a periostial hemocyte if it was adjacent to an ostium, and a cell was counted as a non-periostial, sessile hemocyte if it was attached to the abdominal wall in an area that was outside of the periostial regions (23, 52). Periostial hemocytes were counted within abdominal segments 2-7 whereas non-periostial, sessile hemocytes were only counted on the dorsal abdominal wall of segments 4 and 5. Hemocytes were not counted on the aorta, the excurrent openings or the thoraco-abdominal ostia because few hemocytes are present there, and infection does not induce the aggregation of hemocytes at those locations (33, 34). Each treatment group contained a minimum of 16 mosquitoes that were assayed across 3 independent trials. The data were combined and analyzed by two-way ANOVA, followed by Dunnett's

multiple comparison test. The ds*BLA(Ap^R)*-injected mosquitoes were used as the reference group.

Quantification of GFP fluorescence at the periostial regions

GFP fluorescence intensity at the periostial regions was calculated from EDF images by measuring the sum pixel intensity above a threshold in NIS Elements (112, 123). The threshold was defined as the pixel intensity that distinguished GFP emitted by *E. coli* rods (pixel intensity above the threshold) from background fluorescence intensity (pixel intensities below the threshold). Then, each periostial regions was delineated using the region of interest (ROI) tool, and the sum pixel intensity within each ROI was measured. Each treatment group contained a minimum of 15 mosquitoes that were assayed across 3 independent trials. The data were combined and analyzed by two-way ANOVA, followed by Dunn's multiple comparison test. The ds*BLA(Ap^R)*-injected mosquitoes were used as the reference group.

Quantification of dark deposits at the periostial regions

Dark deposits that result from melanization were quantified from EDF images by measuring the area of pixels with intensities below a threshold using NIS Elements (112). For this, images were first examined to determine a pixel intensity that distinguished melanized areas (pixel intensities below the threshold) from non-melanized areas (pixel intensities above the threshold). Then, the area of pixels below the melanization threshold was measured for each periostial region ROI. A minimum of 19 mosquitoes across 3 independent trials were assayed for each treatment group. The data were combined and

analyzed by two-way ANOVA, followed by Dunn's multiple comparison test. The ds*BLA(Ap^R)*-injected mosquitoes were used as the reference group.

Quantification of bacterial infection intensity

Infected mosquitoes were homogenized individually in PBS, and a dilution of each homogenate was spread on an LB agar plate containing tetracycline. Each plate was incubated at 37°C overnight, and the resulting colony forming units (CFUs) were screened for GFP fluorescence on a Nikon SMZ1500 stereomicroscope and counted. The number of CFUs was used to calculate the number of live GFP-*E. coli* in each mosquito at the time of homogenization. Three independent trials were conducted with a minimum of 24 mosquitoes in each treatment group. For statistical analyses, data were transformed by log 10 to satisfy the assumptions of ANOVA, and the transformed data were analyzed by two-way ANOVA, followed by Dunnett's multiple comparison test. The ds*BLA(Ap^R)*-injected mosquitoes were used as the reference group.

Results

TEP1, TEP3 and TEP4 are involved in infection-induced periostial hemocyte aggregation

To test whether TEPs are involved in periostial hemocyte aggregation, we knocked down the expression of *TEP1*, *TEP3* and *TEP4* by RNAi, which resulted in a >71% reduction in mRNA levels relative to the control ds*BLA(Ap^R)*-injected mosquitoes (Appendix A). Having established successful gene knockdown, we next quantified the number of periostial hemocytes in ds*TEP1-,* ds*TEP3*-, ds*TEP4*- and ds*BLA(Ap^R)*-injected

mosquitoes that were naïve or had been infected with *E. coli* for 4 h or 24 h (Figure 1). We found that the number of periostial hemocytes in naïve mosquitoes remained unchanged regardless of gene knockdown. Furthermore, at 4 h and 24 h post *E. coli* infection, the ds*BLA(Ap^R)* mosquitoes had 3.2 and 2.9-fold more periostial hemocytes than their naïve counterparts, respectively, again showing that periostial hemocyte aggregation is induced by infection. TEP knockdown also resulted in an infection-induced increase in the number of periostial hemocytes, but this increase was significantly smaller than when mosquitoes were treated with ds*BLA(Ap^R)*. Specifically, at 4 h post-infection, the number of periostial hemocytes was 1.3-, 1.7-, and 2.1-fold higher in *TEP1*, *TEP3* and *TEP4* knockdown mosquitoes, relative to their respective naïve counterparts, and this modest increase remained stable in *TEP1* and *TEP3* knockdown mosquitoes at 24 h post-infection. Therefore, these data show that knocking down the expression of *TEP1*, *TEP3* and *TEP4* does not affect the number of periostial hemocytes in naïve mosquitoes, but reduces the infection-induced aggregation of hemocytes at the periostial regions, with the phenotype being stronger in *TEP1*- and *TEP3*-depleted mosquitoes.

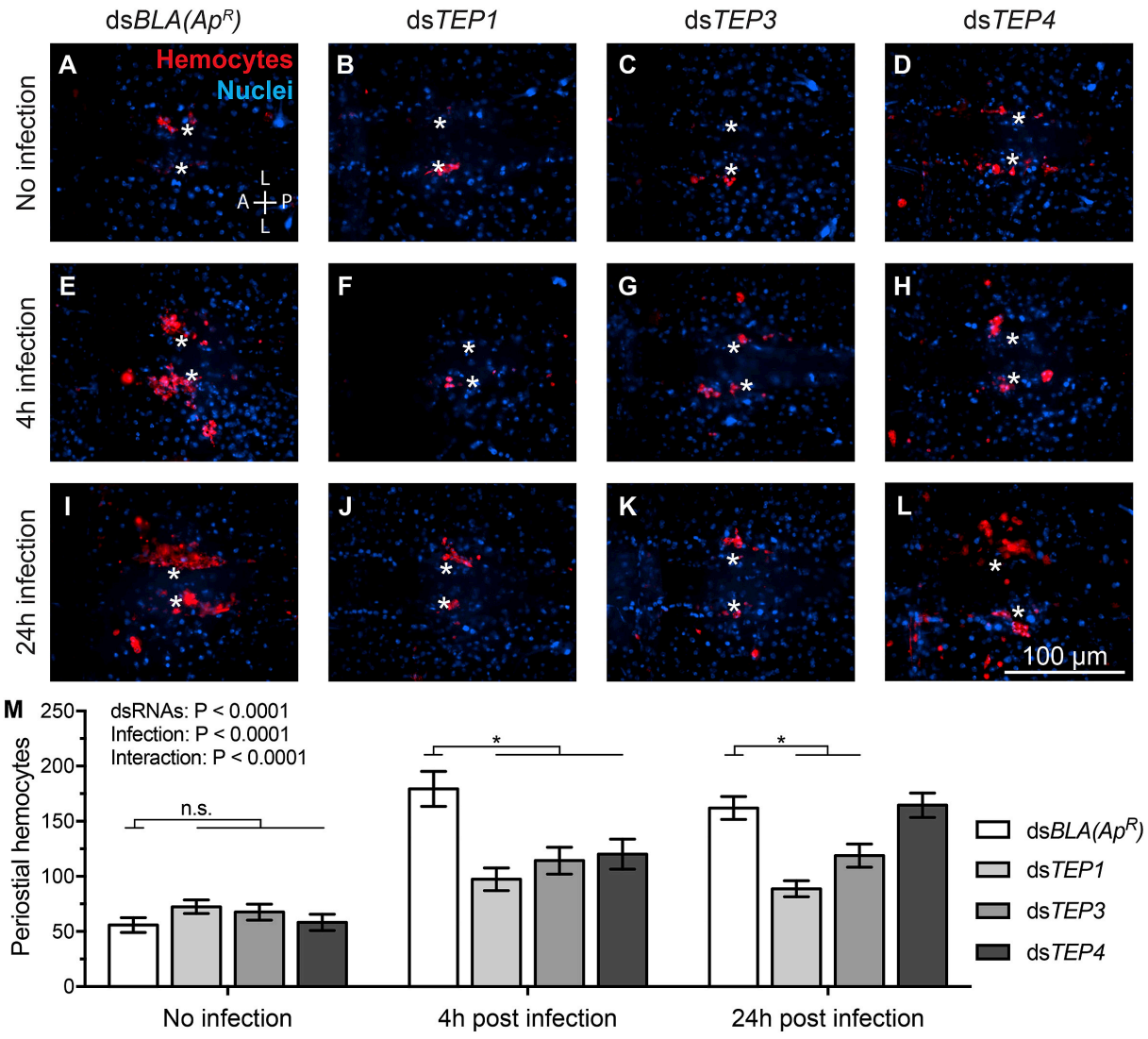

Figure 1 *TEP1*, *TEP3* and *TEP4* knockdown mosquitoes have fewer periostial hemocytes following *E. coli* infection.

(A-L) Fluorescence images of a single abdominal segment showing periostial hemocytes (stained red with CM-DiI) surrounding the ostia (asterisks) in naïve mosquitoes (A-D), and mosquitoes at 4 h (E-H) and 24 h (I-L) post-infection. Prior to infection, mosquitoes had been treated with ds*BLA(Ap^R)* (A, E, I), ds*TEP1* (B, F, J), ds*TEP3* (C, G, K) or ds*TEP4* (D, H, L). Nuclei were stained blue with Hoechst 33342. A, anterior; P, posterior; L, lateral. (M) Columns show the average number of periostial hemocytes in ds*BLA(Ap^R)*-, ds*TEP1*-, ds*TEP3*- and ds*TEP4*-injected mosquitoes that were not infected or had been infected with *E. coli* for 4 h or 24 h. Whiskers mark the standard error of the mean (S.E.M). Data were analyzed by two-way ANOVA, followed by Dunnett's post-hoc test. Asterisks indicate $P < 0.05$ (n.s., nonsignificant).

TEPs do not alter the spatial distribution of periostial hemocytes across segments

Periostial hemocytes preferentially aggregate around the ostia of abdominal segments 4, 5 and 6, which are the ostia that receive the majority of hemolymph flow (112). Having established that TEPs facilitate the infection-induced aggregation of periostial hemocytes, we next sought to determine whether TEPs influence the spatial distribution of periostial hemocytes across the six periostial regions (Figure 2). In naïve mosquitoes, the majority of periostial hemocytes were located in abdominal segments 4-7, and dsRNA treatments did not affect the segmental distribution of periostial hemocytes (interaction $P = 0.4062$). At 4 h post-infection, all segments had fewer periostial hemocytes in TEP knockdown mosquitoes than in ds*BLA(Ap^R)*-injected mosquitoes, but most periostial hemocytes remained in abdominal segments 4-6 and there was no difference in the spatial distribution of periostial hemocytes between the dsRNA groups. The same was true at 24 h post-infection, except that there was an interaction between the segmental distribution of periostial hemocytes and dsRNA treatment. Visual inspection of the data suggests that this change was due to *TEP4*-depleted mosquitoes displaying a non-proportional increase in periostial hemocytes within abdominal segments 4, 5 and 7, relative to segment 6. Altogether, these data show that knocking down the expression of TEPs does not have a meaningful effect on the spatial distribution of periostial hemocytes.

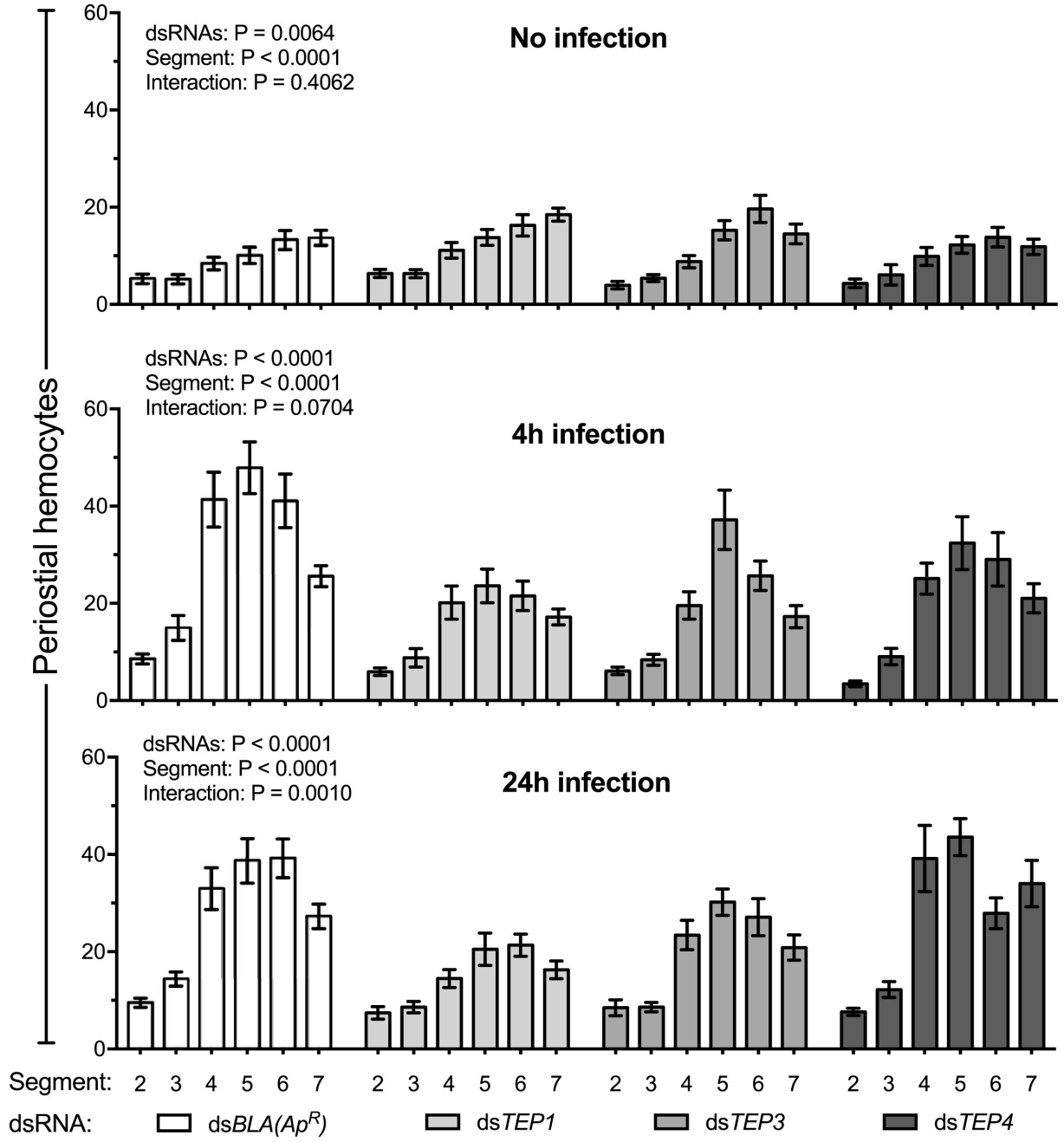

Figure 2 TEPs do not meaningfully alter the spatial distribution of periostial hemocytes.

Columns show the average number of periostial hemocytes at each periostial region in abdominal segments 2-7 in ds*BLA(Ap^R)*-, ds*TEP1*-, ds*TEP3*- and ds*TEP4*-injected mosquitoes that were not infected, or had been infected with *E. coli* for 4 h or 24 h. Whiskers mark the S.E.M. Data were analyzed by two-way ANOVA, followed by Dunnett's post-hoc test.

TEPs do not affect the number of sessile hemocytes outside the periostial regions

We next tested whether TEPs influence the aggregation of sessile hemocytes outside of the periostial regions, and did so to determine whether the effect of TEP depletion is limited to the periostial regions. To achieve this, we examined the same mosquitoes analyzed for figures 1 and 2 (the same Z-stacks), and quantified the number of non-periostial sessile hemocytes present on the dorsal portion of abdominal segments 4 and 5. We found that infection induces a modest increase in the number of non-periostial sessile hemocytes (Figure 3; e.g., at 24 h post-infection there was a 40% increase in segment 4 for naïve ds*BLA(Ap^R)*-injected mosquitoes), but this increase is small relative to the increase in the number of periostial hemocytes (Figure 1; e.g., at 24 h post-infection there was a 293% increase in segment 4 for naïve ds*BLA(Ap^R)*-injected mosquitoes). Furthermore, the number of non-periostial sessile hemocytes in TEP knockdown mosquitoes was similar to the number of non-periostial sessile hemocytes in ds*BLA(Ap^R)*-injected mosquitoes (Figure 3). Therefore, knocking down the expression of TEPs does not affect sessile hemocytes located outside of the periostial regions.

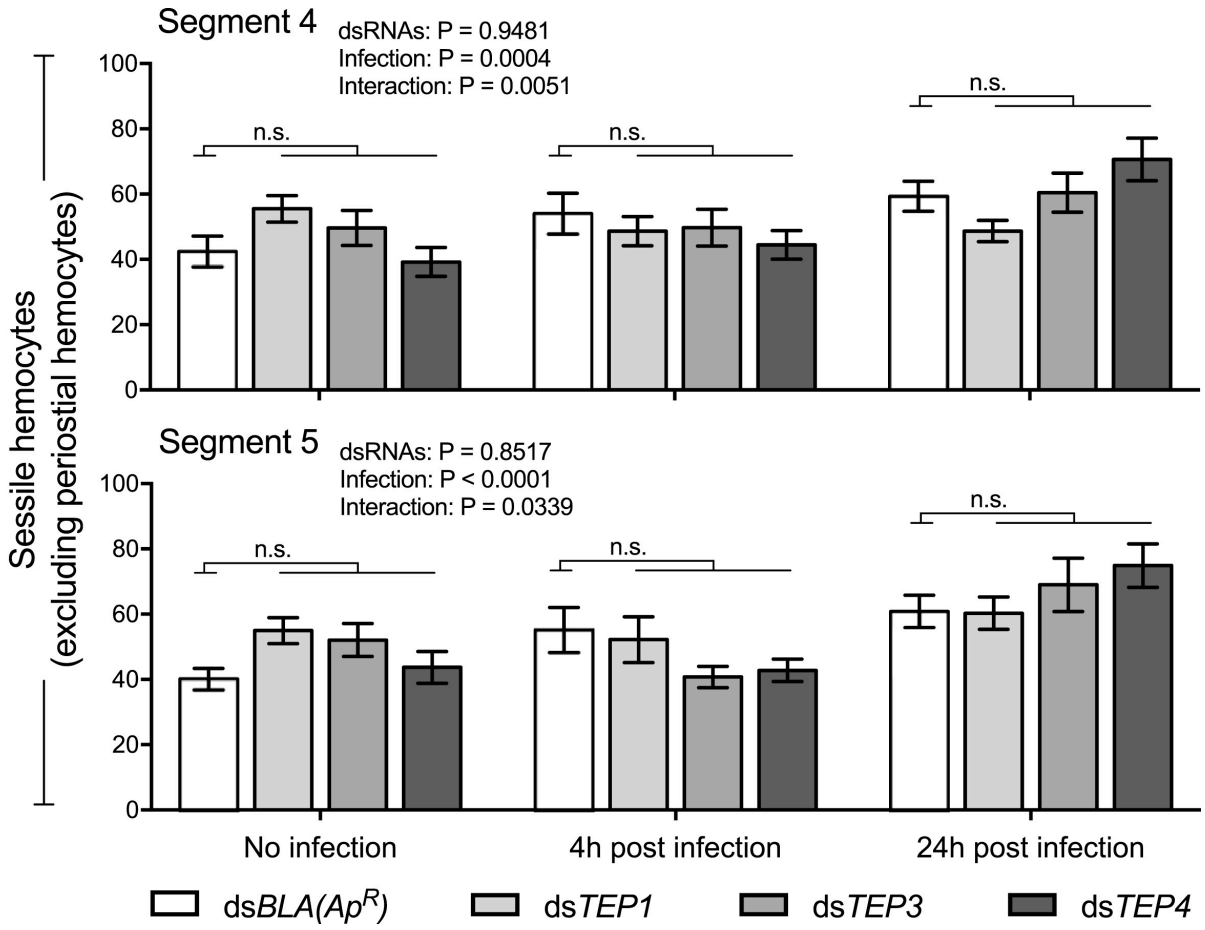

Figure 3 TEPs do not affect the aggregation of sessile hemocytes outside the periostial regions.
Columns show the average number of non-periostial sessile hemocytes on the dorsal abdomen of segments 4 (top) and 5 (bottom) in ds*BLA(Ap^R)*-, ds*TEP1*-, ds*TEP3*- and ds*TEP4*-injected mosquitoes that were not infected, or had been infected for 4 h or 24 h. Whiskers mark the S.E.M. Data were analyzed by two-way ANOVA, followed by Dunnett's post-hoc test (n.s., nonsignificant).

TEPs do not play a major role in the accumulation of live bacteria at the periostial regions

Periostial hemocytes eliminate pathogens by phagocytosis, a cellular immune process that occurs within the periostial regions and elsewhere, and results in the capture and degradation of microbes (23, 51). The hemocyte-based capture of GFP-*E. coli* at the periostial regions results in green fluorescence that accumulates as additional bacteria are phagocytosed, but dissipates as the bacteria are degraded (112). Given that TEPs

regulate periostial hemocyte aggregation, and that TEPs are regulators of the phagocytosis response (105, 107), we next sought to assay whether knocking down the expression of TEPs affects *E. coli* accumulation at the periostial regions. To achieve this, we quantified the fluorescence intensity of GFP-*E. coli* at the periostial regions of dsTEP- and ds*BLA(Ap^R)*-injected mosquitoes at 4 h or 24 h post-infection. To our surprise, we did not detect significant differences in the fluorescence intensity of GFP-*E. coli* between the TEP knockdown and ds*BLA(Ap^R)*-injected mosquitoes at either 4 h or 24 h post-infection (Figure 4). However, there was a trend for all dsTEP groups to have less fluorescence at the periostial regions than the ds*BLA(Ap^R)* group at 4 h – providing weak evidence of phagocytic reduction in TEP knockdown mosquitoes – and there was also a trend for all dsTEP groups to have more fluorescence at the periostial regions than the ds*BLA(Ap^R)* group at 24 h – providing weak evidence of impaired bacterial killing. Furthermore, between 4 h and 24 h post-infection the ds*BLA(Ap^R)*- and ds*TEP4*-injected mosquitoes experienced significant reductions ($p<0.05$) in GFP fluorescence intensity at the periostial regions – 68% and 55% reductions, respectively – whereas ds*TEP1*- and ds*TEP3*-injected mosquitoes experienced smaller, nonsignificant reductions ($p>0.05$) of 39% and 41%, respectively. Overall, these data suggest that TEPs are not major regulators of bacterial accumulation at the periostial regions, although knocking down *TEP1* or *TEP3* results in slower bacterial clearance at the periostial regions.

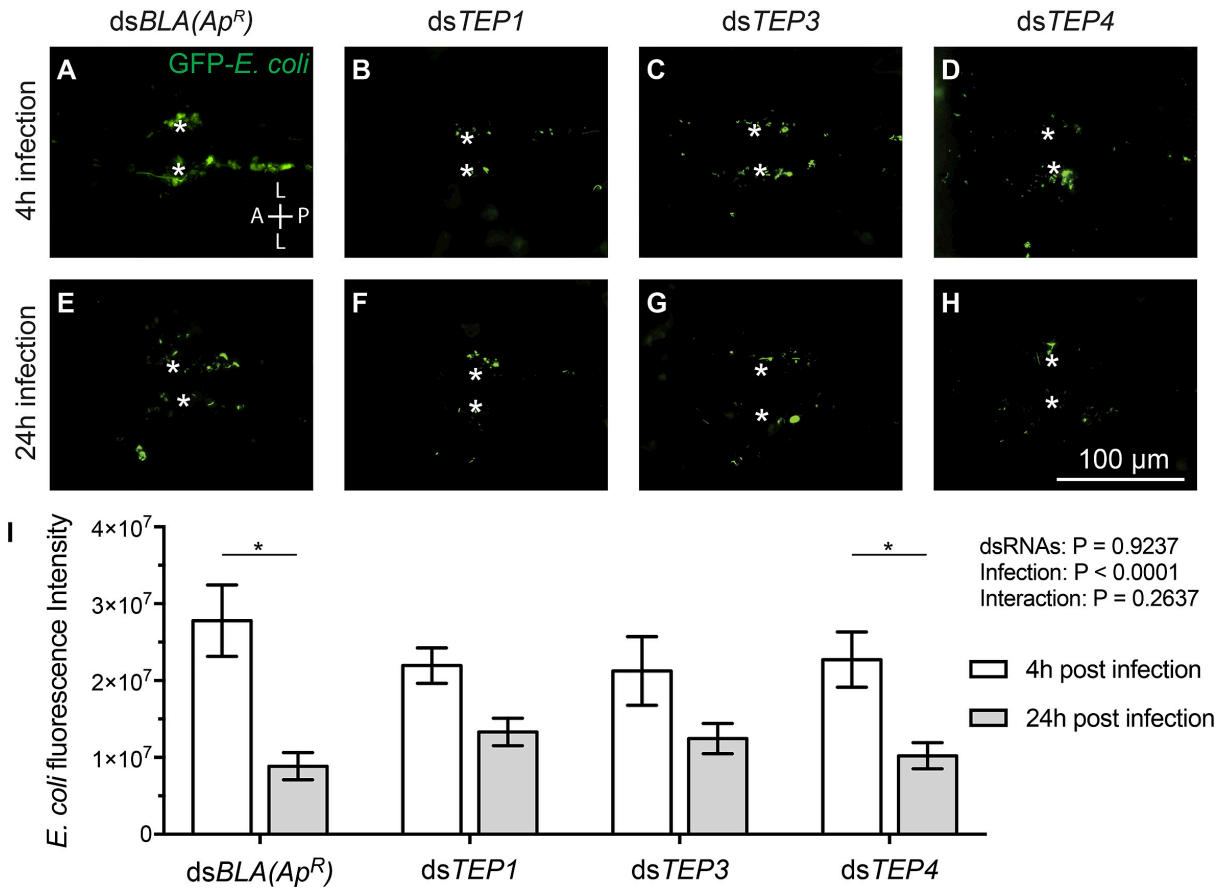

Figure 4 TEPs do not play a major role in *E. coli* accumulation in the periostial regions.
(A-H) Fluorescence images of a single abdominal segment showing GFP-*E. coli* around the ostia (asterisks) at 4 h (A-D) and 24 h (E-H) post-infection. Prior to infection, mosquitoes had been treated with ds*BLA(Ap^R)* (A, E), ds*TEP1* (B, F), ds*TEP3* (C, G) or ds*TEP4* (D, H). A: anterior; P: posterior; L: lateral. (I) Columns show the average GFP-*E. coli* fluorescence intensity in ds*BLA(Ap^R)*-, ds*TEP1*-, ds*TEP3*- and ds*TEP4*-injected mosquitoes that had been infected with *E. coli* for 4 h or 24 h. Whiskers mark the S.E.M. Data were analyzed by two-way ANOVA, followed by Dunnett's post-hoc test. Asterisks indicate $P < 0.05$.

TEPs regulate melanin accumulation on the surface of the heart

Hemocytes produce and secrete the enzymes that drive the phenoloxidase-based enzymatic cascade that leads to the melanization of pathogens, and when visualized by bright-field microscopy, the products of melanization can be seen as dark deposits (48, 70, 112, 113, 132). At the periostial regions, these dark deposits appear because of the

phagocytosis of melanized pathogens by periostial hemocytes (112). Given that TEPs regulate hemocyte aggregation but do not appear to play a major role in the accumulation of live bacteria at the periostial regions, we tested whether TEPs influence the accumulation of melanin at the periostial regions by means of a microscopy-based optical density assay (Figure 5). As expected, melanin was absent in the periostial regions of naïve mosquitoes, regardless of dsRNA treatment. In ds*BLA(Ap^R)*-injected mosquitoes, by 4 h post-infection the area of the periostial regions that contained melanin increased 1,922% relative to naïve mosquitoes, and by 24 h post-infection it increased 3,750% (Figure 5). But in ds*TEP1*-, ds*TEP3*- and ds*TEP4*-injected mosquitoes, at 4 h post-infection the melanized area increased only slightly – 168%, 455% and 579%, respectively, and this modest increase was sustained at 24 h post-infection in ds*TEP1*- and ds*TEP3*-injected mosquitoes. Therefore, this shows that knocking down the expression of *TEP1*, *TEP3* and *TEP4* reduces melanin accumulation at the periostial regions, with the phenotype being stronger in *TEP1*- and *TEP3*-depleted mosquitoes. These data, together with the GFP-*E. coli* fluorescence intensity data, suggest that *TEP1* and *TEP3* regulate pathogen elimination at the periostial regions.

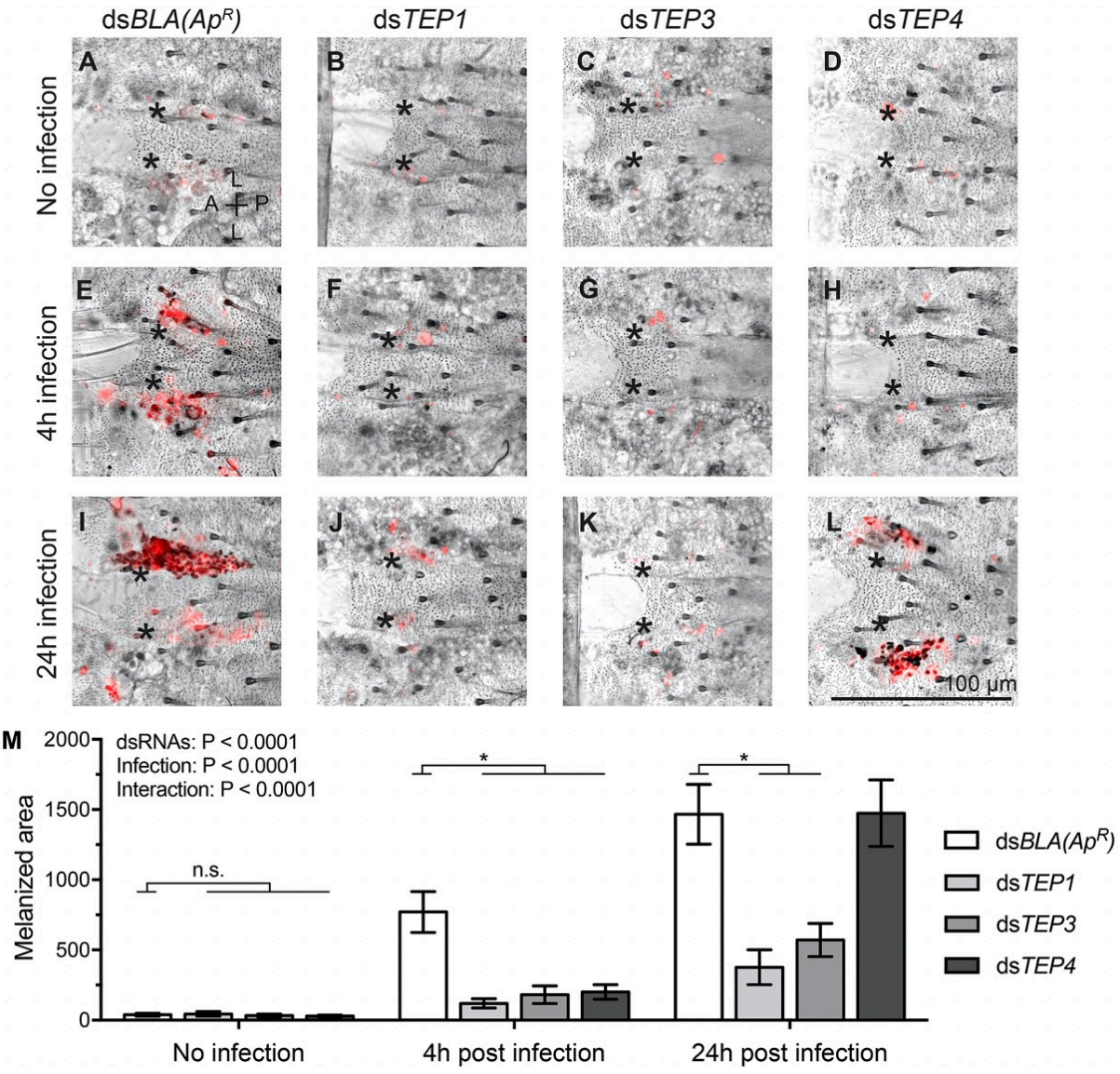

Figure 5 TEPs regulate melanin accumulation at the periostial regions.
(A-L) Bright field images of a single abdominal segment showing melanin deposits (black) and periostial hemocytes (red) surrounding the ostia (flanking the center of the image) in naïve mosquitoes (A-D), and mosquitoes at 4 h (E-H) and 24 h (I-L) post-infection. Prior to infection, mosquitoes had been treated with ds*BLA(Ap^R)* (A, E, I), ds*TEP1* (B, F, J), ds*TEP3* (C, G, K) or ds*TEP4* (D, H, L). A: anterior; P: posterior; L: lateral. (M) Columns show the average area with melanin deposits in ds*BLA(Ap^R)*-, ds*TEP1*-, ds*TEP3*- and ds*TEP4*-injected mosquitoes that were not infected or had been infected with *E. coli* for 4 h or 24 h. Whiskers mark the S.E.M. Data were analyzed by two-way ANOVA, followed by Dunnett's post-hoc test. Asterisks indicate $P < 0.05$ (n.s., nonsignificant).

TEP1 regulates the antibacterial responses in the whole body

Having established that TEPs regulate periostial hemocyte aggregation as well as the accumulation of melanin at the periostial regions, we tested whether knocking down TEPs affects the overall antibacterial immune response. For this, we used a plating assay to measure the number of *E. coli* in the whole body of dsTEP- and ds*BLA(Ap^R)*-injected mosquitoes that had been infected for 4 h or 24 h. The bacterial intensities were similar between the dsRNA groups at 4 h post-infection, however, at 24 h post-infection the TEP1-depleted mosquitoes had 251% more bacteria in their hemocoel than the ds*BLA(Ap^R)*-injected mosquitoes (Figure 6). These data show that *TEP1* depletion suppresses the systemic antibacterial response.

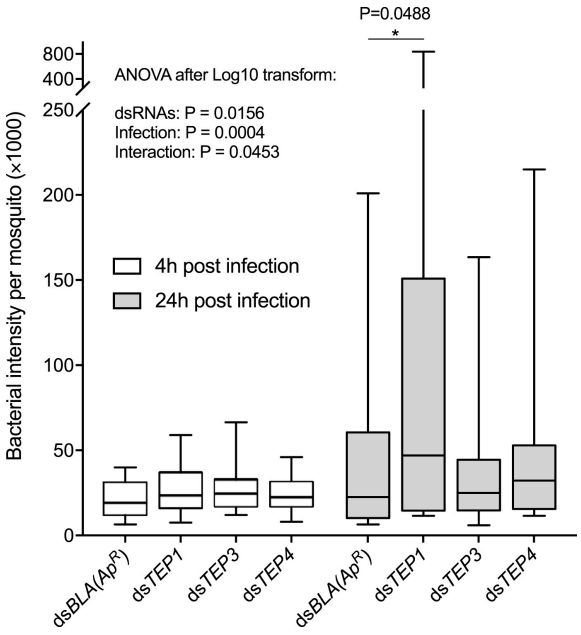

Figure 6 TEP1 regulates the antibacterial response in the mosquito hemocoel.
In this box plot, the center line marks the median, the box shows 50% of the data, and the whiskers delineate the range of live, tetracycline-resistant, GFP-*E. coli* in the whole body of ds*BLA(Ap^R)*-, ds*TEP1*-, ds*TEP3*- and ds*TEP4*-injected mosquitoes at 4 h or 24 h post-infection. For statistical analyses, bacterial intensity was transformed by log 10 to conform to a normal distribution and then analyzed by two-way ANOVA, followed by Dunnett's post-hoc test. Asterisk indicated a significant difference at $P < 0.05$.

Discussion

The aggregation of hemocytes and pathogens on the heart of mosquitoes has been observed in larvae and adults – albeit differently in the two life stages – as well as in several other insects (32, 113-115, 120, 121, 133, 134). However, the genetic mechanisms that leads to the physiological interaction between the immune and circulatory systems remain poorly understood. In this study, we show that *TEP1*, *TEP3* and *TEP4* positively regulate periostial hemocyte aggregation, and also influence the accumulation of bacteria on the surface of the heart. Therefore, *TEP1*, *TEP3* and *TEP4* are positive regulators of the functional integration between the immune and circulatory systems.

TEPs serve important roles in the immunological function of hemocytes. For example, TEPs are secreted by hemocytes and fat body and bind to bacteria in the hemocoel and *Plasmodium* parasites in the midgut, leading to their killing (63, 64, 69, 71, 75, 80, 105, 107, 129). When TEPs bind bacteria, this promotes phagocytosis by hemocytes via two pathways: the *TEP1-TEP3-LRP1-CED6L* pathway and the *TEP4-BINT2-CED2L-CED5L* pathway (107). Two downstream molecules – LRP1 and BINT2 – are transmembrane proteins that have overlapping functions in phagocytosis and adhesion (135, 136). In this study, we found evidence that *TEP1*, *TEP3* and *TEP4* regulate another hemocyte function: the infection-induced aggregation of hemocytes on the surface of the heart. We propose that when a TEP binds and opsonizes a pathogen, it activates signal transduction pathways that activate the phagocytic and adhesive

properties of hemocytes, leading to their attachment to the periostial regions by adhesive capture. Throughout this study, we found that *TEP1* and *TEP3* have stronger effects on periostial responses than *TEP4*. The stronger phenotypes associated with *TEP1* and *TEP3* knockdown could be because (i) the TEP1/TEP3 signal transduction pathway has a stronger regulatory function in periostial hemocyte aggregation, (ii) TEP1 and TEP3 play a more prominent role in the response against *E. coli*, or (iii) TEP1 and TEP3 play a more prominent role in the general immune response. We hypothesize that the latter is most likely for two reasons. First, TEP1 and TEP3 eliminate more malaria oocysts and combat more *Plasmodium* species than TEP4 (67, 69). Second, LRP1 – which is downstream of TEP1 and TEP3 – plays a stronger role in phagocytosis by non-periostial, sessile hemocytes than BINT2 – which is downstream of TEP4 (107).

We also found that although TEPs regulate periostial hemocyte aggregation, they do not play a major role in the aggregation of sessile hemocytes in non-periostial regions. Indeed, a previous report – as well the present study – showed that an infection induces minimal hemocyte aggregation at non-periostial regions, relative to the intense aggregation seen on the surface of the heart (52). We propose that the specific effect observed on the heart is in large part because of circulatory currents, especially given that the periostial regions experience 20 times more hemolymph flow than the rest of the abdomen (30, 31). Therefore, circulating hemocytes flow through the periostial regions more frequently than through any other region of the abdomen, and we hypothesize that once activated by TEPs, hemocytes have a higher chance of attaching to the periostial regions than elsewhere. This hypothesis is further supported by the observation that more periostial hemocytes aggregate in the middle abdominal segments, which are the regions

of the heart that receive the most hemolymph flow (112). Examination of images published by others also show a similar spatial distribution of hemocytes, pathogens or melanin in mosquitoes (70, 108, 112, 132, 133). However, flow alone does not explain the specific aggregation of hemocytes on the surface of the heart because TEP knockdown does not affect non-periostial areas. Thus, other forces or factors must also be involved.

Circulating, sessile and periostial hemocytes phagocytose both unmelanized and melanized pathogens (23, 49, 50, 112). Here, we found that depleting TEPs slightly impairs the accumulation of live pathogens at 4 h post-infection, and we propose that this is due to impaired phagocytic activity by periostial hemocytes. Indeed, an earlier study found that *TEP1*, *TEP3* and *TEP4* knockdown decreases the phagocytic activity of sessile hemocytes present on the lateral abdominal wall by 63%, 48% and 64%, respectively, so the trend we observed was not surprising (107). What was surprising was that the magnitude in the reduction was small, but this may be because of differences in the methods used in the two studies. First, we used live *E. coli* instead of dead *E. coli* particles and quantified pathogen accumulation at 4 h instead of 30 minutes post-challenge – meaning that bacterial replication was occurring in our study. Second, Moita et al (2005) quenched the fluorescence of non-phagocytosed FITC bioparticles (107) – which is something we were unable to do for GFP-expressing live *E. coli* – and so, in our study the bacteria present on the surface of hemocytes yielded a signal even without being phagocytosed. In addition to the differences in methodology, there is an alternate explanation that we believe is even more likely. We have reported that melanin mask the fluorescence emitted by GFP-*E. coli* (113). Therefore, we hypothesize that, because

mosquitoes treated with ds*BLA(Ap^R)* have more melanin in the periostial regions than mosquitoes treated with dsTEP, the fluorescence values measured for ds*BLA(Ap^R)* mosquitoes are an underestimate of the amount of bacteria in the periostial regions, meaning that the real difference between ds*BLA(Ap^R)* and dsTEP knockdown mosquitoes is larger than measured. Regardless, our finding that depleting TEPs reduces melanin accumulation in the periostial regions, together with evidence that (i) melanized or partially melanized bacteria are phagocytosed by hemocytes and (ii) uncontrolled TEP1 activation results in melanin accumulation on the heart even in the absence of infection, supports the role of TEPs in influencing phagocytosis at the periostial regions (49, 50, 70, 112).

Periostial hemocyte aggregation is a general immune response that is elicited by multiple types of infection (23, 112), and therefore, we hypothesize that multiple immune pathways drive this process. Previously, our lab showed that two members of the Nimrod gene family – the transmembrane proteins *Eater* and *Draper* – are regulators of periostial hemocyte aggregation (123). Knocking down *Eater* and TEPs results in a similar phenotype – fewer periostial hemocytes – whereas knocking down *Draper* results in a marginal increase in the number of periostial hemocytes. Regardless, the phenotypes observed following TEP knockdown were generally stronger than the phenotypes observed following the knockdown of *Eater* or *Draper*.

To successfully transmit malaria to a vertebrate host, *Plasmodium* parasites must complete an obligatory migration inside the mosquito. As part of this migration, sporozoites released from oocysts on the midgut circulate with the hemolymph as they seek to invade the salivary glands (128, 137-139). While sporozoites circulate with the

hemolymph, only 19% invade salivary glands (128). The specific mechanisms for sporozoite killing in the hemocoel remain largely unknown, but some are captured and killed by the periostial hemocytes, which highlights the advantage of having hemocytes reside in areas of high hemolymph flow (23, 128). TEP1 and TEP3 bind and mediate the killing of *Plasmodium* in the midgut (63, 64, 69, 71). We hypothesize that TEP1 and TEP3 have additional roles in reducing the number of malaria parasites in mosquitoes, and propose that future studies investigate whether TEPs are involved in the periostial hemocyte-mediated killing of sporozoites circulating with the hemolymph.

CHAPTER III

The IMD and JNK pathways drive the functional integration of the immune and circulatory systems in mosquitoes

Preface

This chapter utilized RNA sequencing and found that infection highly induces several components of the IMD and JNK pathways in periostial hemocytes. RNAi-based knockdown showed that the IMD and JNK pathways drive periostial hemocyte aggregation and immune responses on the heart, highlighting their roles in the interaction between the mosquito immune and circulatory systems. The RNAseq project was initiated prior to me joining the Hillyer lab. Dr. Leah Sigle and my advisor, Dr. Julián Hillyer, designed the RNAseq experiment. Dr. Sigle and Ms. Tania Estévez-Lao conducted the RNAseq experiments. Drs. David Rinker and John (Tony) Capra mapped the reads. I assisted them in narrowing the candidate gene lists and I conducted the subsequent RNAi experiments. Ms. Estévez-Lao assisted in the qPCR analysis. Dr. Hillyer and I wrote the manuscript, as it is presented in this chapter. Dr. Hillyer provided the funding and resources for this study. I thank Dr. Scott B. Williams and Ms. Luísa Jabbur for helpful discussions and feedback on this manuscript. This chapter was included in this dissertation with the permissions of my collaborators, Leah Sigle, Tania Estévez-Lao, David Rinker, John Capra and Julián Hillyer.

Abstract

The immune and circulatory systems are functionally integrated across insect evolution. In the African malaria mosquito, *Anopheles gambiae*, immune cells called periostial hemocytes reside around the heart's ostia (valves), where they readily phagocytose pathogens in the areas of the body that experience the swiftest hemolymph (blood) flow. An infection recruits additional periostial hemocytes, amplifying this heart-associated immune response. Although the structural mechanics of periostial hemocyte aggregation have been defined in mosquitoes, the genetic factors that drive heart-associated immune responses remain less understood. Here, we conducted RNAseq analyses and discovered that, during an infection, multiple components of the IMD and JNK pathways are more highly upregulated in periostial hemocytes than in circulating hemocytes or the rest of the abdomen. RNAi-based knockdown showed that the IMD and JNK pathways drive periostial hemocyte aggregation and immune responses on the heart, thereby showing their involvement in the functional integration between the immune and circulatory systems of mosquitoes.

Introduction

Insect immune cells – called hemocytes – produce pattern recognition receptors that detect pathogens, activate immune signaling pathways such as TOLL, IMD, JNK and JAK/STAT, and eventually kill pathogens via phagocytosis, lysis, melanization and other mechanisms (48). These hemocytes exist in the hemocoel, which is a dynamic environment where the hemolymph constantly circulates them to all regions of the body. But not all hemocytes circulate; one quarter of the hemocytes are attached to tissues and remains sessile (52). A sub-population of these sessile hemocytes concentrates on the outer surface of the heart, and more specifically, in the regions surrounding heart valves called ostia (23, 112). These heart-associated hemocytes – called periostial hemocytes – reside in the locations of the body that experience the highest hemolymph flow and intensely phagocytose bacteria and malaria parasites within seconds of their entry into the hemocoel. As this is happening, additional hemocytes leave circulation and aggregate in the periostial regions of the heart, thereby augmenting the heart-associated immune response (23, 112). Although the structural mechanics of periostial immunity has only been comprehensively described in the African malaria mosquito, *Anopheles gambiae* (23, 33, 34, 112-114), the functional integration between the immune and circulatory systems is conserved across the entire insect lineage (140).

Despite its significance in the insect fight against infection, the genetic mechanisms that drive heart-associated immune responses remain largely unknown. In mosquitoes, pattern recognition receptors in the thioester-containing protein family and adhesion/phagocytosis factors in the Nimrod protein family regulate immune responses

on the heart (123, 127). Here, we used RNA sequencing (RNAseq) on periostial hemocytes and other tissues of *A. gambiae* to uncover immune signaling pathways and other factors that drive heart-associated immune responses. Combined with functional studies, we discovered that the IMD and JNK pathways drive the functional integration between the immune and circulatory systems of mosquitoes.

Results

Infection upregulates immune genes in periostial hemocytes.

To identify the candidate genes that drive periostial hemocyte aggregation, RNAseq was carried out on tissues from mosquitoes that were naïve, injured, or infected with Gram(-) GFP-*Escherichia coli* or Gram(+) *Staphylococcus aureus* (Figure 1). Three tissues were isolated at 4 hours (hr) after treatment: (i) the heart containing periostial hemocytes, (ii) the hemolymph containing circulating hemocytes, and (iii) the entire abdomen. Prior to submitting the samples to sequencing, a subset of mosquitoes was used to confirm that infection induces heart-associated cellular responses at 4 hr after infection. Indeed, a resident population of periostial hemocytes was present in both the naïve and the injured mosquitoes, and the number of periostial hemocytes increased 1.8- and 1.6-fold after GFP-*E. coli* and *S. aureus* infection, respectively (Figure 1*B*).

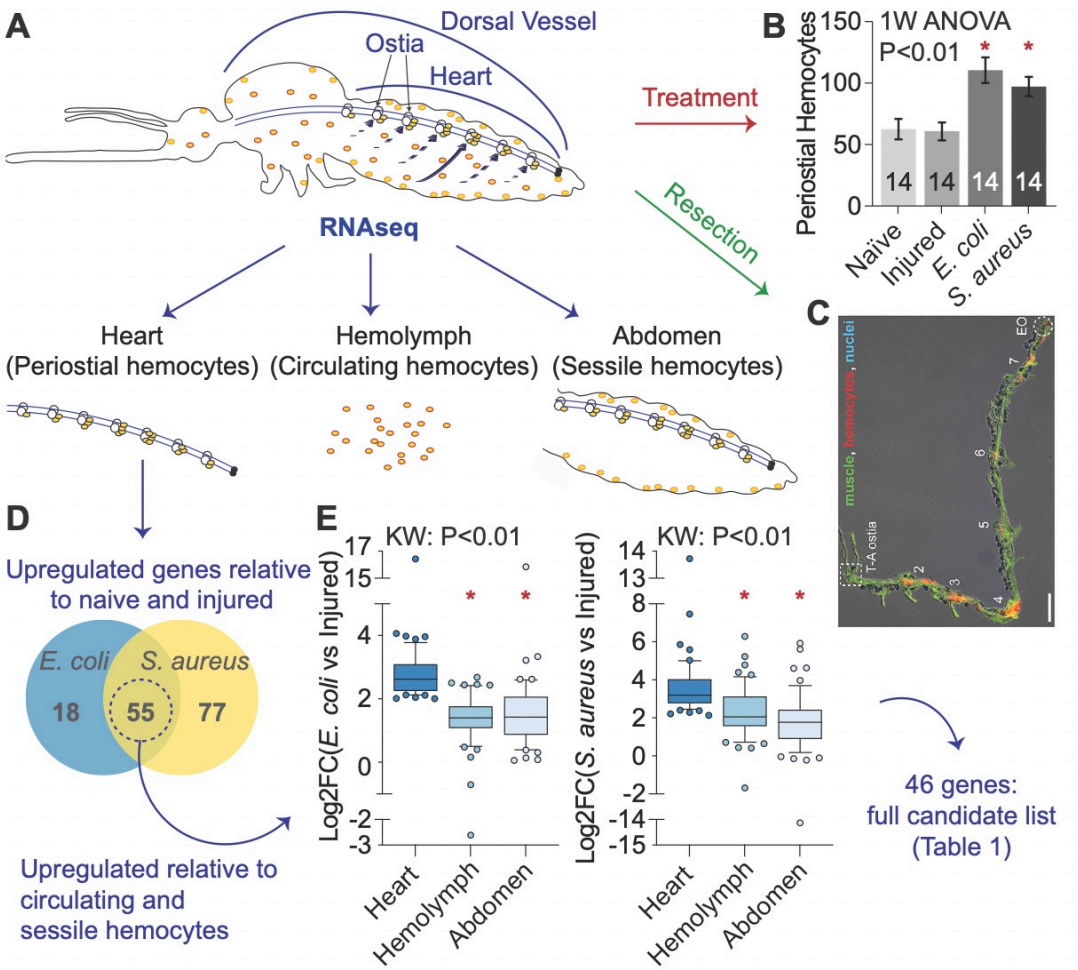

Figure 1 Infection induces the preferential upregulation of immune genes in periostial hemocytes.

(*A*) The heart with periostial hemocytes, the circulating hemocytes and the abdomen of mosquitoes that were naïve, injured, or infected with GFP-*E. coli* or *S. aureus* were sequenced by RNAseq. (*B*) Naïve and injured mosquitoes have a basal number of periostial hemocytes, but infection for 4 hr with GFP-*E. coli* or *S. aureus* – the time of tissue isolation for RNAseq – induces the aggregation of additional hemocytes at the periostial regions. Naïve mosquitoes were used as the reference group. Whiskers show the standard error of the mean (S.E.M.) (*C*) A representative image shows the periostial hemocytes (red) remain attached to a resected heart (green). Image is modified from Sigle and Hillyer (34), and reproduced according to Creative Commons Attribution License CC BY. (*D*) Venn diagram shows that 55 genes were significantly upregulated in the heart with periostial hemocytes during both GFP-*E. coli* and *S. aureus* infections. (*E*) Box plots show that the 55 infection-induced genes in panel *D* were more highly upregulated in the heart with periostial hemocytes than in the circulating hemocytes and abdomens during GFP-*E. coli* (left) or *S. aureus* (right) infections. The box indicates the median and quartiles, and between the whiskers is the 10-90 percentile. The heart tissue was used as the reference group. 1W ANOVA, one-way ANOVA; KW, Kruskal-Wallis test. Asterisks indicate $P < 0.05$.

RNAseq revealed that 73 and 132 genes are upregulated in the heart and periostial hemocytes of mosquitoes infected with GFP-*E. coli* and *S. aureus*, respectively, relative to the heart and periostial hemocytes of naïve and injured mosquitoes (Figure 1*D*). Because periostial hemocyte aggregation is a dynamic immune response that occurs during any bacterial infection, we hypothesized that its core molecular drivers must be preferentially upregulated in periostial hemocytes following both *E. coli* and *S. aureus* infection. We found that 55 genes met this overlap criterion (Appendix I).

To further narrow down this list, we reasoned that the molecular drivers of periostial hemocyte aggregation should be more highly expressed in periostial hemocytes than in circulating hemocytes or any other tissues. Therefore, we carried out parallel RNAseq analyses of (i) circulating hemocytes (hemolymph) and (ii) the entire abdomen. Infection upregulated fewer genes in the circulating hemocytes and the abdomen than in the periostial hemocytes (Appendix C and I-K). We then compared the infection-induced fold change of the 55 genes that were upregulated in the periostial hemocytes to their fold change in the circulating hemocytes and abdomens (Figure 1*E*). During a GFP-*E. coli* infection, these genes had a median $\log_2$ fold change of 2.6 in the periostial hemocytes of infected mosquitoes when compared to the periostial hemocytes of injured mosquitoes, whereas their median $\log_2$ fold change was only 1.4 in both the circulating hemocytes and the abdomens of infected mosquitoes relative to their respective injured counterparts. Similarly, during the *S. aureus* infection, these 55 genes had a median $\log_2$ fold change of 3.2 in the periostial hemocytes of infected mosquitoes when compared to the periostial

hemocytes of injured mosquitoes, whereas this value was 2.1 and 1.8 in the circulating hemocytes and abdomens, respectively.

Because we hypothesized that the gene/pathways that drive periostial hemocyte aggregation are overrepresented in the heart and periostial hemocytes, we removed from the list of 55 genes any gene that was more highly regulated in the circulating hemocytes or abdomens relative to the periostial hemocytes. Among the 46 genes remaining in the list, 27 have an annotated function, and 10 function in immunity (Table 1). Interestingly, 6 of the 10 immune genes are involved in the immune deficiency (IMD) and c-Jun N-terminal kinase (JNK) pathway: *PGRP-LA* (141), *IAP2* (142), *REL2* (79, 80), *CEC3* (79), *DEF1* (82, 143), and *JNK3* (98, 144) (Appendix D). All aspects of the IMD/JNK pathway are represented: upstream components such as *PGRP-LA* and *IAP2*, and downstream elements from both branches of the pathway: the classical IMD cascade represented by *REL2*, *CEC3* and *DEF1*, and the bifurcation into the JNK pathway that is represented by *JNK3* (141, 142, 145-147). In *Drosophila*, the JNK pathway is associated with cell adhesion and phagocytosis by regulating the cytoskeleton (144, 148). The JNK pathway also induces the expression of *Draper* (149) and *TEP1* (98), which affect periostial hemocyte aggregation in mosquitoes (123, 127). Therefore, we hypothesized that the main driver of periostial hemocyte aggregation is the IMD/JNK pathway.

Table 1 Candidate genes that drive periostial hemocyte aggregation.

Gene ID	Gene name	Gene description
AGAP000694	*CEC3*	cecropin anti-microbial peptide
AGAP000786		
AGAP001160		
AGAP001508		
AGAP001563		glycerol kinase
AGAP001610		
AGAP001634		
AGAP001828		
AGAP002064		
AGAP002065		alpha-tocopherol transfer protein
AGAP002323		
AGAP002536		
AGAP002883		
AGAP003488		nucleotide exchange factor SIL1
AGAP004170		
AGAP004181		fibroblast growth factor
AGAP004826		
AGAP005205	*PGRPLA*	peptidoglycan recognition protein (long)
AGAP005839		MFS transporter, FLVCR family
AGAP006426		cyanogenic beta-glucosidase
AGAP006670		gamma-glutamyl hydrolase
AGAP006671		
AGAP006674		chymotrypsin-like protease (Precursor)
AGAP006745		
AGAP006747	*REL2*	NF-kappaB Relish-like transcription factor
AGAP007659		
AGAP008279	*D7L2*	D7 long form salivary protein
AGAP008851		E3 ubiquitin-protein ligase mind-bomb
AGAP009091	*DDC*	dopa decarboxylase
AGAP009099	*TGase3*	transglutaminase
AGAP009100	*TGase1*	protein-glutamine gamma-glutamyltransferase E
AGAP009213	*SRPN16*	serine protease inhibitor (serpin) 16
AGAP009214	*CLIPB11*	CLIP-domain serine protease
AGAP009460	*JNK3*	c-Jun N-terminal kinase
AGAP009985		4-nitrophenylphosphatase
AGAP010197		SPRY domain-containing SOCS box protein 1
AGAP010934		
AGAP011294	*DEF1*	defensin anti-microbial peptide
AGAP011326	*IAP2*	inhibitor of apoptosis 2
AGAP011588		
AGAP011654		membrane dipeptidase
AGAP011764		
AGAP011992		lysosomal acid lipase
AGAP012166		
AGAP013506	*UPD3A*	JAK/STAT pathway cytokine unpaired 3 variant A
AGAP028615	*NAT5*	nutrient amino acid transporter 5

Underline indicates genes with immune functions.

The IMD pathway positively regulates periostial hemocyte aggregation.

To determine whether the IMD pathway drives periostial hemocyte aggregation, we first used qPCR to confirm the expression of its transcription factor, *rel2*, and its negative regulator, *caspar*, in the mosquito whole-body. Injury alone did not change the mRNA abundance of *rel2*, but GFP-*E. coli* infection for 4 and 24 hr increased *rel2* mRNA abundance by 3.4- and 2.4-fold, respectively (Figure 2*A*). For *caspar*, injury and infection increased the mRNA abundance at 4 hr post treatment by 1.7- and 2.1-fold, respectively, but this effect was gone by 24 hr. As expected, the mRNA abundance of the housekeeping gene, *Rps17*, was unaltered by treatment. Next, we synthesized double-stranded RNA (dsRNA) to target *rel2* and *caspar*, and achieved RNAi-based silencing of 43% and 37%, respectively, compared to the control ds*bla(Ap^R)*-injected mosquitoes (Appendix E).

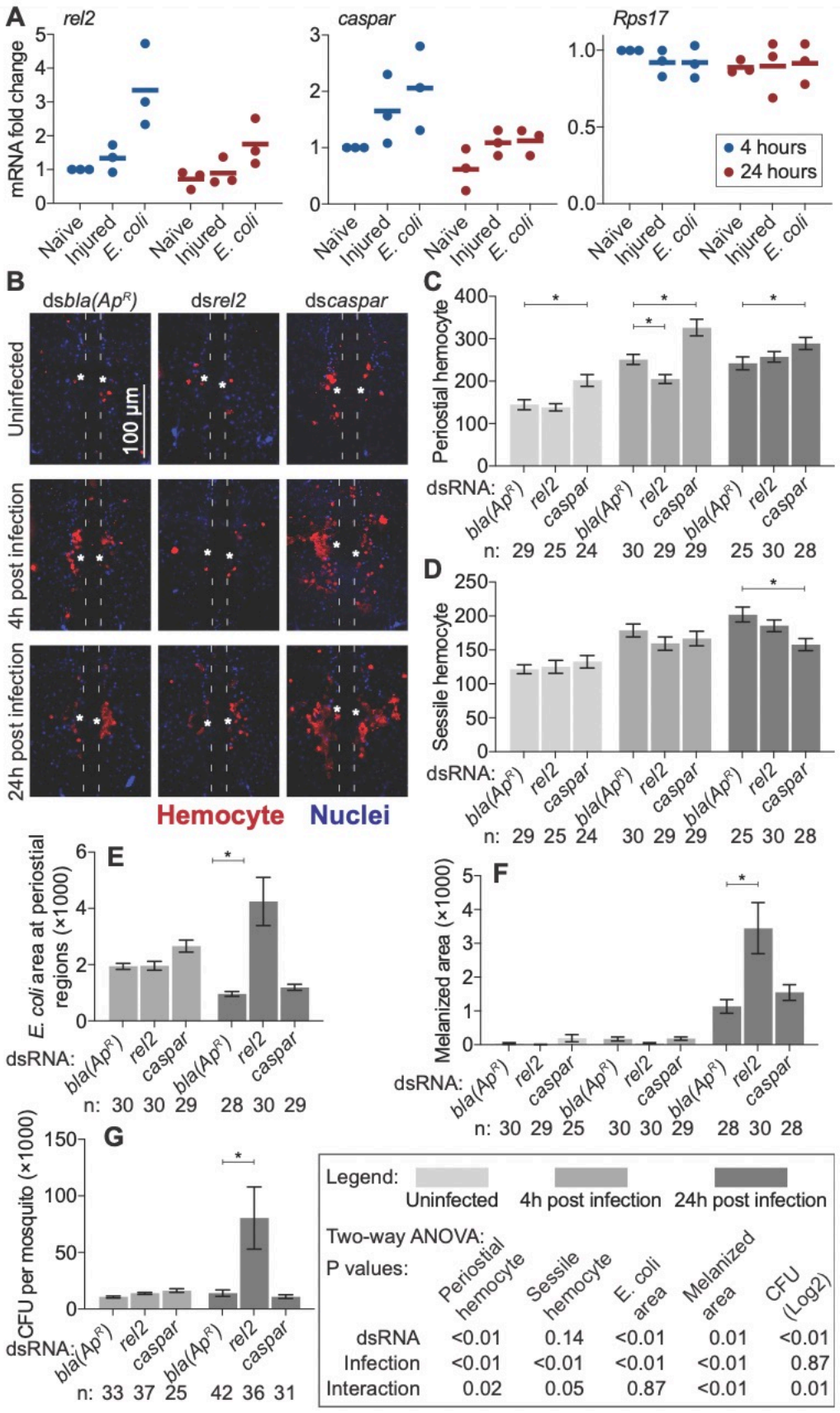
A
rel2
caspar
Rps17
mRNA fold change
Naïve
Injured
E. coli
4 hours
24 hours
B
dsbla(Ap^R)
dsrel2
dscaspar
Uninfected
4h post infection
24h post infection
100 µm
Hemocyte
Nuclei
C
Periostial hemocyte
dsRNA:
n: 29 25 24 30 29 29 25 30 28
D
Sessile hemocyte
E
E. coli area at periostial regions (×1000)
n: 30 30 29 28 30 29
F
Melanized area (×1000)
n: 30 29 25 30 30 29 28 30 28
G
CFU per mosquito (×1000)
n: 33 37 25 42 36 31
Legend:
Uninfected
4h post infection
24h post infection
Two-way ANOVA:
P values:
Periostial hemocyte
Sessile hemocyte
E. coli area
Melanized area
CFU (Log2)
dsRNA <0.01 0.14 <0.01 0.01 <0.01
Infection <0.01 <0.01 <0.01 <0.01 0.87
Interaction 0.02 0.05 0.87 <0.01 0.01

Figure 2 The IMD pathway drives periostial hemocyte aggregation.
(*A*) mRNA abundance of *rel2*, *caspar* and *Rps17* (control) in the whole-body of naïve, injured and *E. coli*-infected mosquitoes at 4 and 24 hr after treatment. Horizontal line, median; Circles, individual biological trials. (*B*) Fluorescence images show the periostial hemocytes (CM-DiI; red) surrounding a single pair of ostia (asterisks) on a segment of the heart (outlined by dotted lines) of ds*bla(Ap^R)*-, ds*rel2*- and ds*caspar*-injected mosquitoes that were not infected or had been infected with GFP-*E. coli* for 4 or 24 hr. (*C*-*G*) Graphs showing for ds*bla(Ap^R)*-, ds*rel2*- and ds*caspar*-injected mosquitoes that were not infected or had been infected with GFP-*E. coli* for 4 or 24 hr: (*C*) average number of periostial hemocytes; (*D*) average number of sessile hemocytes outside of periostial regions; (*E*) pixel area of GFP-*E. coli* in the periostial regions; (*F*) pixel area of melanin in the periostial regions; and (*G*) the systemic GFP-*E. coli* infection intensity. The data were analyzed by two-way ANOVA, followed by Dunnett's multiple comparison test. The ds*bla(Ap^R)*-injected mosquitoes were used as the reference group. Whiskers show S.E.M. and the asterisks indicates $P < 0.05$.

To assess whether the IMD pathway drives heart-associated immune responses, we compared the number and activity of periostial hemocytes in *rel2* and *caspar* RNAi mosquitoes, relative to ds*bla(Ap^R)* control mosquitoes (Figure 2 *B*-*F*). Analysis of the ds*bla(Ap^R)*-injected mosquitoes revealed that, as expected, infection for 4 hr induces the aggregation of hemocytes at the periostial regions, and this aggregation remains in place at 24 hr. In uninfected mosquitoes, knocking down *rel2* did not change the number of periostial hemocytes (Figure 2 *B* and *C*). However, at 4 hr following infection, knockdown of *rel2* decreased the number of periostial hemocytes by 18%, relative to ds*bla(Ap^R)* mosquitoes. At 24 hr post-infection, the effect of *rel2* RNAi on periostial hemocyte aggregation was diminished. When we instead knocked down *caspar*, the number of periostial hemocytes increased by 39% in uninfected mosquitoes, and infection for 4 and 24 hr increased in the number of periostial hemocytes by 30% and 19%, respectively, relative to the infected control mosquitoes. This shows that *rel2* positively regulates periostial hemocyte aggregation whereas *caspar* is a negative regulator of this process.

To determine whether the IMD pathway specifically affects periostial hemocytes and not sessile hemocytes in general, we counted the number of non-periostial sessile hemocytes in the dorsal tergum of abdominal segments 4 and 5 in the same mosquitoes that were examined for periostial hemocytes (Figure 2*D*). Knockdown of *rel2* or *caspar* did not alter the number of non-periostial sessile hemocytes in uninfected mosquitoes or mosquitoes that were infected for 4 hr. However, at 24 hr following infection, knockdown of *caspar* caused a 22% decrease in the number of non-periostial sessile hemocytes. Taken altogether, these results suggest that the IMD pathway regulates periostial hemocyte aggregation while having a minimal effect on the rest of the sessile hemocytes.

Periostial hemocytes phagocytose and destroy pathogens that circulate with the hemolymph. To determine whether the IMD pathway affects the phagocytic activity of periostial hemocytes, we measured the GFP-*E. coli* pixel area in the periostial regions (Figure 2*E* and Appendix F). At 4 hr following infection, the GFP-*E. coli* area was similar regardless of dsRNA treatment. At 24 hr after infection, this area decreased in ds*bla(Ap^R)*- and ds*caspar*-injected mosquitoes, indicating that periostial hemocytes efficiently destroyed the pathogens. However, the opposite occurred in *rel2* RNAi mosquitoes: at 24 hr following infection, GFP-*E. coli* at the periostial regions significantly increased.

Periostial hemocytes also phagocytose melanized bacteria. Therefore, we measured melanin accumulation in the periostial regions (Figure 2*F* and Appendix F). Melanin was absent in uninfected mosquitoes and mosquitoes that were infected for 4 hr. However, at 24 hr following infection, *rel2* RNAi increased melanin deposits at the periostial regions, whereas *caspar* RNAi had no effect.

The increased accumulation of GFP-*E. coli* and melanin in *rel2* RNAi mosquitoes could be due to either (i) enhanced phagocytosis by periostial hemocytes, or (ii) higher bacterial proliferation in the hemocoel, which places increased pressure on the phagocytosis response. To differentiate between these two scenarios, we measured the systemic GFP-*E. coli* infection intensity and observed that, at 4 hr after infection, the bacterial intensity was similar for all dsRNA treatments, but at 24 hr, knockdown of *rel2* resulted in a higher infection intensity than treatment with ds*caspar* or ds*bla(Ap^R)* (Figure 2*G*). This suggests that *rel2* is essential for proper bacterial killing in the hemocoel, and therefore, knocking it down increases infection intensity and causes increased phagocytosis in the periostial regions. However, because silencing *rel2* and *caspar* has opposite effects on periostial hemocyte aggregation but silencing *caspar* does not impact infection intensity, we conclude that the IMD pathway is a positive regulator of periostial hemocyte aggregation.

PRGP-LA is one of the upstream activators of the IMD pathway (141), and was upregulated in the heart and periostial hemocytes (Table 1). Therefore, we tested its involvement in periostial hemocyte aggregation. *PGRP-LA* has three splice forms. To knock it down, we designed ds*PGRP-LA-RARB* to target the *RA* and *RB* splice forms and ds*PGRP-LA-RC* to target the *RC* splice form (Appendix E). *PGRP-LA* knockdown with either dsRNA did not alter the number of periostial hemocytes, the number of non-periostial sessile hemocytes, or melanin accumulation at periostial regions (Appendix G). However, knockdown of *RC* led to increased phagocytosis of GFP-*E. coli* in the periostial regions. This suggests that PGRP-LA does not play a major role in periostial hemocyte aggregation but may be involved in the phagocytosis response by periostial hemocytes.

The JNK pathway positively regulates phagocytosis by periostial hemocytes and hemocyte adhesion.

We next tested whether the JNK pathway regulates periostial hemocyte aggregation. The mosquito genome encodes two JNK genes: *JNK1* and *JNK3* (150). We measured the expression of *JNK1*, *JNK3* and the negative regulator of the JNK pathway, *puckered* (*puc*), in the same cDNAs used to measure mRNA abundance of IMD components in the whole body. The mRNA abundance of *JNK1* remained unchanged regardless of treatment and time (Figure 3*A*). Injury and infection for 4 hr increased the mRNA abundance of *JNK3* by 2.0- and 3.3-fold, respectively, but this upregulation disappeared by 24 hr of infection. The expression of *puc* increased 1.6-fold at 4 hr following infection, but was unaffected in injured mosquitoes or mosquitoes infected for 24 hr. Because of the high sequence identity between *JNK1* and *JNK3*, we synthesized ds*JNK1/3* to simultaneously target both positive regulators of the pathway, and ds*puc* to target the negative regulator of the pathway. RNAi-based knockdown resulted in 33%, 44% and 31% reduction in mRNA abundance of *JNK1*, *JNK3* and *puc*, respectively (Appendix E).

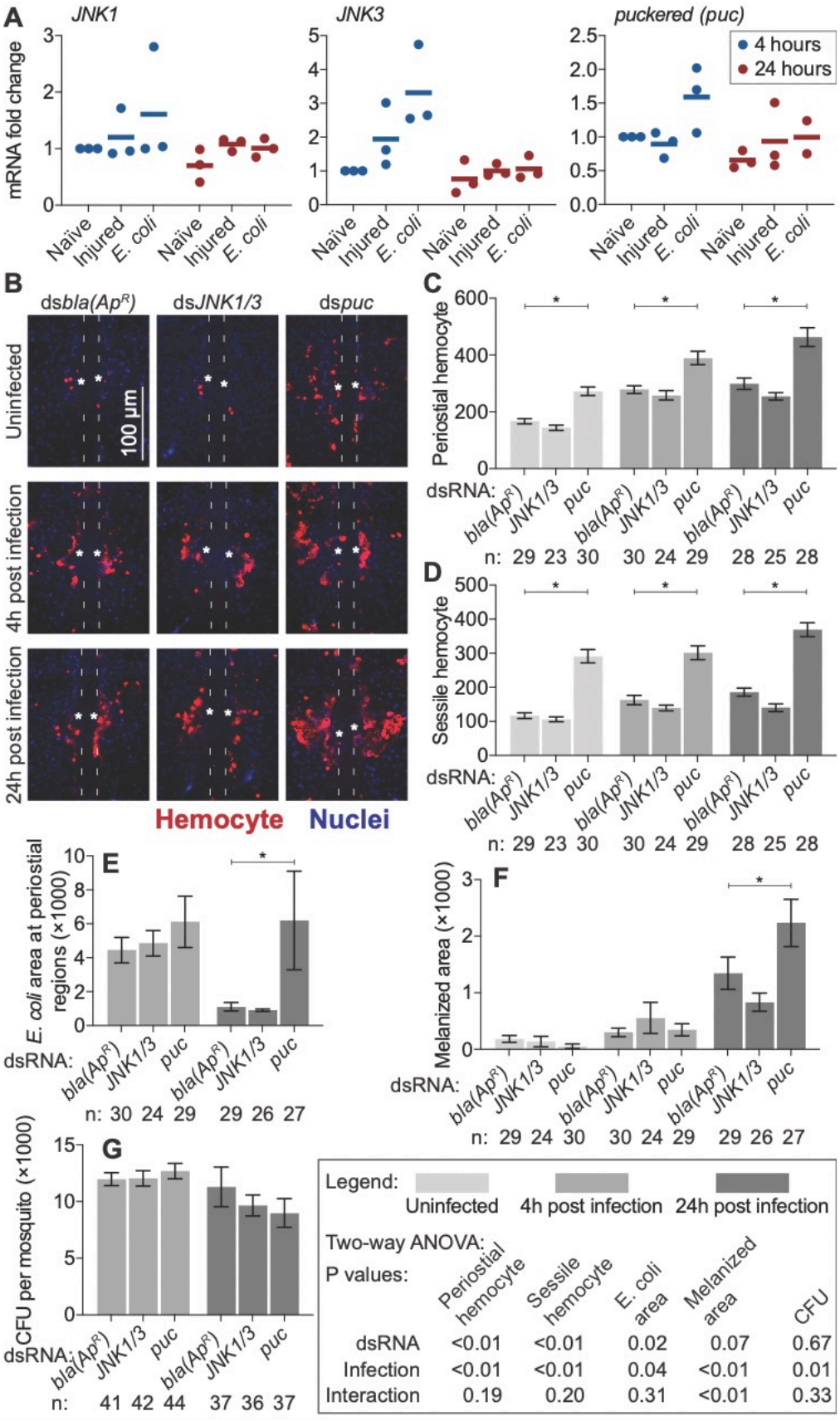
A
JNK1
JNK3
puckered (puc)
mRNA fold change
4 hours
24 hours
Naïve
Injured
E. coli
B
dsbla(ApR)
dsJNK1/3
dspuc
Uninfected
4h post infection
24h post infection
100 µm
Hemocyte
Nuclei
C
Periostial hemocyte
D
Sessile hemocyte
dsRNA:
n: 29 23 30 30 24 29 28 25 28
E
E. coli area at periostial regions (×1000)
n: 30 24 29 29 26 27
F
Melanized area (×1000)
n: 29 24 30 30 24 29 29 26 27
G
CFU per mosquito (×1000)
n: 41 42 44 37 36 37
Legend:
Uninfected
4h post infection
24h post infection
Two-way ANOVA:
P values:
Periostial hemocyte
Sessile hemocyte
E. coli area
Melanized area
CFU
dsRNA <0.01 <0.01 0.02 0.07 0.67
Infection <0.01 <0.01 0.04 <0.01 0.01
Interaction 0.19 0.20 0.31 <0.01 0.33

Figure 3 The JNK pathway drives periostial hemocyte aggregation.
(*A*) mRNA abundance of *JNK1*, *JNK3* and *puc* in the whole-body of naïve, injured and *E. coli*-infected mosquitoes at 4 and 24 hr after treatment. Horizontal line, median; Circles, individual biological trials. (*B*) Fluorescence images show the periostial hemocytes (CM-DiI; red) surrounding a single pair of ostia (asterisks) on a segment of the heart (outlined by dotted lines) of ds*bla(Ap^R)*-, ds*JNK1/3*- and ds*puc*-injected mosquitoes that were not infected or had been infected with GFP-*E. coli* for 4 or 24 hr. (*C*-*G*) Graphs showing for ds*bla(Ap^R)*-, ds*JNK1/3*- and ds*puc*-injected mosquitoes that were not infected or had been infected with GFP-*E. coli* for 4 or 24 hr: (*C*) average number of periostial hemocytes; (*D*) average number of sessile hemocytes outside of periostial regions; (*E*) pixel area of GFP-*E. coli* in the periostial regions; (*F*) pixel area of melanin in the periostial regions; and (*G*) the systemic GFP-*E. coli* infection intensity. The data were analyzed by two-way ANOVA, followed by Dunnett's multiple comparison test. The ds*bla(Ap^R)*-injected mosquitoes were used as the reference group. Whiskers show S.E.M. and the asterisks indicates $P < 0.05$.

To assess whether the JNK pathway drives heart-associated immune responses, we compared the number and activity of periostial hemocytes in *JNK1/3* and *puc* RNAi mosquitoes, relative to ds*bla(Ap^R)* control mosquitoes (Figure 3 *B*-*F*). Regardless of infection status, the number of periostial hemocytes was statistically similar between ds*JNK1/3*- and ds*bla(Ap^R)*-injected mosquitoes, although ds*JNK1/3* mosquitoes averaged fewer periostial hemocytes than control mosquitoes for all treatments (Figure 3 *B* and *C*). Knockdown of *puc*, however, increased the number of periostial hemocytes 1.6-fold in uninfected mosquitoes, and 1.4- and 1.5-fold at 4 and 24 hr following GFP-*E. coli* infection, respectively. To further determine whether *puc* specifically affects periostial hemocytes or sessile hemocytes in general, we quantified the number of non-periostial sessile hemocytes on the dorsal tergum of segments 4 and 5 in the same mosquitoes (Figure 3*D*). ds*JNK1/3* RNAi mosquitoes showed a trend of fewer non-periostial sessile hemocytes than control mosquitoes regardless of infection status. Treatment with ds*puc*, however, increased the number of non-periostial sessile hemocytes for all treatments.

This suggests that *puc* negatively regulates both periostial and non-periostial sessile hemocyte abundance.

To determine whether the JNK pathway affects the phagocytic activity of periostial hemocytes, we measured the GFP-*E. coli* pixel area in the periostial regions (Figure 3*E* and Appendix H). At 4 hr following infection, the GFP-*E. coli* pixel area was similar regardless of dsRNA treatment. However, at 24 hr following infection, periostial hemocytes in ds*puc* RNAi mosquitoes sequestered more GFP-*E. coli* than the ds*bla(Ap^R)* mosquitoes. We then quantified the melanized bacteria that were sequestered by periostial hemocytes (Figure 3*F* and Appendix H). Melanin deposits were undetectable in uninfected mosquitoes and mosquitoes at 4 hr post infection; however, at 24 hr following GFP-*E. coli* infection, more melanin was present in ds*puc* RNAi mosquitoes relative to the controls. The difference in GFP-*E. coli* and melanin accumulation in ds*puc* RNAi mosquitoes can be due to (i) enhanced phagocytosis by periostial hemocytes, or (ii) higher bacterial proliferation in the hemocoel. To differentiate between these two scenarios, we quantified the systemic *E. coli* infection intensity and found that the bacterial intensity was similar regardless of dsRNA treatment (Figure 3*G*). Therefore, this suggests *puc* negatively regulates hemocyte adhesion and phagocytic activity, and indicates that the JNK pathway is a positive regulator of periostial immune responses.

Discussion

Microarray and RNAseq have revealed immune genes and signaling pathways that are active in hemocytes (60, 151-156), including those that are activated in specific

subpopulations of hemocytes (58, 59, 157). However, these studies only focused on the circulating hemocytes, and therefore, failed to capture the biology of sessile hemocytes. Yet, one quarter of hemocytes are sessile, and they play significant roles in hematopoiesis (53, 158), wound healing (55), and pathogen killing (113, 117, 125, 159). Therefore, extrapolating the molecular signatures of circulating hemocytes to those of sessile hemocytes likely miss the essential factors that make sessile hemocytes conduct their specific immune activities. Periostial hemocytes, in particular, reside on the heart and perform an intense pathogen killing response. To better understand how an infection drives the migration of hemocytes to the heart and how they kill pathogens at the periostial regions, we sequenced the periostial hemocyte transcriptome and discovered that the IMD and JNK pathway drives periostial immune responses.

The IMD pathway is commonly known for controlling the production of antimicrobial peptides. Here, we show that the IMD pathway also regulates a cellular immune response, namely the transition of hemocytes from a circulating to a sessile state on the heart. Specifically, knockdown of the positive regulator of the IMD pathway, *rel2*, decreases infection-induced periostial hemocyte aggregation, whereas knockdown of the negative regulator of the IMD pathway, *caspar*, increases the number of periostial hemocytes. We hypothesize that the IMD pathway drives periostial hemocyte aggregation via two cascades that are related to phagocytosis: the *TEP1-TEP3-LRP1-CED6L* pathway and the *TEP4-BINT2-CED2L-CED5L* pathway (107). This is because the IMD pathway induces the expression of *TEP1* and *TEP4* (15, 82, 143), and both positively regulate periostial hemocyte aggregation (127). Moreover, two downstream molecules – LRP1 and BINT2 – are transmembrane proteins that have overlapping functions in phagocytosis

and adhesion (135, 136, 160), which likely facilitate the adhesion of hemocytes to the heart. In this study, we also confirmed the positive role of rel2 in pathogen killing, especially at the later stages of infection (14, 15, 79, 84, 87, 161-165). When we systemically knocked down the expression of *rel2*, bacteria proliferated uncontrollably during the later stages of infection. For that reason, *rel2* RNAi mosquitoes had fewer periostial hemocytes early in infection, but after knocking down the pathway increased infection intensity later on, the number of periostial hemocytes increased, as did *E. coli* and melanin deposits on the heart. Overall, this suggests that the IMD pathway drives periostial hemocyte aggregation during the early stages of infection and limits systemic bacterial infection during the later stages of infection.

The JNK pathway modulates mosquito longevity, regulates oviposition and limits malaria parasites and viruses (97-101, 166). Here, we found that overexpressing the JNK pathway by knocking down the negative regulator, *puc*, increases the number of periostial and the adjacent sessile hemocytes. This suggests that the JNK pathway positively regulates hemocyte adhesion. Indeed, the *Drosophila* ortholog of mosquito *JNK1* and *JNK3*, called *basket*, is involved in the formation of actin- and focal adhesion kinase-rich placodes in hemocytes (167). The JNK pathway also induces hemocyte differentiation in *Drosophila*, producing large lamellocytes that adhere and encapsulate parasitic eggs (168). We found that overexpressing the JNK pathway does not alter the infection intensity, but increases the accumulation of *E. coli* and melanin deposits on the heart, suggesting that the JNK pathway positively regulates the phagocytosis and melanization response. Indeed, JNK1 in mosquitoes that are refractory to malaria positively regulates the melanization response (97), and overexpressing the JNK pathway in aphids increases

phenoloxidase activity and the hemocyte phagocytic index (169). We hypothesize that the JNK pathway regulates phagocytosis by periostial hemocytes in a manner that involves TEP1 and draper. This is because the JNK pathway induces the expression of both (98, 99, 170), and TEP1 opsonizes pathogens for phagocytoses whereas draper participates in the degradation of phagocytosed bacteria (107, 123, 127, 129, 171, 172). In our study, we could not distinguish between the roles that *JNK1* and *JNK3* play in periostial hemocyte aggregation; however, knockdown of both resulted in phenotypes that were opposite of *puc* knockdown, strongly suggesting that JNK1 or JNK3 – or both – positively regulate(s) periostial hemocyte aggregation. Therefore, these data show that the JNK pathway positively regulates the periostial hemocyte aggregation response, presumably via adhesion and phagocytosis.

Because both the IMD and JNK pathways induce the production of *TEP1*, we hypothesize that they share the *TEP1-TEP3-LRP1-CED6L* phagocytosis cascade that leads to hemocyte aggregation. However, we also hypothesize that the IMD and JNK pathways use additional, independent mechanisms to regulate periostial hemocyte aggregation for the following reasons. First, even though the two pathways share upstream signaling molecules, they bifurcate and activate their own set of effector genes, suggesting they perform different functions (146, 147). Second, knocking down the components of the IMD and JNK pathways resulted in different phenotypes, especially for periostial and non-periostial sessile hemocytes. Third, in *Drosophila*, co-silencing of draper and Integrin $\beta\nu$ suggests that they function in parallel pathways (173), and in mosquitoes, draper is regulated by the JNK pathway, whereas the homolog of Integrin $\beta\nu$,

BINT2, is involved in IMD-induced, TEP4-mediated phagocytosis cascade (107, 135, 143, 170).

Bacteria, malaria parasites, and fungal infections all induce periostial hemocyte aggregation, and this process is structurally conserved across the entire insect lineage (23, 112, 140). Therefore, we expect that a conserved pathway or pathways induce this process (96, 174). Indeed, infection induces the production of *Upd3* by periostial hemocytes (Table 1), and *Upd3* functions as a ligand for the receptor of the JAK/STAT pathway (119, 144, 175, 176). The TOLL pathway also induces hemocyte proliferation (177, 178) and the expression of *TEP1* (87), which positively regulate periostial hemocytes aggregation (127). Beyond immune pathways, periostial hemocyte aggregation may also be under the influence of neuronal and hormonal control. Injecting mosquitoes with the neuropeptide, Allatotropin, increases the number of hemocytes on the mosquito heart (133), whereas depletion of the juvenile hormone binding protein reduces the number of hemocytes and their phagocytic capacity (179).

To date, we have tested the involvement of several hemocyte-producing factors on periostial hemocyte aggregation. However, the heart itself may also produce factors that drive this immune response. For example, a fibroblast growth factor is highly regulated in the heart and periostial hemocytes in mosquitoes (Table 1). In *Drosophila*, its ortholog, *Branchless*, is expressed in heart and pericardial cells and regulates hemocyte differentiation in the lymph glands of the larval heart (180, 181). Moreover, reducing the expression of the *Drosophila* cardiac extracellular matrix (ECM) protein, *Pericardin*, disrupts the formation of the cardiac ECM and lowers the number of hemocytes on the heart (116). These data suggest that the heart and its associated

structures (e.g. cardiac ECM) facilitate the binding of circulating hemocytes to the periostial regions. Other factors – like transglutaminases – are expressed in both the heart and hemocytes and may play a role in periostial hemocyte aggregation (182, 183).

Heart-associated immune responses have been observed in insects from 14 different taxonomic orders, including important agricultural, urban, and medical insect pests (140). Therefore, understanding the genetic factors that drive periostial hemocyte aggregation in *A. gambiae* will shed light on how this medically important insect and other insects of societal importance fight the pathogens that they carry. Indeed, TEP proteins, Nimrod proteins and the JNK pathway are conserved amongst insects (150, 184-186), and although some insects in the order of Hemiptera lack components of the IMD pathway, all insects queried to date still have a functional IMD immune response (187-190). Therefore, we conclude that the IMD and JNK pathways, together with TEP and Nimrod proteins, are the primary drivers of the heart-associated immune responses in insects.

Materials and Methods

Mosquitoes, bacteria, and infection

Anopheles gambiae, Giles sensu stricto (G3; Diptera: Culicidae), were maintained at 27 °C, 75% relative humidity, and a 12h:12h light:dark photoperiod (30). Experiments were done using female adults fed 10% sucrose. Tetracycline resistant, GFP-expressing *E. coli* (modified DH5α; GFP-*E. coli*) and *S. aureus* (RN6390) were grown in Luria-Bertani (LB) and tryptic soy (TSB) broth, respectively, at 37 °C in a shaking incubator. The bacterial cultures were diluted and injected into the thoracic anepisternal cleft using a

Nanoject III (Drummond Scientific Company, Broomall, PA, USA). The infection dose was determined by plating the cultures and counting the colony forming units (CFUs).

RNAseq: treatment, tissue collection, RNA isolation and library preparation

Six-day-old mosquitoes were divided into four groups: (i) naïve (unmanipulated), (ii) injured by injecting 69 nL of sterile LB, (iii) infected by injecting 69 nL of GFP-*E. coli* (~75,779 CFUs), and (iv) infected by injecting 69 nL of *S. aureus* (~39,451 CFUs). Four hours after treatment, three tissues were isolated: (i) the heart with periostial hemocytes, (ii) hemolymph with circulating hemocytes, and (iii) the entire abdomen. To isolate the heart, mosquitoes were bisected along the coronal plane in RNase-free PBS, and the heart with the periostial hemocytes was resected by severing the alary muscles and detaching it from the cuticle (34). To isolate circulating hemocytes, hemolymph was perfused by making an incision in the last abdominal segment, injecting RNase-free PBS into the hemocoel through the cervical membrane, and collecting the first 2 drops that exited the abdomen (57). The abdomens were isolated by bisecting mosquitoes on the transverse plane along the thoraco-abdominal junction.

To isolate RNA from hearts or abdomens, samples were homogenized in TRIzol Reagent (Invitrogen, Carlsbad, CA, USA), extracted following the TRIzol protocol, and resuspended in Buffer RLT (Qiagen, Hilden, Germany) with 2% 2-Mercaptoethanol (Fisher Scientific, Pittsburgh, PA, USA). The RNA was further purified using the RNeasy Micro Kit (Qiagen), DNase treated, and eluted in RNase-free water. To isolate RNA from circulating hemocytes, perfused hemolymph was collected in Buffer RLT (Qiagen) and 2% 2-Mercaptoethanol (Fisher Scientific), and RNA was isolated using the RNeasy Micro Kit.

Three biological replicates were done; each heart sample contained 72 hearts, the hemolymph sample contained perfusate from 108 mosquitoes, and each abdomen sample contained 36 abdomens.

The integrity and quantity of RNA was assessed on a 2100 Bioanalyzer (Agilent Technologies, Santa Clara, CA) using an RNA 6000 Series II Nano kit for abdomen samples and a Pico kit for the heart and hemolymph samples. The library for sequencing was prepared using 1 μg of RNA and the NEBNext Ultra kit (New England BioLabs, Ipswich, MA), according to the protocol for low-input samples. Library quality and concentration were assessed using a DNA 1000 Series II kit on the 2100 Bioanalyzer.

Illumina sequencing and differential gene expression analysis

All 36 samples – 4 treatments, 3 tissue types and 3 replicates – were sequenced across 3 lanes on an Illumina HiSeq 3000 (paired-end, 75 base pair read) at Vanderbilt University's Vantage facility. Reads were mapped to the *A. gambiae* genome (AgamP4.7) by STAR (191, 192). The number of uniquely mapped reads per sample averaged 23,698,077 (range: 18,487,153 – 31,487,002), which represented 94.03% of the total reads in a sample. Differential expression was calculated based on reads per kilobase per million by DESeq2 (193). Genes were considered significantly regulated at $\log_2$ fold change ≥ 2 or $\log_2$ fold change ≤ -2 and the adjusted P value < 0.05.

Gene expression by Real-time quantitative PCR (qPCR)

Six-day-old mosquitoes were separated into three groups: (i) naïve, (ii) injured, and (iii) infected with GFP-*E. coli* (~12,282 CFUs). RNA was isolated using TRIzol from 10

whole bodies at 4 and 24 hours after treatment, and repurified using the RNeasy Mini Kit (Qiagen). RNA was treated with RQ1 RNase-free DNase (Promega, Madison, WI, USA), and used for cDNA synthesis using Oligo$(dT)_{20}$ primers and the SuperScript III First-Strand Synthesis System for RT-PCR (Invitrogen).

qPCR was conducted using cDNA as template, gene-specific primers (Appendix L), and Power SYBR Green PCR Master Mix (Applied Biosystems, Foster City, CA) on an ABI 7300 Real-Time PCR System. Relative quantification was conducted using the $2^{-\Delta\Delta C_T}$ method, with *RPS7* as the reference and *RPS17* as a control (114). Three independent trials were conducted, each with 2-3 technical replicates. For each trial, mRNA abundance was calculated relative to the naïve group at 4 hr. The absence of genomic DNA in the cDNA preparations was confirmed by melting curve analysis and amplicon size.

Double-stranded RNA (dsRNA) synthesis

Double-stranded RNA was synthesized for *rel2*, *caspar*, *PGRP-LA*, *JNK1* and *JNK3*, and *puc*. *PGRP-LA* has three splice variants; ds*PGRP-LA-RARB* targets the *RA* and *RB* splice forms and ds*PGRP-LA-RC* targets the *RC* splice form. Because of high sequence identity, the *JNK1/3* dsRNA targets both *JNK1* and *JNK3*. *A. gambiae* cDNA was amplified by PCR using gene-specific primers with T7 promoter tags (Appendix L). Amplicons were separated by gel electrophoresis and purified using Qiagen's QIAquick Gel Extraction kit. Each amplicon was re-amplified in a second PCR reaction using the same primers, purified using Qiagen's QIAquick PCR Purification Kit, and used as template for dsRNA synthesis using the MEGAscript T7 Kit (Applied Biosystems). The

dsRNA was ethanol precipitated and re-suspended in PBS. dsRNA concentration was quantified spectrophotometrically and the integrity was verified by gel electrophoresis. As a negative control, dsRNA was synthesized for the non-mosquito gene, *bla(Ap^R)*, using DNA from *E. coli* BL21(DE3) containing the pET-46 plasmid as template (EMD Chemicals, Gibbstown, NJ, USA) (123, 127).

RNA interference (RNAi)

Two or three-day-old mosquitoes were intrathoracically injected 300 ng of dsRNA. Four days later, mosquitoes were divided into two groups: (i) uninfected and (ii) infected with GFP-*E. coli* (~16,528 CFUs). Injured mosquitoes were not assayed because injury does not induce periostial hemocyte aggregation (23, 52, 112). RNAi efficiency was determined by extracting RNA, synthesizing cDNA, and conducting qPCR. Three independent trials were conducted per gene, except for *PGRP-LA*, for which only two trials were done.

Fluorescence labeling and mosquito dissection

Hemocytes were labeled with the Vybrant CM-DiI Cell-Labeling Solution (Invitrogen) as we described (23). Live mosquitoes were injected ~0.4 μl of 67 μM CM-DiI and 1.08 mM Hoechst 33342 (nuclear stain; Invitrogen) in PBS, incubated at 37 °C for 20 min, and injected 16% paraformaldehyde. Ten min later, abdomens were bisected along a coronal plane, and the dorsal portions containing the heart and periostial hemocytes were mounted on glass slides using Aqua-Poly/Mount (Polysciences; Warrington, PA, USA).

Microscopy and image acquisition

Specimens were imaged under bright-field and fluorescence illumination on a Nikon Eclipse Ni-E compound microscope connected to a Nikon Digital Sight DS-Qi1 camera and Advanced Research NIS Elements (Nikon, Tokyo, Japan). Z-stacks for bright field, red fluorescence (hemocytes), green fluorescence (GFP-*E. coli*) and blue fluorescence (nuclei) were acquired using a linear encoded Z-motor. For image presentation and pixel intensity measurement, specific channels were selected and all images within a stack were combined into a two-dimensional image using the Extended Depth of Focus (EDF) function in NIS Elements.

Quantification of hemocytes

Hemocytes, labeled with both CM-DiI and Hoechst 33342, were counted manually by examining all images within a Z-stack (127). A cell was counted as a periostial hemocyte if adjacent to an ostium, and as a non-periostial, sessile hemocyte if attached to the abdominal wall outside of a periostial region (23, 52). Periostial hemocytes were counted within abdominal segments 2-7 whereas non-periostial, sessile hemocytes were counted on the tergum of segments 4 and 5. Hemocytes were not counted on the aorta, the thoraco-abdominal ostia or the excurrent openings because few hemocytes are there, and infection does not induce aggregation at those locations (33, 34). Data were analyzed by two-way ANOVA, followed by Dunnett's multiple comparison test, with ds*bla(Ap^R)*-injected mosquitoes as the reference.

Quantification of GFP-*E. coli* and melanin deposits at the periostial regions

GFP-*E. coli* at the periostial regions was calculated in NIS Elements by delineating in EDF images each periostial region using the region of interest (ROI) tool and measuring the area of pixels with intensities above a threshold that distinguished GFP-*E. coli* from background fluorescence (127). Dark, melanin deposits were quantified in NIS Elements by delineating in EDF images each periostial region using the ROI tool and measuring the area of pixels with intensities below a threshold that distinguished melanized areas (dark) from non-melanized areas (127). For GFP-*E. coli* or melanin, data from all ROIs within an image were combined and analyzed by two-way ANOVA, followed by Dunnett's multiple comparison test, with ds*bla(Ap^R)*-injected mosquitoes as the reference.

Quantification of bacterial infection intensity

Mosquitoes infected with GFP-*E. coli* for 4 or 24 hr were homogenized individually in PBS, a dilution was spread on LB agar containing tetracycline, and plates were incubated overnight at 37 °C. The resulting CFUs were counted and used to calculate infection intensity. Data were analyzed by two-way ANOVA, followed by Dunnett's multiple comparison test, with ds*bla(Ap^R)*-injected mosquitoes as the reference group. For *rel2* and *caspar* RNAi mosquitoes, data were first $\log_2$ transformed to achieve normality, and then analyzed by two-way ANOVA.

CHAPTER IV

Transglutaminase 3 negatively regulates immune responses on the heart of the mosquito, *Anopheles gambiae*

Preface

This chapter utilized the list of candidate genes from chapter III and tested whether transglutaminases (TGase) are involved in periostial hemocyte aggregation. RNAi-based knockdown showed that TGase3 – but not TGase1 and TGase2 – negatively regulates this heart-associated immune response. This work gave me the opportunity to mentor a very talented undergraduate, Ms. Abinaya Ramakrishnan. I led the project and we conducted the experiments together; I did the organismal manipulation, while Ms. Ramakrishnan collected the quantitative data. Ms. Tania Estévez-Lao assisted in the qPCR analysis. Dr. Julián Hillyer and I wrote the manuscript, as it is presented in this chapter. Dr. Hillyer provided the funding and resources for this study. I thank Dr. Scott B. Williams and Ms. Luísa Jabbur for helpful discussions and feedback on this manuscript. This chapter was included in this dissertation with the permissions of my collaborators, Abinaya Ramakrishnan, Tania Estévez-Lao and Julián Hillyer.

Abstract

The immune and circulatory systems of insects are functionally integrated. Following infection, immune cells called hemocytes specifically aggregate around the ostia (valves) of the heart. An earlier RNA sequencing project in the African malaria mosquito, *Anopheles gambiae*, revealed that the heart-associated hemocytes, called periostial hemocytes, express transglutaminases more highly than hemocytes elsewhere in the body. Here, we further queried the expression of these transglutaminase genes and examined whether they play a role in heart-associated immune responses. We found that, in the whole body, injury upregulates the expression of *TGase2*, whereas infection upregulates *TGase1*, *TGase2* and *TGase3*. RNAi-based knockdown of *TGase1* and *TGase2* did not alter periostial hemocyte aggregation, but knockdown of *TGase3* increased the number of periostial hemocytes during the early stages of infection and the sequestration of melanin by periostial hemocytes during the later stages of infection. In uninfected mosquitoes, knockdown of *TGase3* also slightly reduced the number of sessile hemocytes outside of the periostial regions. Taken altogether, these data show that TGase3 negatively regulates periostial hemocyte aggregation, and we hypothesize that this occurs via negative regulation of the immune deficiency (IMD) pathway and alteration of hemocyte adhesion. In conclusion, TGase3 is involved in the functional integration between the immune and circulatory systems of mosquitoes.

Introduction

Pathogens often invade the hemocoel of a mosquito, but they are immediately confronted by two forces: hemolymph currents and immune responses (21, 48). The circulatory organ that maintains the hemolymph currents is a dorsal vessel that extends the entire length of the body and is subdivided into an aorta in the thorax and a heart in the abdomen (22). The aorta is not meaningfully involved in the pumping of hemolymph. Instead, the heart contracts in a manner that aspirates hemolymph from the hemocoel via six pairs of abdominal ostia (heart valves) and one pair of thoraco-abdominal ostia, and propels it to the anterior or posterior ends of the body (30, 33, 34).

The primary cellular drivers of immune responses in the hemocoel are the hemocytes (51). In mosquitoes, three quarters of hemocytes circulate with the hemolymph whereas one quarter attaches to tissues and is sessile (52). The distribution of sessile hemocytes is not homogenous, and many aggregate in the areas surrounding the heart's ostia, and are called periostial hemocytes (23). During an infection, periostial hemocytes sequester and kill pathogens that are about to be swept into the heart by the flow of hemolymph (23, 128). As this is happening, additional hemocytes aggregate at the periostial regions, which amplifies the pathogen killing response (23, 112). As a result, the most intense immune responses and the highest concentration of hemocytes coincide with the regions of the body that receive the most hemolymph flow, and therefore, periostial hemocyte aggregation highlights the functional integration between the immune and circulatory systems (23, 112).

The periostial response to infection is not restricted to mosquitoes. Infection induces hemocyte aggregation on the heart of insects from all major branches of the class Insecta, which illustrates the evolutionary conservation of this immune process (140). Despite its significance in insect immunity, the genetic factors that govern heart-associated immune responses remain largely unknown. Genes belonging to the Nimrod gene family – *Eater* and *Draper* – and the Thioester-containing protein gene family – *TEP1*, *TEP3* and *TEP4* – regulate periostial hemocyte aggregation in the mosquito, *Anopheles gambiae* (123, 127). Moreover, chapter III shows that the IMD and JNK pathways – two of the major innate immune signaling pathways – also positively regulate periostial hemocyte aggregation. That latter study also showed that the mRNA abundance of two of the three transglutaminase genes in *A. gambiae* – *TGase1* and *TGase3* – is enriched in the periostial hemocytes of infected mosquitoes relative to circulating hemocytes or the rest of the body. Therefore, we hypothesize that transglutaminases are involved in heart-associated immune responses.

Transglutaminases catalyze the formation of isopeptide bonds between glutamine and lysine residues, and are encoded in the genomes of bacteria, plants and animals (194-196). The transglutaminases that are encoded in the *Drosophila melanogaster* genome perform pleiotropic functions, including cuticular morphogenesis, hemolymph coagulation, pathogen entrapment, signal transduction and peritrophic matrix formation (197, 198). Transglutaminases in other arthropods have similar pleiotropic functions, and of interest to the present study is that they coagulate wounds in horseshoe crabs (199, 200) and crayfish (201, 202), and are involved in immune defenses against viruses, bacteria and fungi in shrimps (203, 204), crabs (205) and termites (206, 207).

The *A. gambiae* genome encodes three transglutaminase genes: *TGase1*, *TGase2* and *TGase3*. The function of TGase1 remains unknown, but TGase2 functions in the wound-induced antimalarial response (166, 208), and TGase3 cross-links seminal secretions to form a gelatinous mating plug that is transferred to the female during mating and is essential for sperm storage in the spermatheca (209-211). Here, we investigated whether transglutaminases are involved in heart-associated immune responses. We show that TGase3 – but not TGase1 or TGase2 – negatively regulates periostial hemocyte aggregation during the early stages of infection, indicating that it plays a role in the functional integration between the mosquito immune and circulatory systems.

Results

Infection induces the expression of transglutaminase genes

Our previous RNA sequencing study showed that an infection with *E. coli* or *S. aureus* upregulates the expression of *TGase1* and *TGase3* in periostial hemocytes relative to other tissues. To explore this further, we examined the expression of all three members of the transglutaminase family – *TGase1* (AGAP009100), *TGase2* (AGAP009098) and *TGase3* (AGAP009099) – by qPCR in the whole body of female mosquitoes that were naïve, injured, or had been infected with tetracycline resistant, GFP-expressing *Escherichia coli* (GFP-*E. coli*) for 4 or 24 hr (Figure 1). For *TGase1*, mRNA abundance was similar between naïve and injured mosquitoes, but increased 3.8- and 4.8-fold after infection for 4 and 24 hr, respectively. For *TGase2*, injury induced a 3.3-fold increase in expression at 4 hr but only marginally changed expression at 24 hr, and

infection increased the mRNA abundance by 9.3- and 4.0-fold at 4 and 24 hr respectively. For *TGase3*, mRNA abundance doubled following injury but increased 7.2- and 10.4-fold after infection for 4 and 24 hr, respectively. As expected, the mRNA abundance of the control gene, *Rps17*, remained unchanged regardless of treatment and time. Overall, these data show that injury upregulates the expression of *TGase2*, while infection upregulates the expression of *TGase1*, *TGase2* and *TGase3*.

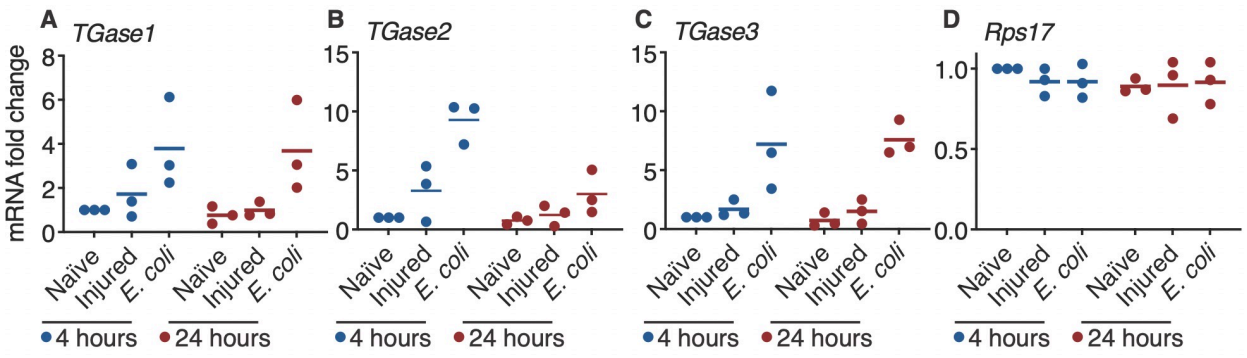

Figure 1 Transglutaminase genes are transcriptionally upregulated following infection.
Graphs show the relative mRNA level of *TGase1* (A), *TGase2* (B), *TGase3* (C) and *Rps17* (D; negative control; data shared with chapter III), in naïve (unmanipulated), injured and *E. coli*-infected mosquitoes at 4 or 24 hr post-treatment. Each circle represents an independent trial, and the value is the average mRNA abundance relative to naïve mosquitoes at 4 hr across 2-4 technical replicates within the trial. The horizontal line marks the average.

TGase3 negatively regulates infection-induced periostial hemocyte aggregation during the early stages of infection

To determine whether transglutaminases play a role in periostial hemocyte aggregation, we individually knocked down the expression of *TGase1*, *TGase2* or *TGase3* by RNA interference (RNAi) and evaluated the number of periostial hemocytes before infection and at 4 and 24 hr after *E. coli* infection. The RNAi-based knockdown

efficiency for *TGase1*, *TGase2* and *TGase3* was 57%, 79% and 41%, respectively, compared to the control ds*bla(Ap^R)*-injected mosquitoes (Appendix M).

The number of periostial hemocytes in uninfected mosquitoes was the same regardless of dsRNA treatment, indicating that transglutaminases do not regulate the basal abundance of periostial hemocytes in uninfected mosquitoes (Figure 2). At 4 hr following infection, the number of periostial hemocytes in ds*bla(Ap^R)*-injected mosquitoes increased 2.8-fold compared to their naïve counterparts, and remained elevated at 24 hr after infection. This reiterates that infection induces periostial hemocyte aggregation (23, 112). The number of periostial hemocytes in ds*TGase1* and ds*TGase2* mosquitoes increased at 4 and 24 hr after infection in a manner that was similar to the increase seen for ds*bla(Ap^R)* mosquitoes, indicating that knocking down these two genes does not impact periostial hemocyte aggregation. However, relative to ds*bla(Ap^R)* mosquitoes, knockdown of *TGase3* resulted in a disproportionately large, 27% increase in periostial hemocyte aggregation at 4 hr post-infection, although this effect disappeared by 24 hr.

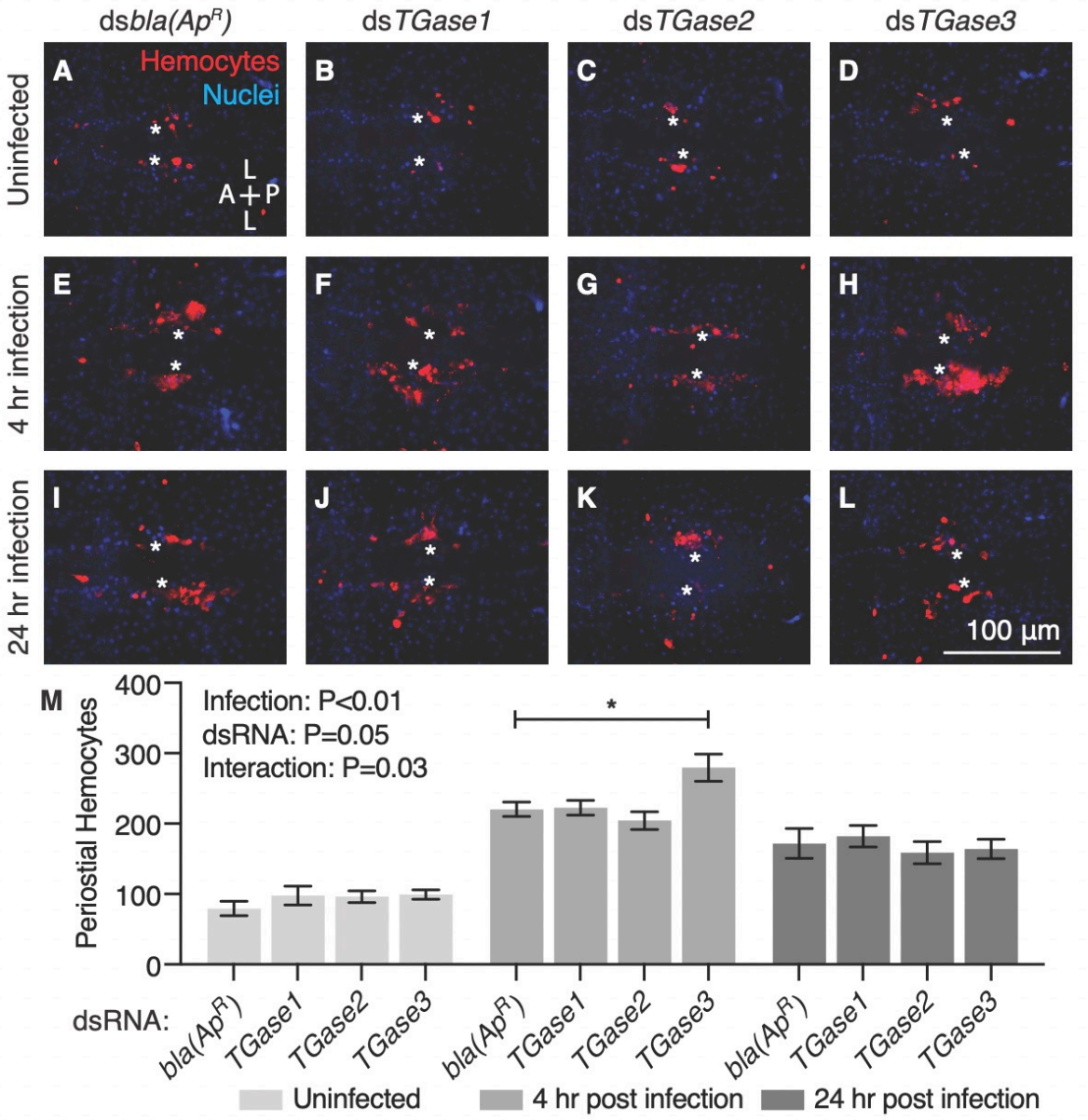

Figure 2 RNAi-based knockdown of *TGase3* increases the number of periostial hemocytes during the early stages of *E. coli* infection.

(A-L) Each fluorescence image shows a single abdominal segment with periostial hemocytes (CM-DiI; red) surrounding the ostia (asterisks) in uninfected mosquitoes (A-D), and mosquitoes at 4 (E-H) or 24 hr (I-L) post-infection. Four days prior to infection, mosquitoes had been injected with ds*bla(Ap^R)* (A, E, I), ds*TGase1* (B, F, J), ds*TGase2* (C, G, K) or ds*TGase3* (D, H, L). Nuclei were stained blue with Hoechst 33342. A, anterior; P, posterior; L, lateral. (M) Graph shows the average number of periostial hemocytes in ds*bla(Ap^R)*-, ds*TGase1*-, ds*TGase2*- and ds*TGase3*-injected mosquitoes that were uninfected or had been infected with GFP-*E. coli* for 4 or 24 hr. Data were analyzed by two-way ANOVA followed by Dunnett's post-hoc test, using ds*bla(Ap^R)* mosquitoes as the reference. Column heights mark the means, whiskers show the standard error of the mean (S.E.M.), and the asterisk indicates $P < 0.05$.

There is a trend for TGase3 to positively regulate non-periostial, sessile hemocyte abundance in uninfected mosquitoes

We next counted the number of non-periostial sessile hemocytes in the dorsal tergum of abdominal segments 4 and 5 in the same mosquitoes that were examined for periostial hemocytes. The rationale for collecting this measurement was to determine whether transglutaminases affect the general abundance of sessile hemocytes, and more specifically, whether the effect seen for TGase3 at 4 hr after infection was a general phenomenon that affects all sessile hemocytes, or whether it is specific to the periostial regions. In uninfected mosquitoes, and relative to ds*bla(Ap^R)* injection, knockdown of *TGase3* reduced the number of non-periostial sessile hemocytes by 26% (P = 0.07), whereas knockdown of *TGase1* or *TGase2* had a minimal effect on the number of non-periostial hemocytes (Figure 3). Infection induced a modest increase in the number of non-periostial sessile hemocytes, but this increase was unaffected by dsRNA treatment (Figure 3). The magnitude of the infection-induced increase was small relative to the increase seen within the periostial regions.

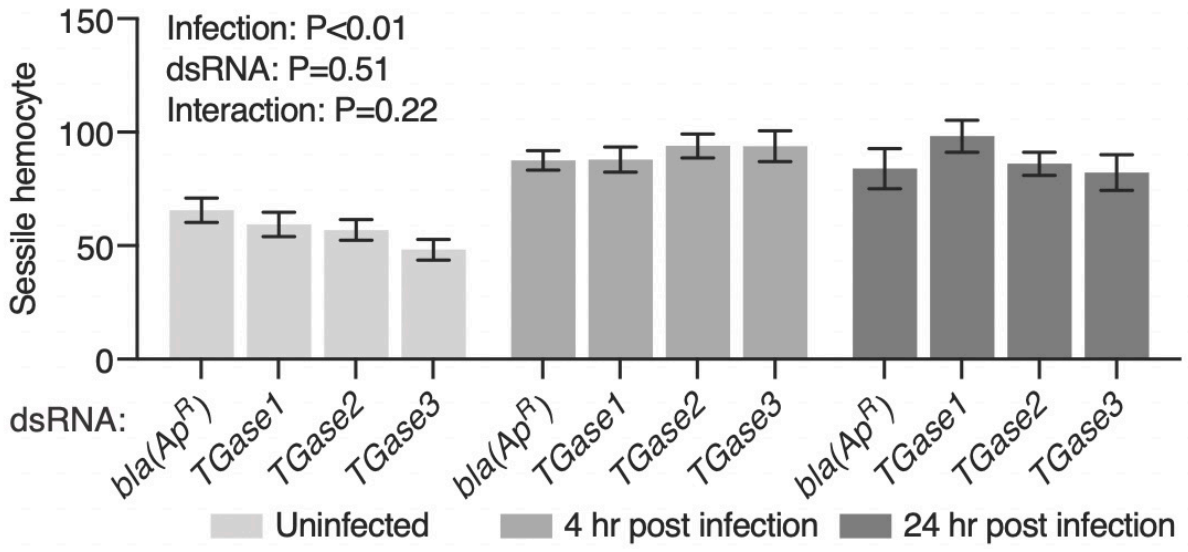

Figure 3 RNAi-based knockdown of transglutaminase genes has limited effect on the aggregation of sessile hemocytes outside of the periostial regions.
Graph shows the average number of non-periostial, sessile hemocytes on the integument of dorsal abdominal segments 4 and 5 in ds*bla(Ap^R)*-, ds*TGase1*-, ds*TGase2*- and ds*TGase3*-injected mosquitoes that were uninfected or had been infected with GFP-*E. coli* for 4 or 24 hr. Data were analyzed by two-way ANOVA followed by Dunnett's post-hoc test, using ds*bla(Ap^R)* mosquitoes as the reference. Column heights mark the means, and whiskers show the S.E.M.

Transglutaminases do not modulate the phagocytosis of bacteria on the surface of the heart

Hemocytes phagocytose and destroy pathogens that circulate with the hemolymph, and this phagocytic activity is strongly manifested at the periostial regions (23, 48, 112, 128). Given that *TGase3* knockdown increases the infection-induced aggregation of periostial hemocytes during the early stages of infection, we next sought to assay whether knocking down transglutaminases affects the accumulation of phagocytosed GFP-*E. coli* at the periostial regions. To our surprise, the GFP-*E. coli* pixel area in the periostial regions was similar between the ds*bla(Ap^R)*-injected mosquitoes and the ds*TGase1*-, ds*TGase2*- and ds*TGase3*-injected mosquitoes at both 4 and 24 hr post-infection (Figure

4). For all dsRNA groups, the presence of fluorescent bacteria at the periostial regions significantly dropped between 4 and 24 hr following infection, which shows that phagocytosed bacteria are destroyed and that the immune response at the periostial regions is effective. Overall, these data show that transglutaminases do not modulate the hemocyte-mediated phagocytosis of bacteria at the periostial regions.

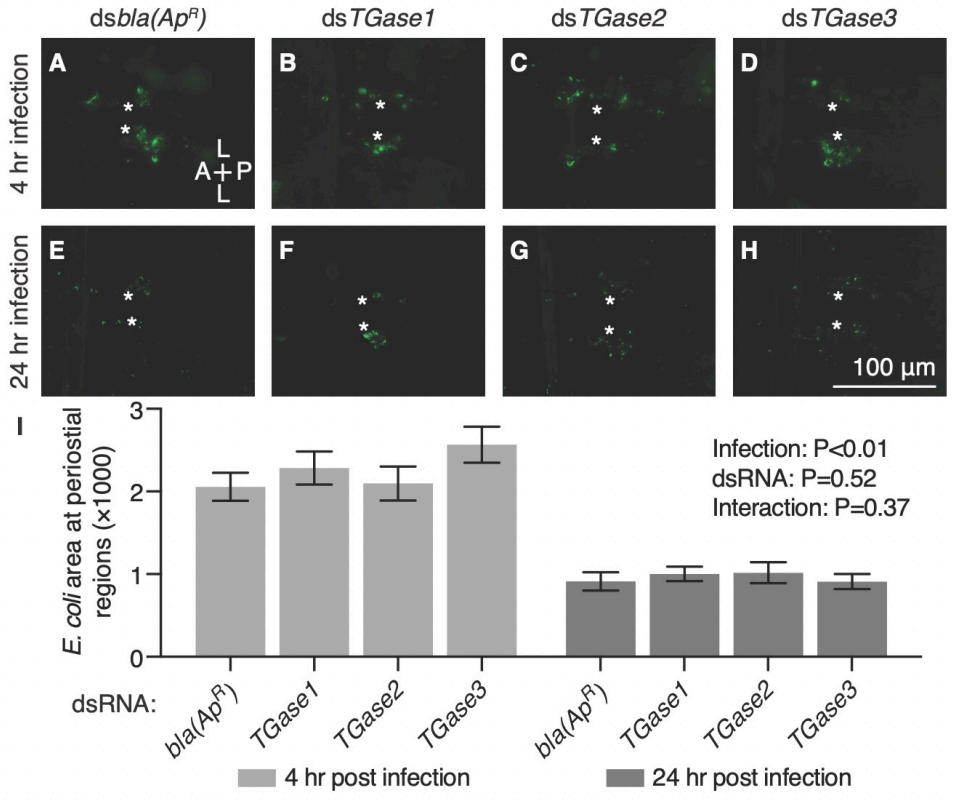

Figure 4 RNAi-based knockdown of transglutaminase genes does not alter the accumulation of GFP-*E. coli* in the periostial regions.
(A-H) Fluorescence images show a single abdominal segment with phagocytosed bacteria (green) surrounding the ostia (asterisks) in mosquitoes that had been infected with GFP-*E. coli* for 4 h (A-D) or 24 hr (E-H). Prior to infection, mosquitoes had been treated with ds*bla(Ap^R)* (A, E), ds*TGase1* (B, F), ds*TGase2* (C, G) or ds*TGase3* (D, H). A, anterior; P, posterior; L, lateral. (I) Graph shows the average area of GFP-*E. coli* in ds*bla(Ap^R)*-, ds*TGase1*-, ds*TGase2*- and ds*TGase3*-injected mosquitoes that had been infected with GFP-*E. coli* for 4 or 24 hr. Data were analyzed by two-way ANOVA followed by Dunnett's post-hoc test, using ds*bla(Ap^R)* mosquitoes as the reference. Column heights mark the means, and whiskers show the S.E.M.

TGase3 negatively regulates melanin accumulation on the surface of the heart during the later stages of infection

Hemocytes produce enzymes that catalyze the melanization cascade that encases and kills pathogens (50, 56, 57, 212, 213). Melanization is a humoral response that occurs in circulation, but this response leads to the eventual phagocytosis of dark, melanized pathogens by periostial hemocytes and the capture of smaller, melanized debris by pericardial cells (23, 49, 112, 127, 214). Given that *TGase3* knockdown increases the number of periostial hemocytes at 4 hr after infection but does not affect the phagocytosis of live bacteria, we tested whether transglutaminases are involved in the accumulation of melanin on the surface of the heart. To achieve this, we measured the cumulative area of dark melanin deposits within the periostial regions of the same mosquitoes examined for GFP-*E. coli* accumulation. Melanin was undetectable in uninfected mosquitoes or in mosquitoes that had been infected with *E. coli* for 4 hr. However, at 24 hr post-infection, knockdown of *TGase3* increased the melanized area within the periostial regions when compared to ds*bla(Ap^R)*-injected mosquitoes (Figure 5). Knockdown of *TGase1* and *TGase2* also slightly increased the melanized area, but this difference was smaller and not statistically significant. Overall, these data show that TGase3 negatively regulates the accumulation of melanized bacteria at the periostial regions.

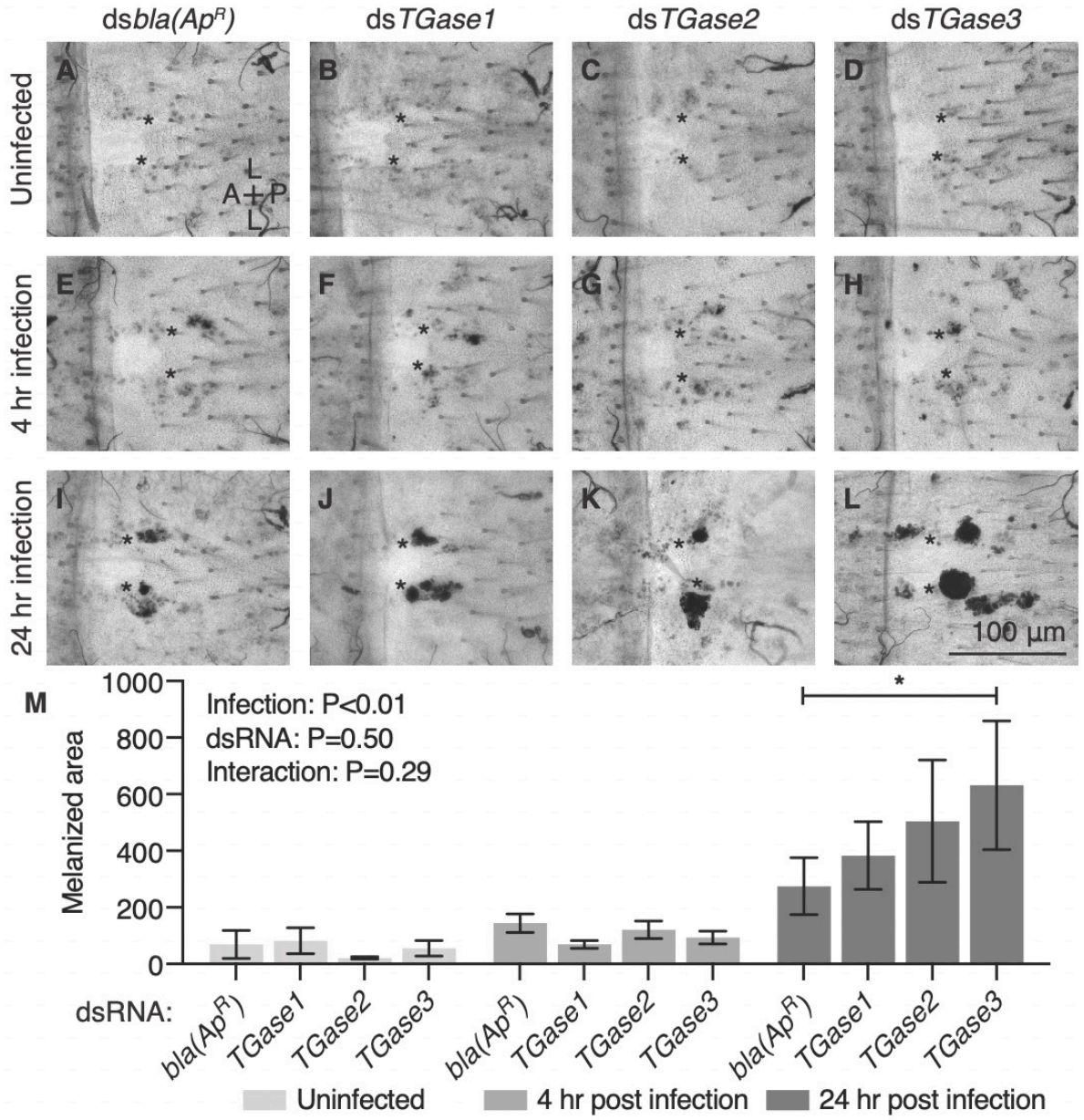

Figure 5 RNAi-based knockdown of *TGase3* increases melanin accumulation at the periostial regions.

(A-L) Brightfield images show a single abdominal segment with melanin deposits (black) surrounding the ostia (asterisks) in uninfected mosquitoes (A-D), and mosquitoes that had been infected with GFP-*E. coli* for 4 (E-H) or 24 hr (I-L). Prior to infection, mosquitoes had been treated with ds*bla(Ap^R)* (A, E, I), ds*TGase1* (B, F, J), ds*TGase2* (C, G, K) or ds*TGase3* (D, H, L). A, anterior; P, posterior; L, lateral. (M) Graph shows the average area of melanin deposits in ds*bla(Ap^R)*-, ds*TGase1*-, ds*TGase2*- and ds*TGase3*-injected mosquitoes that were not infected or had been infected with GFP-*E. coli* for 4 or 24 hr. Data were analyzed by two-way ANOVA followed by Dunnett's post-hoc test, using ds*bla(Ap^R)* mosquitoes as the reference. Column heights mark the means, whiskers show the S.E.M. and asterisks indicate $P < 0.05$.

Discussion

Here we show that TGase3 plays a negative role in periostial hemocyte aggregation during the early stages of infection. In contrast, we also detected a trend that TGase3 positively regulates sessile hemocyte attachment to the abdominal integument in uninfected mosquitoes. We hypothesize that TGase3 regulates periostial hemocyte aggregation by inhibiting the immune deficiency (IMD) pathway and altering hemocyte adhesion.

In *D. melanogaster*, some infections activate the IMD pathway, which leads to the cleavage of the NF-κB transcription factor, Relish. The N-terminal region of Relish translocates into the nucleus, binds to DNA, and induces the expression of antimicrobial peptides and the activation of other immune responses that kill pathogens (142). Interestingly, *Drosophila* transglutaminase negatively regulates the IMD pathway (215, 216). Specifically, *Drosophila* transglutaminase cross-links the N-terminal region of Relish and forms a polymer that prevents its translocation into the nucleus (215). This transglutaminase also incorporates natural primary amines into the DNA binding site of Relish, thereby providing a second layer of IMD pathway inhibition (216). Here, we did not test the direct relationship between *A. gambiae* TGase3 and the IMD pathway. However, we show that TGase3 negatively regulates periostial hemocyte aggregation during the early stages of infection and melanin accumulation in the periostial regions during the later stages of infection. Moreover, in an earlier study we demonstrated that the IMD pathway positively regulates periostial hemocyte aggregation [CITATION].

Specifically, silencing the *A. gambiae* ortholog of *D. melanogaster Relish*, *rel2*, reduces periostial hemocyte aggregation whereas silencing the negative regulator of the IMD pathway, *caspar*, increases the periostial immune response. Therefore, given these findings and the direct links between transglutaminases and NF-κB signaling pathways, we hypothesize that mosquito TGase3 negatively regulates periostial hemocyte aggregation by inhibiting the IMD pathway.

Silencing *TGase3* slightly reduces the number of sessile hemocytes in uninfected mosquitoes. A plausible explanation is that silencing *TGase3* causes sessile hemocytes to detach from the abdominal wall, trachea and other tissues, thereby forcing them into circulation. This would increase circulating hemocyte numbers, thus increasing the number of hemocytes available to aggregate within the periostial regions of infected mosquitoes. Whether TGase3 regulates hemocyte attachment in mosquitoes is unknown, but two human transglutaminase homologs – Factor XIII and tissue transglutaminase 2 (hTGase2) (210, 211) – are involved in cell-substrate binding (217-221). Moreover, in a freshwater crayfish, transglutaminase is expressed in hematopoietic cells and functions to maintain cells within the hematopoietic organ (222). Follow-up experiments showed that inhibiting transglutaminase activity – either via dsRNA treatment or by introducing the inhibitor Astakine 1 – enables hemocytes to differentiate such that their morphology and shape resembles that of mature hemocytes that have been released from the hematopoietic organ (222-224). In another crustacean, the white shrimp, reducing transglutaminase expression increases the circulating hemocyte population, possibly because of the detachment of sessile hemocytes (204). Overall, this suggests that reduced levels of transglutaminase are associated with morphological changes in

hemocytes, and the release of sessile hemocytes into circulation. This explains why mosquitoes with silenced *TGase3* tended to have fewer non-periostial, sessile hemocytes than mosquitoes with a natural amount of *TGase3*.

In this study, we found that TGase1 and TGase2 are not involved in periostial hemocyte aggregation. This was expected for TGase2 because it is involved in wound-induced immunity (166), and injury does not induce periostial hemocyte aggregation (23, 52, 112). However, it is surprising that TGase1 does not play a role in periostial hemocyte aggregation, as infection upregulates the expression of both *TGase1* and *TGase3* more highly in periostial hemocytes than in other tissues. A previous study also found that TGase1 is not involved in the immune response against malaria parasites (166). It appears that TGase1 has an alternate function in periostial hemocytes or within the heart, especially because its ortholog in *Drosophila* is highly expressed in the ostia of the embryo (182). Instead, we found that TGase3 is involved in periostial hemocyte aggregation. Prior to this study, TGase3 was only known to be essential for the formation of the anopheline-specific mating plug (209). A previous study suggested that *TGase3* is expressed in the male accessory glands of *A. gambiae*, but that it is not expressed in female mosquitoes (209). However, we detected *TGase3* expression in the heart, periostial hemocytes and whole body of female mosquitoes by both RNA sequencing, quantitative PCR, and conventional PCR. Altogether, this suggests that the three transglutaminases in *A. gambiae* have different functions. Based on our limited knowledge of mosquito transglutaminases, we conclude that (i) TGase1 plays a lesser role or no role in immunity, (ii) TGase2 is involved in wound-related immunity, and (iii) TGase3 is involved in both mating biology and periostial hemocyte aggregation.

Alternatively, the lack of a phenotype in ds*TGase1* and ds*TGase2* RNAi mosquitoes could be due to the residual amount of transglutaminase protein that remains after partial silencing or because of a redundant mechanism involving TGase3. This would not be entirely surprising because our treatments were conducted four days after the onset of RNAi, and some *Drosophila* transglutaminase can still be detected 12 days after the initiation of RNAi (215).

Transglutaminases participate in many physiological processes. Here we show that TGase3 is involved in heart-associated immune responses. Based on what is already known about arthropod transglutaminases, we hypothesize that this occurs via two complementary mechanisms: (i) modification of the infection-induced activation of the IMD pathway and (ii) modulating hemocyte adhesion. In conclusion, this study shows that a factor that is not classically associated with immunity or circulatory physiology is involved in the functional integration of the immune and circulatory systems of mosquitoes.

Methods

Mosquitoes, bacteria, and infection

Anopheles gambiae, Giles sensu stricto (G3 strain; Diptera: Culicidae), were reared and maintained in an environmental chamber at 27 °C and 75% relative humidity, with a 12 hr:12 hr light:dark photoperiod (30). Adults were fed 10% sucrose *ad libitum*, and only females were used for experimentation. GFP-*E. coli* (modified DH5α) were grown overnight in Luria-Bertani's (LB) rich nutrient medium in a 37 °C shaking incubator (New Brunswick Scientific, Edison, NJ, USA). On average, 17,388 GFP-*E. coli* were

injected into the thoracic anepisternal cleft using a Nanoject III Programmable Nanoliter Injector (Drummond Scientific Company, Broomall, PA, USA).

Treatments, RNA extraction and cDNA synthesis

Six-day-old mosquitoes were cold-anesthetized and separated into three groups: (1) naïve (unmanipulated), (2) injured by injecting 69 nL of sterile LB medium, and (3) infected by injecting 69 nL of GFP-*E. coli*. RNA was extracted and isolated from a pool of 10 whole-body mosquitoes at 4 and 24 hr after treatment using TRIzol Reagent (Invitrogen, Carlsbad, CA, USA), and purified using the RNeasy Mini Kit (Qiagen, Valencia, CA, USA). The concentration of RNA was quantified using a BioPhotometer Plus spectrophotometer (Eppendorf AG, Hamburg, Germany), and up to 5 µg of RNA was treated with RQ1 RNase-free DNase (Promega, Madison, WI, USA). The extracted RNA was then used for cDNA synthesis using Oligo$(dT)_{20}$ primers and the SuperScript III First-Strand Synthesis System for RT-PCR (Invitrogen).

Gene expression and Real-time quantitative PCR (qPCR)

qPCR was conducted using cDNA as template, gene-specific primers (Appendix O), and Power SYBR Green PCR Master Mix (Applied Biosystems, Foster City, CA) on an ABI 7300 Real-Time PCR System. Relative quantification of mRNA levels was conducted using the $2^{-\Delta\Delta C_T}$ method, with the housekeeping gene *RPS7* as the reference gene and *RPS17* as a control (130, 131). To assess gene expression following treatment, three independent trials were conducted, each with two to four technical replicates. The absence of genomic DNA in the cDNA preparations was confirmed by (i) conducting a

melting curve analysis at the end of each qPCR run to show that there is only one peak, and (ii) testing each cDNA with primers that span an intron to show that only one amplicon that is of the predicted mRNA size amplified. Gene expression analyses for this study and for the study in chapter III were conducted concurrently and using the same cDNAs, and hence, the *RPS17* data are the same for both studies.

Double-stranded RNA (dsRNA) synthesis

Double-stranded RNA was synthesized for three mosquito genes – *TGase1*, *TGase2* and *TGase3* – using methods we have described (123, 126, 127). Specifically, a fragment of each gene was amplified using *A. gambiae* cDNA as the template and gene-specific primers with T7 promoter tags (Appendix O). The amplicons were separated by agarose gel electrophoresis, excised, and purified using Qiagen's QIAquick Gel Extraction kit. Each amplicon was then used as the template for a second PCR reaction using the same primers. The product was purified using the QIAquick PCR Purification Kit (Qiagen), and the concentration was quantified spectrophotometrically. Up to 1 µg of the second PCR product was used as the template for *in vitro* dsRNA synthesis using the MEGAscript T7 Kit (Applied Biosystems). The resultant dsRNA was precipitated with ethanol and re-suspended in phosphate-buffered saline (PBS). The concentration of dsRNA was quantified spectrophotometrically and the integrity of dsRNA was verified by agarose gel electrophoresis. The same procedure was used for synthesis a non-mosquito gene – *bla(Ap^R)* (beta-lactamase) – except that the template was DNA extracted from *E. coli* BL21(DE3) containing the pET-46 plasmid (EMD Chemicals, Gibbstown, NJ).

RNA interference

Two-day-old female mosquitoes were injected with 300 ng of dsRNA. Four days later, mosquitoes were divided into two groups: (1) uninfected and (2) infected with GFP-*E. coli*. An injury group (e.g., sham injection) was not assayed because injury does not induce periostial hemocyte aggregation (23, 52, 112). To assess RNAi efficiency, RNA was purified from whole bodies at 4 days after dsRNA injection, cDNA was synthesized, and qPCR was conducted with gene-specific primers (Appendix O). For qPCR, three to four independent trials were conducted with two to four technical replicates each.

Hemocyte staining and mosquito dissections

Hemocytes were stained *in vivo* using Vybrant CM-DiI Cell-Labeling Solution (Invitrogen) as we have previously described (23). Briefly, live mosquitoes were injected with ~0.4 µL of a solution consisting of 67 µM CM-DiI and 1.08 mM Hoechst 33342 (nuclear stain; Invitrogen) in PBS. Mosquitoes were incubated in the environmental chamber for 20 min, and then fixed by injecting 16% paraformaldehyde into the hemocoel. Ten minutes later, a razor blade was used to separate the abdomen from the head and thorax, and to bisect the abdomen along a coronal plane such that the dorsal and ventral sides were separated. The dorsal abdomens were then immersed in PBS containing 0.1% Triton X-100 and the internal organs were removed. The dorsal abdomens – containing the heart, periostial hemocytes and pericardial cells – were rinsed briefly in PBS and mounted between a glass slide and a coverslip using Aqua-Poly/Mount (Polysciences; Warrington, PA, USA).

Microscopy and image acquisition

Each dorsal abdomen was imaged using a Nikon Eclipse Ni-E compound microscope connected to a Nikon Digital Sight DS-Qi1 monochrome digital camera and Nikon's Advanced Research NIS Elements software (Nikon, Tokyo, Japan). Z-stacks of bright-field, red fluorescence (hemocytes), green fluorescence (GFP-*E. coli*) and blue fluorescence (nuclei) channels were acquired using a linear encoded Z-motor. For image presentation and pixel measurements, a specific channel (or channels) was (were) selected and all images within a stack were combined into a two-dimensional, focused image using the Extended Depth of Focus (EDF) function in NIS Elements.

Hemocyte counting

Hemocytes were counted manually by examining all images within a Z-stack. A cell was counted as a hemocyte if it measured 9–18 μm in diameter and was labeled with both CM-DiI and Hoechst 33342 (112). A cell was counted as a periostial hemocyte if it was adjacent to an ostium, and a cell was counted as a non-periostial, sessile hemocyte if it was attached to the dorsal abdominal wall in an area that was outside of the periostial regions (23, 52, 127). Periostial hemocytes were counted within abdominal segments 2–7 whereas non-periostial, sessile hemocytes were only counted on the dorsal abdominal wall of segments 4 and 5. Hemocytes were not counted on the aorta, the excurrent openings of the heart or the thoraco-abdominal ostia because few hemocytes are present there, and infection does not induce the aggregation of hemocytes at those locations (33, 34). Each treatment group contained between 22 and 37 mosquitoes, which were

assayed across 3-4 independent trials. Periostial and non-periostial sessile hemocytes were counted in the same specimens.

Quantification of GFP-*E. coli* at the periostial regions

GFP-*E. coli* in the periostial regions was quantified by measuring the area of pixels with intensities above a threshold. Images were first examined to determine a pixel intensity threshold that distinguished GFP emitted by *E. coli* (pixel intensities above the threshold) from background fluorescence intensity (pixel intensities below the threshold). Then, each of the periostial regions was delineated using the region of interest (ROI) tool in NIS Elements, and the sum binary area of pixels above the threshold was measured for each periostial region ROI. Each treatment group contained between 22 and 38 mosquitoes, which were assayed across 3-4 independent trials.

Quantification of melanin at the periostial regions

Dark melanin deposits in the periostial regions were quantified by measuring the area of pixels with intensities below a threshold (112). Images were first examined to determine a threshold of pixel intensity that distinguished melanized areas (pixel intensities below the threshold) from non-melanized areas (pixel intensities above the threshold). Then, each periostial region was delineated using the ROI tool, and the sum binary area of pixels below the threshold was measured for each periostial region ROI. Each treatment group contained between 22 and 38 mosquitoes, which were assayed across 3-4 independent trials. Phagocytosis (GFP-*E. coli*) and melanization were quantified in the same specimens.

Statistical analysis

Data on hemocyte, pathogen or melanin aggregation were analyzed by two-way ANOVA, followed by Dunn's multiple comparison test. The ds*bla(Ap^R)*-injected mosquitoes were used as the reference group. A two-way ANOVA yields three distinct P values that examine the following: (i) whether dsRNA treatment affects the outcome, regardless of infection status; (ii) whether infection status affects the outcome, regardless of dsRNA treatment; (iii) whether the infection status has effects that depend on the dsRNA treatment, and vice versa. All data analysis was done in GraphPad Prism version 8.4.3.

CHAPTER V

The immune and circulatory systems are functionally integrated across insect evolution

Preface

Instead of deciphering the genetic mechanisms, this chapter took an evolutionary approach and determined whether periostial hemocyte aggregation occurs in insects other than *A. gambiae*. This chapter analyzed 68 species of insects in 51 families from 16 orders and discovered that the functional integration between the immune and circulatory systems is conserved throughout insect evolution. This shows that insects, and not just mosquitoes, utilize this heart-associated immune response to combat infections. Dr. Julián Hillyer provided the funding and resources for this study. I conducted the experiments. We designed the experiments, analyzed and visualized the data, and wrote the manuscript. I thank Drs. Patrick Abbot, Antonis Rokas, Scott B. Williams, and Anderson de Sá Nunes for commenting on this manuscript. I thank Ms. Luísa Jabbur, Drs. James Sears, and Michael Tackenberg for useful discussions and our friends and colleagues that assisted in insect collection (see Appendix Z). This chapter is adapted from "*The immune and circulatory systems are functionally integrated across insect evolution*" published in 2020 in the journal *Science Advances* (140) and has been reproduced with the permission of the publisher and my co-author, Julián Hillyer.

Abstract

The immune and circulatory systems of mammals are functionally integrated, as exemplified by the immune function of the spleen and lymph nodes. Similar functional integration exists in the malaria mosquito, *Anopheles gambiae*, as exemplified by the infection-induced aggregation of hemocytes around the valves of the heart. However, whether this is specific to mosquitoes or a general characteristic of insects remained unknown. We analyzed 68 species from 51 families representing 16 orders, and discovered that infection induces the aggregation of hemocytes and pathogens on the heart of insects from all major branches of class Insecta. An expanded analysis in the holometabolous mosquito, *Aedes aegypti*, and the hemimetabolous bed bug, *Cimex lectularius*, showed that infection induces the aggregation of phagocytic hemocytes on the hearts of distantly related insects, with aggregations mirroring the patterns of hemolymph flow. Therefore, the functional integration of the immune and circulatory systems is conserved across the insect tree of life.

Introduction

The insect body cavity is a dynamic environment where the insect blood, called hemolymph, constantly and rapidly flows in a manner that bathes all tissues (30, 32, 41). This flow is primarily driven by a dorsal vessel that is structurally divided into an aorta in the thorax and a heart in the abdomen (22, 24). When pathogens invade an adult mosquito and reach its hemocoel, the flow of hemolymph disperses them to all regions of the body (21, 22). Hemolymph flow also circulates immune cells called hemocytes that survey the body for invaders. However, not all hemocytes circulate. Sessile hemocytes exist attached to tissues yet their distribution is not homogeneous; they concentrate on the outer surface of the dorsal vessel, and specifically, in the regions of the heart that surround the valves, or ostia – locations called the periostial regions (23, 52). Within seconds of infection, these heart-associated hemocytes, called periostial hemocytes, phagocytose circulating pathogens, and soon thereafter, additional hemocytes migrate to the periostial regions and amplify the phagocytosis response (23, 112). Periostial immune responses are advantageous because they occur in areas of high hemolymph flow, placing hemocytes where they are most likely to encounter and destroy pathogens (112). Thus, in a manner functionally similar to how the spleen and lymph nodes of vertebrate animals capture pathogens circulating in the blood and lymph (111), the function of periostial hemocytes exemplifies the functional integration of the immune and circulatory systems of mosquitoes (Figure 1).

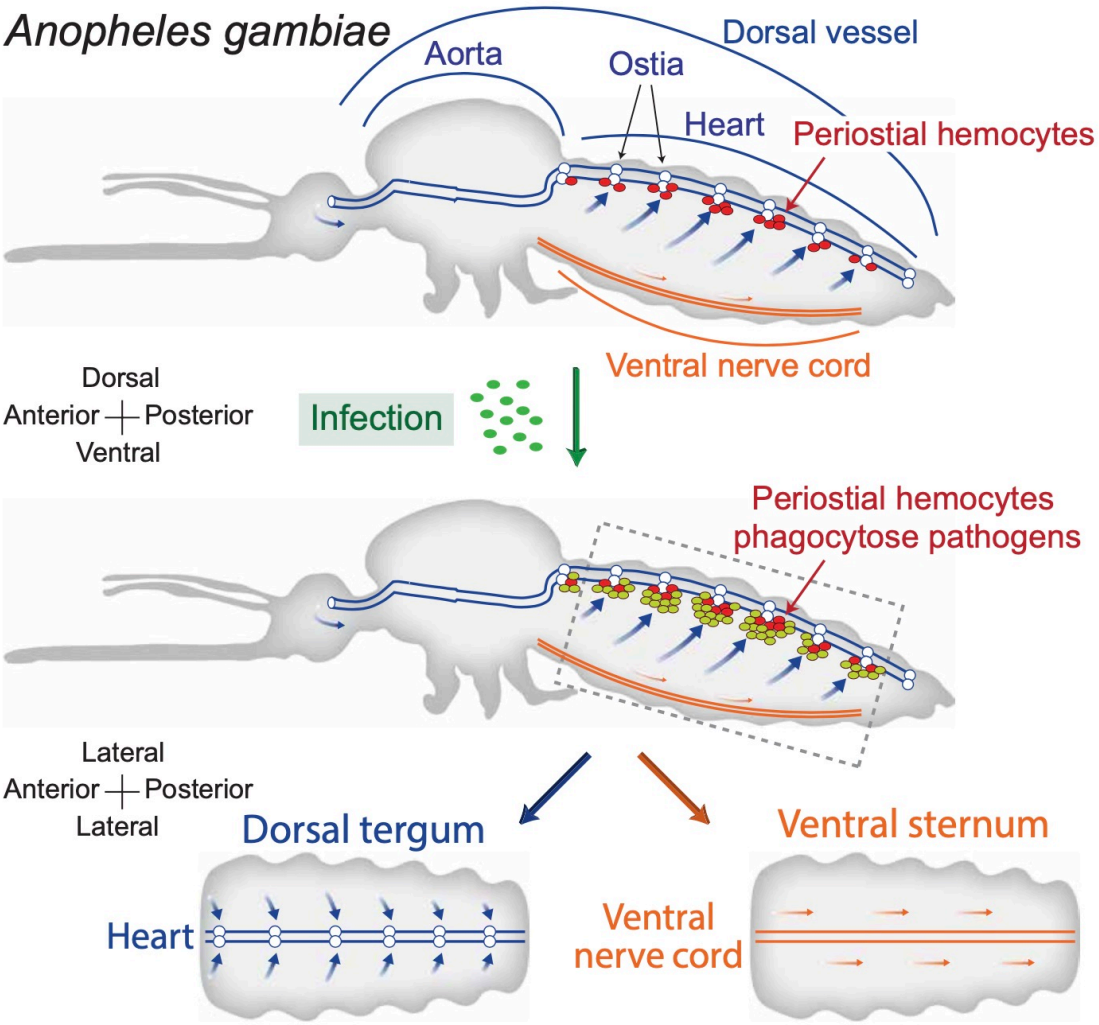

Figure 1 Diagram that illustrates periostial hemocyte aggregation and the experimental design of this study.
The top shows a lateral view of an entire mosquito and marks the position of the dorsal vessel (divided into a thoracic aorta and an abdominal heart), periostial hemocytes (red circles) surrounding the ostia (white circles), and the ventral nerve cord. The middle shows that infection induces the aggregation of additional hemocytes (olive green circles) and the phagocytosis of pathogens around the heart's ostia. The bottom shows a coronal view of the dorsal (tergum) and ventral (sternum) abdomen, which represents how they were visualized and photographed for this study. The arrows mark the direction of hemolymph flow during periods of anterograde heart contractions.

The biology of periostial hemocytes has only been characterized in the African malaria mosquito, *Anopheles gambiae* (23, 52, 112, 123, 127), but hemocytes have also been detected in the lumen of the heart of a stick insect and on the surface of the heart

of adult fruit flies and larvae of the greater wax moth (115-117, 120, 121). Whether the hemocytes of these insects are present near the ostia or whether their response to infection is linked to circulatory currents remained unknown. Hence, we asked whether the functional integration of the immune and circulatory systems is a novel trait specific to mosquitoes or a general characteristic of insects. To answer this question, we analyzed 68 species from 51 families representing 16 orders, and discovered that an infection induces the aggregation of hemocytes and pathogens on the heart of insects from all major branches of class Insecta. Therefore, the functional integration of the immune and circulatory systems is conserved across the insect tree of life.

Results

Infection induces the aggregation of phagocytic hemocytes on the heart of holometabolous and hemimetabolous insects

Having observed the interaction between the immune and circulatory systems in the mosquito, *An. gambiae* (Figure 1), we conducted a comprehensive analysis of infection-induced hemocyte aggregation on the heart of the yellow fever mosquito, *Aedes aegypti,* and the bed bug, *Cimex lectularius*. These two insect pests diverged ~370 million years ago and have different developmental trajectories: one is holometabolous and the other is hemimetabolous (225). Moreover, both are societally important; *Ae. aegypti* transmit human diseases such as dengue and Zika, and *C. lectularius* are notorious hematophagous pests.

In preparation for studying the functional integration of the immune and circulatory systems of *Ae. aegypti* and *C. lectularius*, we quantified how efficiently their hemocytes could be labeled by injecting Vybrant CM-DiI into the hemocoel and examining their perfused hemocytes 20-30 min later (Appendix P). Vybrant CM-DiI is a lipophilic dye that in *An. gambiae* labels the circulating and sessile hemocytes, but does not label the heart, pericardial cells, integument or any other tissue (23, 52, 112). Moreover, this dye has also been used to label the hemocytes of *Ae. aegypti* and *Apis mellifera* (Hymenoptera) (133, 226), and therefore, we hypothesized that it could label the hemocytes of any insect. We found that CM-DiI efficiently stains the hemocytes of naïve, injured and *Escherichia coli*-infected mosquitoes and bed bugs. On average, 84%, 83% and 77% of the hemocytes from naïve, injured and *E. coli*-infected *Ae. aegypti*, respectively, stained with CM-DiI. Similarly, 84%, 90% and 89% of the hemocytes from naïve, injured and *E. coli*-infected *C. lectularius*, respectively, stained with CM-DiI. Fat body and other cells were seldomly stained with CM-DiI, similar to what we have observed for *An. gambiae* (23, 34, 52, 112).

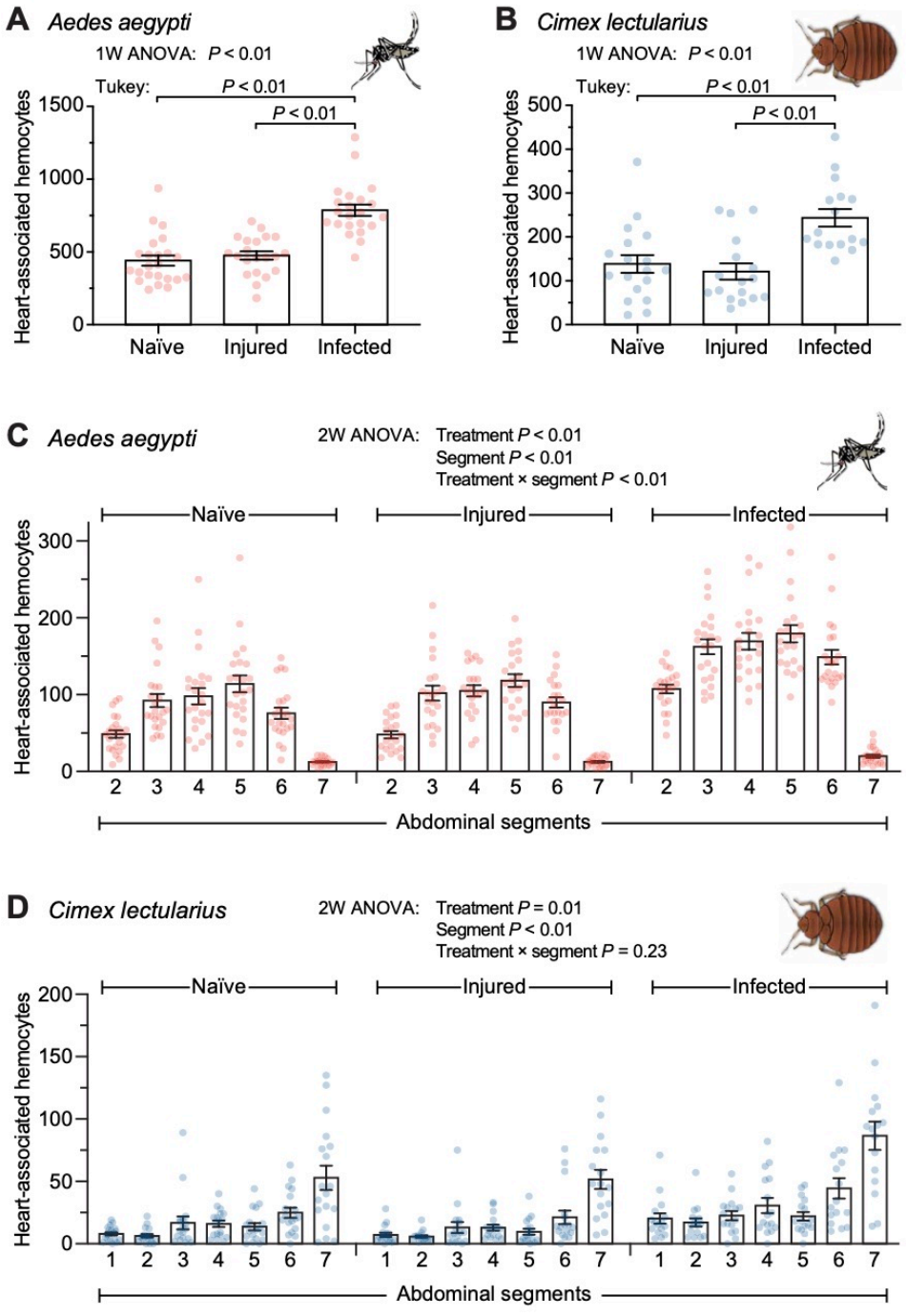

Figure 2 Infection induces the aggregation of phagocytic hemocytes on the heart of *Aedes aegypti* and *Cimex lectularius*.

A, B. Hemocytes on the heart of naïve, injured and *E. coli*-infected *Ae. aegypti* (**A**) and *C. lectularius* (**B**). **C, D.** Spatial distribution of hemocytes along the heart in the different abdominal segments of naïve, injured and *E. coli*-infected *Ae. aegypti* (**C**) and *C. lectularius* (**D**). Column heights mark the mean and the whiskers denote the standard error of the mean. Each circle represents the number of heart-associated hemocytes in an individual insect.

We then assayed for the presence of hemocytes on the heart of mosquitoes and bed bugs by injecting CM-DiI into the hemocoel, bisecting their abdomen, and examining the tubular heart that extends across the dorsal tergum. For *Ae. aegypti*, approximately 440 hemocytes reside on the heart of a naïve mosquito (Figure 2A). Injury does not alter the number of periostial hemocytes, but infection results in a 1.7-fold increase in the number of periostial hemocytes. This indicates that, much like occurs in adult *An. gambiae* (23), an infection induces the recruitment of additional hemocytes to the heart. A more detailed analysis of the spatial distribution of hemocytes revealed that most hemocytes aggregate in the periostial regions of abdominal segments 3-6 (Figure 2C). Again, this aggregation pattern resembles that of *An. gambiae*, which is advantageous because these middle abdominal segments are the locations that have the swiftest hemolymph flow (112). In bed bugs we observed similar results. Specifically, the average naïve and injured bed bug has 140 and 120 hemocytes on the heart, respectively, but infection induces a 2-fold increase in the number of heart-associated hemocytes (Figure 2B). In *C. lectularius*, hemocytes predominantly aggregate in the portions of the heart of abdominal segments 6 and 7 (Figure 2D). This spatial distribution occurs because this portion of the heart is enlarged and is where the incurrent ostia are located, as evidenced by structural analyses of the heart of other hemipterans, such as the kissing bug, *Rhodnius prolixus* (227), and the boxelder bug, *Leptocris trivittatus* (228).

To determine whether the hemocytes that aggregate on the heart are immunologically active, we injected *Ae. aegypti* and *C. lectularius* with *E. coli* bioparticles conjugated to pHrodo, which is a pH sensitive dye that only fluoresces in an acidic environment, such as that of the phagolysosome. Therefore, this dye is an efficient

marker for phagocytosis (112). In naïve mosquitoes and bed bugs, no fluorescence was detected, which was expected because no *E. coli*-pHrodo was injected. However, when mosquitoes and bed bugs were injected with *E. coli*-pHrodo, we detected fluorescence emission soon after injection, and this fluorescence was predominantly in the areas that contain the heart-associated hemocytes (Figure 3). Taken altogether, these data show that, in both holometabolous and hemimetabolous insects, infection induces the aggregation of hemocytes on the heart, and that these hemocytes rapidly phagocytose pathogens that circulate with the hemolymph.

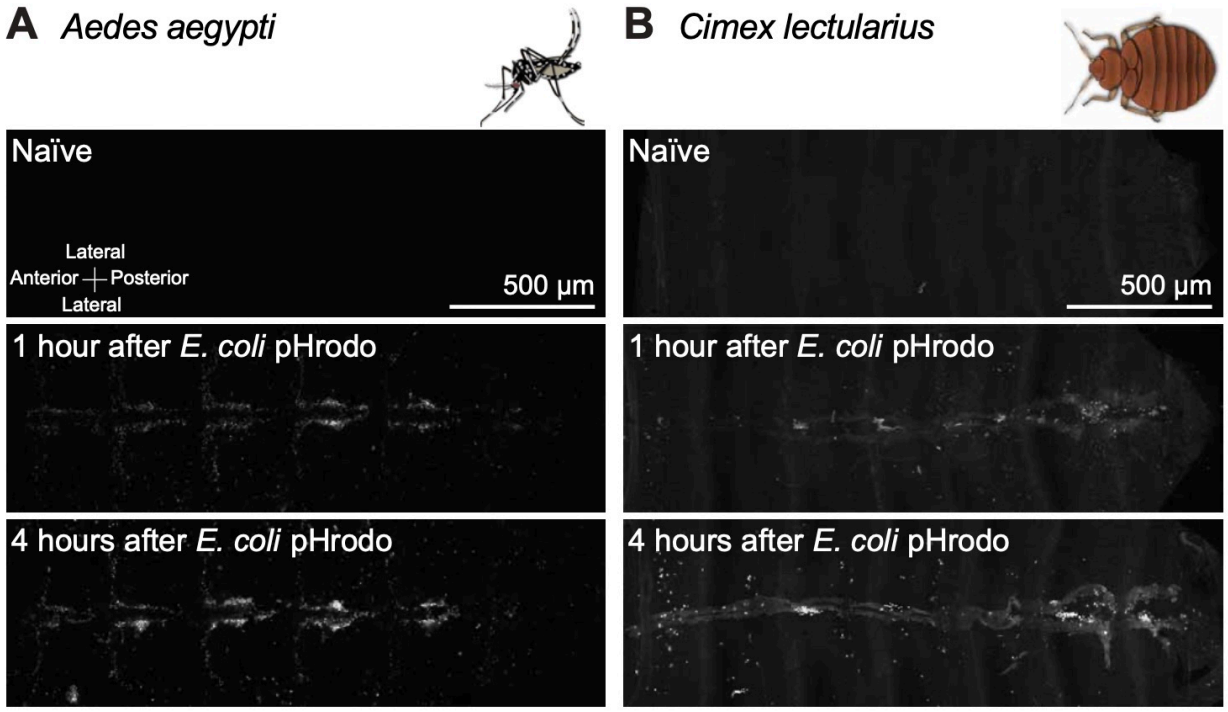

Figure 3 Heart-associated hemocytes phagocytose bacteria in *Aedes aegypti* and *Cimex lectularius*.
A, B. Phagocytosis of *E. coli*-pHrodo by the hemocytes of *Ae. aegypti* (**A**) and *C. lectularius* (**B**). Insects were imaged prior to injection (naïve; negative control) or at 1 hour and 4 hours after injection with *E. coli*-pHrodo. Fluorescence images show the entire length of the dorsal abdomen of each insect, with the heart extending along the horizontal midline. The heart-associated hemocytes, as well as other sessile hemocytes dispersed throughout the abdomen, actively phagocytose pathogens that circulate with the hemolymph.

Hemocytes and pathogens aggregate on the hearts of taxonomically diverse insects

Given that periostial hemocyte aggregation occurs in both holometabolous mosquitoes and hemimetabolous bed bugs, we next sought to assess whether periostial immune responses occur throughout the class Insecta. We initiated this comprehensive survey by infecting field-collected *Anopheles punctipennis* (Diptera: Anophelinae), *Aedes albopictus* (Diptera: Culicinae) and *Culex* sp. (Diptera: Culicinae) with GFP-expressing *E. coli* to induce the hemocyte aggregation response. Following hemocyte labeling with CM-DiI, we bisected the mosquito's abdomen, and visualized the distribution of hemocytes and pathogens on (i) the tubular heart that extends across the dorsal tergum and (ii) the ventral nerve cord that extends across the ventral sternum (Figure 1). Both the dorsal and ventral sides of the abdomen were examined because the ventral nerve cord mirrors the location of the heart but is not in a region of high hemolymph flow (31). Therefore, if an interaction between the immune and circulatory systems were to exist, hemocytes and pathogens would aggregate on the heart but not the ventral nerve cord. Much like we discovered in our *An. gambiae* laboratory colony, in both anopheline and culicine mosquitoes, hemocytes and pathogens aggregate exclusively around the six pairs of cardiac ostia, and nowhere else in the tergum or sternum (Figure 4 and Appendix Q).

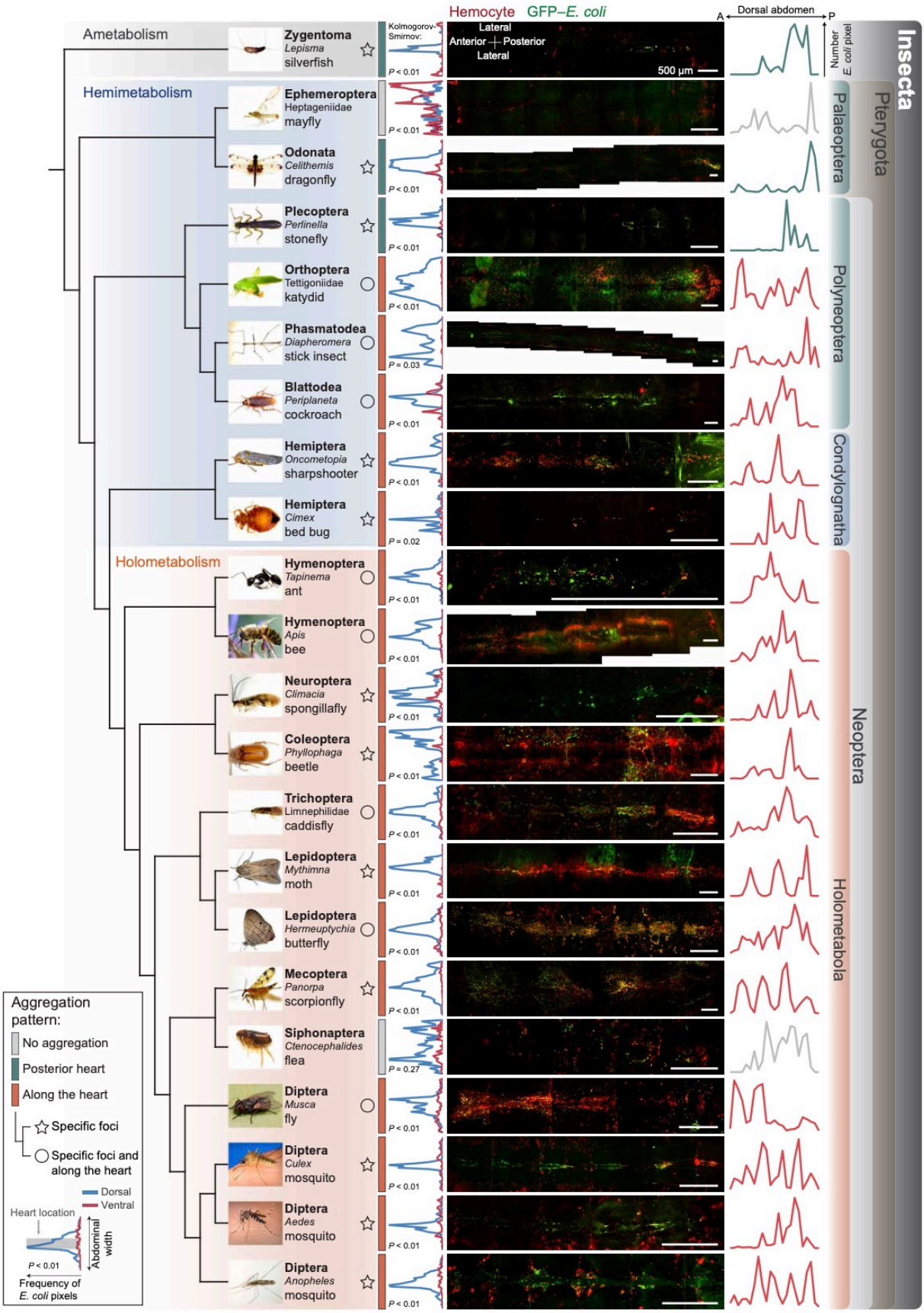
Hemocyte GFP–E. coli
Dorsal abdomen
A
P
Lateral
Anterior
Posterior
Lateral
500 µm
Kolmogorov-Smirnov:
Number of E. coli pixels
Insecta
Pterygota
Palaeoptera
Polyneoptera
Condylognatha
Neoptera
Holometabola
Ametabolism
Hemimetabolism
Holometabolism
Zygentoma
Lepisma
silverfish
Ephemeroptera
Heptageniidae
mayfly
Odonata
Celithemis
dragonfly
Plecoptera
Perlinella
stonefly
Orthoptera
Tettigoniidae
katydid
Phasmatodea
Diapheromera
stick insect
Blattodea
Periplaneta
cockroach
Hemiptera
Oncometopia
sharpshooter
Hemiptera
Cimex
bed bug
Hymenoptera
Tapinema
ant
Hymenoptera
Apis
bee
Neuroptera
Climacia
spongillafly
Coleoptera
Phyllophaga
beetle
Trichoptera
Limnephilidae
caddisfly
Lepidoptera
Mythimna
moth
Lepidoptera
Hermeuptychia
butterfly
Mecoptera
Panorpa
scorpionfly
Siphonaptera
Ctenocephalides
flea
Diptera
Musca
fly
Diptera
Culex
mosquito
Diptera
Aedes
mosquito
Diptera
Anopheles
mosquito
P < 0.01
P = 0.03
P = 0.02
P = 0.27
Aggregation pattern:
No aggregation
Posterior heart
Along the heart
Specific foci
Specific foci and along the heart
Dorsal
Ventral
Heart location
Abdominal width
P < 0.01
Frequency of E. coli pixels

Figure 4 The heart-associated immune response is a trait shared across the insect tree of life.
On the left is a selection of the insects assayed, arranged by insect phylogeny. The fluorescence images near the center show the entire length of the dorsal abdomen of each insect, with the heart extending along the horizontal midline. They show that hemocytes (red) and GFP-*E. coli* (green) aggregate and co-localize on the heart, although more than one pattern was observed (see box for key). To the immediate left of the images are frequency distributions of GFP-*E. coli* positive pixels along the lateral axis of the dorsal (blue lines) and ventral (red lines) abdomens. To the immediate right of the images are frequency distributions of GFP-*E. coli* positive pixels along the anterior-posterior axis of the dorsal abdomen. The data show that, except in the mayfly and flea, pathogens aggregate on the heart (blue peaks in the center of the leftmost graphs) and nowhere else. Moreover, peaks in the rightmost graphs show that hemocytes aggregate in the periostial regions along the length of the heart, except in silverfish, dragonflies and stoneflies, where they aggregate on the periostial regions of the posterior of the heart.

We next used the same approach to examine members of Pterygota within Holometabola (syn. Endopterygota). In 7 species in Diptera, 2 in Mecoptera, 11 in Lepidoptera, 4 in Trichoptera, 9 in Coleoptera, 1 in Neuroptera and 6 in Hymenoptera, we once again found that hemocytes and pathogens aggregate along the entire length of the heart in the dorsal abdomen and nowhere else in the body (Figure 4). Closer examination of the distribution of hemocytes and GFP-*E. coli* revealed two different patterns, but both included hemocyte aggregation around the ostia (Figure 4 and Appendix Q-V). In the first pattern, observed in scorpionflies (Mecoptera: Panorpidae), moths (Lepidoptera: Noctuidae), beetles (Coleoptera: Scarabaeidae) and spongillaflies (Neuroptera: Sisyridae), hemocytes and pathogens aggregate in specific foci on the surface of the heart in a manner that is similar to what occurs in the periostial regions of mosquitoes. In the second pattern, observed in house flies (Diptera: Muscidae), butterflies (Lepidoptera: Nymphalidae), caddisflies (Trichoptera: Limnephilidae), honeybees (Hymenoptera: Apidae) and ants (Hymenoptera: Formicidae), hemocytes and pathogens concentrate in specific foci but they are also sparsely distributed between some of the foci. We failed to

detect heart-associated immune responses in the cat flea (Siphonaptera: Pulicidae), where similar amounts of pathogens were present on the dorsal and ventral abdomen. We hypothesize that this is due to variation in circulatory physiology that is associated with the flea's laterally-flattened body shape.

Once we discovered that heart-associated immune responses occur throughout Holometabola, we investigated hemimetabolous species in Neoptera. In 6 species in Hemiptera, 3 in Blattodea, 1 in Phasmatodea, 7 in Orthoptera and 2 in Plecoptera, we confirmed that hemocyte aggregation only occurs in cardiac tissues and nowhere else in the body (Figure 4 and Appendix W-Y). Within Condylognatha, hemocytes and pathogens aggregate in specific foci on the heart of bed bugs (Hemiptera: Cimicidae) and sharpshooters (Hemiptera: Cicadellidae). Moreover, within Polyneoptera, hemocytes and pathogens are both in foci and sparsely distributed between some foci in cockroaches (Blattodea: Blattidae), walking sticks (Phasmatodea: Diapheromeridae), and katydids (Orthoptera: Tettigoniidae). The pattern seen in these Polyneoptera could be because their elaborate dorsal diaphragm provides a larger and more continuous platform for the aggregation of hemocytes (44). A completely different pattern occurs in one Polyneoptera – the stonefly (Plecoptera: Perlidae) – where hemocytes and pathogens aggregate only in the heart regions located in the posterior abdominal segments. Although plecopterans have segmental ostia (44), it is possible that their distinct pattern of hemocyte aggregation occurs because only the posterior ostia are functional. An alternative explanation is that a reduced dorsal diaphragm reduces the ability of hemocytes to adhere to the heart (229).

We then examined another hemimetabolous group: the Palaeoptera. In two dragonfly species (Odonata: Libellulidae), hemocytes and pathogens aggregate near the

posterior of the heart in a manner that resembles the aggregation pattern in mosquito larvae (Figure 4 and Appendix Y) (113). This makes sense given the parallels in circulatory physiology between dragonfly adults and mosquito larvae; odonate adults only have two pairs of abdominal ostia that are located in the posterior of the abdomen, which is similar to how mosquito larvae only allow hemolymph to enter the heart via a posterior incurrent opening (32, 44). Therefore, it appears that their circulatory physiology drives hemocytes and pathogens only to the posterior of the abdomen. A completely different pattern was observed in two mayfly species (Ephemeroptera: Heptageniidae); few hemocytes and pathogens are attached to the abdominal integument, with slightly more hemocytes in the ventral abdomen than in the dorsal abdomen (Figure 4 and Appendix Y). This suggests that heart-associated immune responses do not occur in Ephemeroptera, even though ostia are present in all or most abdominal segments (230). Because mayfly adults only live ~2 days, we hypothesize that these non-feeding and short-lived adult insects minimize their investment in immunity in favor of reproduction.

Finally, we examined wingless insects that do not undergo metamorphosis (ametabolous), and are the sister group to the Pterygota. Excitingly, infection of silverfish (Zygentoma: Lepismatidae) results in both hemocytes and pathogens distinctively aggregating within the periostial regions – especially toward the posterior end of the heart – although the strength of hemocyte aggregation is less pronounced when compared to more derived insect groups (Figure 4 and Appendix Y). The pattern observed in silverfish mirrors the pattern observed in odonates and plecopterans, raising the possibility that infection-induced hemocyte aggregation at the posterior of the heart is the pleisiomorphic

state. Taken altogether, these data show that the immune and circulatory systems are functionally integrated throughout the insect lineage.

Discussion

Significant efforts have been made to characterize the immunological mechanisms used by insects to fight infection (48), yet less attention has been paid to the structural features and functional mechanics of hemolymph propulsion (22). Moreover, until recently, how circulatory currents affect immune responses has gone ignored (22). This is surprising because the immune responses of vertebrate animals are intrinsically linked to the flow of blood and lymph (111). To address this gap in knowledge, we conducted a comprehensive survey in the class Insecta, and here show that immunologically active hemocytes are present on the hearts of holometabolous, hemimetabolous and ametabolous insects, and that an infection induces the migration of hemocytes to the periostial regions of the heart, therefore amplifying the immune response.

Although this study uncovered the physiological interaction between two major organ systems, the mechanisms governing this interaction remain mostly unknown. Thioester-containing complement-like proteins and Nimrod family proteins are immune factors that influence the migration of hemocytes to the heart of mosquitoes and fruit flies (117, 123, 125, 127). Both of these protein families are encoded in the genomes of diverse insects (186, 231), so their roles in heart-associated responses likely extend beyond Diptera. Additionally, a collagen protein that is part of the cardiac extracellular matrix, called Pericardin, facilitates the aggregation of hemocytes on the heart of fruit flies (116).

Collectively, this means that hemocyte migration to the heart is driven by a combination of immune and cardiac components.

The directional forces of circulatory currents undoubtedly facilitate how hemocytes migrate to the heart. In mosquitoes, hemocytes aggregate in the periostial regions of abdominal segments 2-7, and more precisely, in the locations of the heart that contain the incurrent ostia. Most of these hemocytes aggregate in the periostial regions of the middle abdominal segments, which are the locations of the ostia that receive the most hemolymph flow (112). In a similar circulatory pattern, the hemocytes of dragonflies and silverfish aggregate on the posterior of the heart, which is where their incurrent ostia are located (44). Given that hemocytes aggregate in areas of high hemolymph flow, it is not surprising that allatotropin, which is a neuropeptide that modulates heart rhythmicity (232), also alters the number of hemocytes present on the surface of the heart (133). Also linking immunity and circulation are nitric oxide and lysozymes. They are produced by hemocytes – including periostial hemocytes – to combat bacterial infections but they also decelerate the insect heart contraction rate (48, 120, 233, 234). Nitric oxide also has immune and circulatory functions in vertebrate animals (235, 236). Therefore, the molecular drivers of the physiological interaction between the immune and circulatory systems are undoubtedly complex, but are likely conserved across the insect lineage and beyond.

From an evolutionary perspective, insects are hexapods that are nested within a paraphyletic Crustacea, which, collectively, is called the Pancrustacea (237). Innovation in the hexapod lineage resulted in the evolution of the tracheal system and the decoupling of hemolymph circulation and gas exchange, which led to a decrease in vasculature and a simplification of the major circulatory organs (22, 238). This simplification resulted in a

dorsal vessel that contains ostia and propels hemolymph in three primary ways: (i) bidirectional flow as occurs in Diplura (a non-insect Hexapod) and wingless ametabolous insects, (ii) anterograde flow as occurs in hemimetabolous insects, and (iii) periodic alternation between anterograde and retrograde flow as occurs in holometabolous insects (22, 24). To our knowledge, no studies have investigated how non-insect hexapods (Protura, Collembola and Diplura) immunologically respond to infection. Regardless, there are many similarities in the immune and circulatory systems of insects and crustaceans (239). For example, the primary immune cells in both insects and crustaceans are hemocytes, and the major immune effector pathways are conserved between these two groups (239). Moreover, insects and crustaceans both have open circulatory systems that are composed of a hemocoel, hemolymph, and a heart that is located along the dorsal midline (22, 24). Many of the same neuropeptides (e.g., CCAP and FMRFamide-like peptides) and neurotransmitters (e.g., serotonin and octopamine) influence cardiac physiology in both animal groups (22). Given all these parallels, we hypothesize that the interaction between the circulatory and immune systems extends beyond insects and into non-insect hexapods and crustaceans. Although differences in the architecture of the circulatory systems of insects and crustaceans preclude a direct structural comparison, hemocytes populate the endothelium of the hepatic arterioles of lobsters (240), and following an infection they aggregate on the heart and arterial vessels of prawns and crabs (241, 242). In penaeid shrimp and prawns, heart contractions drive hemolymph into a lymphoid organ, where immune cells destroy circulating pathogens and release humoral immune factors into circulation (159, 243). Therefore, hemocytes in the

circulatory structures of decapod crustaceans function in a manner reminiscent of the periostial hemocytes of insects.

In conclusion, insects emerged ~480 million years, and Zygentoma diverged from Pterygota ~420 million years ago (225). The data presented herein shows the conserved association of hemocytes and immune responses on the heart of species that span the entire insect lineage. Therefore, the functional integration of the circulatory and immune systems of insects likely evolved near the origin of the insect lineage, or predates the divergence of Insecta from other Pancrustacea.

Materials and Methods

Aedes aegypti and *Cimex lectularius* colonies

Aedes aegypti Black Eye Liverpool strain were obtained from BEI Resources (Catalog No. NR-48921; Manassas, VA). Mosquitoes were maintained at 27°C and 75% relative humidity under a 12h:12h light:dark photoperiod. Adults were maintained in 2.4 L plastic buckets and fed 10% sucrose. Five-day-old female mosquitoes were used in the experiments.

Cimex lectularius were obtained from a colony maintained at Purdue University. Bed bugs were starved for 7 days or more at room temperature prior to experimental manipulations. A mixture of male and female adult bed bugs of unknown age was used.

Surveyed insects, identification, and phylogeny

Insects were collected in the wild using a sweep net or a light trap or were obtained from established laboratory colonies. Insects were identified to the family or genus level by their external morphology (Appendix Z), and insect phylogeny was inferred from Misof et. al (225). The following sources were used in the identification of insects: (1) Kaufman Field Guide to Insects of North America (244), (ii) bugguide.net, (iii) and the artificial intelligence model powered by iNaturalist or Seek apps. When identifying insects, consideration was given to their ecology, including geographic distribution, collection site, and time of year. Appendix Z details the insects used in this study, including the location and date of collection, the collectors, the infection doses, and other relevant information. Collecting done in state parks or state natural areas was done pursuant to State of Tennessee, Department of Environment and Conservation, Division of Natural Areas Scientific Study Permit No.: 2019-017. From the time of collection to the time of experimentation, insects were fed a 10% sucrose solution and maintained in a BugDorm (MegaView Science Co., Taiwan) under standard laboratory conditions.

Bacterial growth and insect infection

Tetracycline resistant, GFP-expressing *E. coli* were grown overnight in Luria-Bertani's rich nutrient medium (LB) in a 37 °C shaking incubator (New Brunswick Scientific, Edison, NJ, USA). The absorbance of GFP-*E. coli* cultures was measured spectrophotometrically and normalized to OD_{600} = 5 prior to injection. To initiate infections, insects were briefly anesthetized in a tube or Petri dish held over ice, and then intrathoracically injected using either a Nanoject III Programmable Nanoliter Injector (Drummond Scientific Company, Broomall, PA, USA) when the injected volume was < 2

μL or a calibrated micropipette (Drummond Scientific Company, Broomall, PA, USA) when the injected volume was > 2 μL. The injected volume for each insect was normalized to approximately 69 nL per 1 mg of insect weight. The absolute number of *E. coli* injected into each insect was calculated after plating dilutions of the tetracycline resistant, GFP-*E. coli* culture on an LB plate containing tetracycline and counting the resultant colony forming units.

Aedes aegypti and *Cimex lectularius* CM-DiI hemocyte staining efficiency

Mosquitoes were left unmanipulated (here termed naïve), injured by injecting 69 nL LB medium or infected by injecting 69 nL GFP-*E. coli*. One hour later, each mosquito was injected in the thorax with a solution of 67 μM CM-DiI Cell-Labeling Solution (Thermo Fisher Scientific, Waltham, MA, USA) and 1.08 mM Hoechst 33342 (Thermo Fisher Scientific) in PBS until its abdomen became expanded. This protocol specifically labels circulating and sessile hemocytes with CM-DiI and all cell nuclei with Hoechst 33342 (23). It was crucial that the staining solution was injected within minutes of its preparation because once the CM-DiI is placed in an aqueous environment its hemocyte staining effectiveness begins to decrease, approaching 0% after 10-15 mins of mixing (23). At 20-30 min later, the hemolymph with circulating hemocytes was perfused by making a small incision at the ventral side of the 7th abdominal segment and then injecting PBS through the thoracic anepisternal cleft. The first five drops of hemolymph that exited the abdomen were collected within a 1 cm-diameter etched ring on a glass slide. The circulating hemocytes were allowed to adhere to the slide for 20 minutes in a humidity chamber, fixed for 5 minutes by adding 4% formaldehyde in PBS, washed three times with PBS for

5 minutes each, and a coverslip was mounted using Aqua-Poly/Mount (Polysciences, Warrington, PA, USA). A similar protocol was followed for bed bugs, except that the hemolymph was perfused by making a small incision between the 6th and 7th abdominal segments and PBS was injected through the ventral thorax.

Hemocyte staining efficiency for each insect was measured by examining the first 50 hemocytes that were viewed by simultaneous differential interference contrast (DIC) and fluorescence microscopy on a Nikon 90i compound microscope connected to a Nikon Digital Sight DS-Qi1 monochrome digital camera and Nikon's Advanced Research NIS Elements software (Nikon, Tokyo, Japan). Cells were considered hemocytes if they had both a nucleus (stained with Hoechst 33342 and seen in the blue channel) and a cell membrane (seen in the DIC channel). Then, hemocytes were considered stained if they had incorporated CM-DiI (seen in the red channel). Hemocytes were distinguished from fat body cells by their significantly smaller size and the absence of large, refractive lipid droplets. Hemocytes were distinguished from the nuclei of lysed cells by examining the DIC channel; nuclei from lysed cells lack a cell membrane. Three independent trials were performed for both *Ae. aegypti* and *C. lectularius*. Combined, at least 24 mosquitoes and 15 bed bugs were analyzed per treatment group, respectively. Data were analyzed by one-way ANOVA, followed by Tukey's multiple comparison test (GraphPad Prism, San Diego, CA).

In vivo hemocyte staining and dissection of the dorsal and ventral abdomen

For all insects employed in this study, at 1 or 4 hours following infection, hemocytes were stained *in vivo* using Vybrant CM-DiI as described above. Then, each insect was

fixed for 10 minutes by injecting 16% formaldehyde into the hemocoel until the abdomen began to expand. The head and thorax of each insect were separated from the abdomen using a razor blade, and for insects collected in the wild, the head and thorax were stored in denatured ethanol at -20 °C in case further identification was required. The abdomen was then bisected along a coronal plane, immersed in PBS containing 0.1% Triton X-100, and the internal organs were removed. The dorsal abdomen (containing the heart) and the ventral abdomen (containing the ventral nerve cord) were rinsed briefly in PBS and mounted between a glass slide and a coverslip using Aqua-Poly/Mount. It is important to note that some insects were processed at 1 hour after infection whereas others were processed at 4 hours after infection. For species that were processed at both timepoints, the results were similar, except that stronger aggregations were sometimes seen at 4 hours.

Visualization and quantification of hemocyte aggregation on the heart of *Aedes aegypti* and *Cimex lectularius*

The dissected dorsal abdomens of naïve, injured and GFP-*E. coli*-infected *Ae. aegypti* and *C. lectularius* were imaged under bright-field and fluorescence illumination. Z-stacks were acquired using a linear encoded Z-motor, and for image presentation, all images within a stack were combined into a two-dimensional, focused image using the Extended Depth of Focus (EDF) function in NIS Elements.

The heart-associated hemocytes were counted manually by examining all images within a Z-stack. A cell was counted as a heart-associated hemocyte if it resided near the dorsal vessel and was labeled with both CM-DiI and Hoechst 33342. The heart-

associated hemocytes were counted in abdominal segments 2-7 in *Ae. aegypti* and 1-7 in *C. lectularius*. The heart-associated hemocytes in segment 1 of *Ae. aegypti* were not counted because this is the location of the thoraco-abdominal ostia. This region is structurally conserved across the dipteran lineage and its circulatory physiologically is different from the other abdominal segments, and is a location where few hemocytes are located (27, 34). Three independent trials were performed for both *Ae. aegypti* and *C. lectularius*. Combined, at least 21 mosquitoes and 16 bed bugs were analyzed per treatment group, respectively. Data were analyzed by one-way ANOVA, followed by Tukey's multiple comparison test.

Visualization of the phagocytic activity of heart-associated hemocytes in *Aedes aegypti* and *Cimex lectularius*

E. coli bacterial bioparticles conjugated to pHrodo-Red (Thermo Fisher Scientific) were reconstituted in PBS at 2 mg/mL. *Ae. aegypti* and *C. lectularius* were injected with 0.4 μL and 1 μL of pHrodo-Red *E. coli*, respectively. At 1 hour and 4 hours post-challenge, each insect was injected with 16% formaldehyde and the dorsal abdomen was dissected and mounted as described above. Insects that were not injected were used as negative controls. Each dorsal abdomen was visualized under bright-field and fluorescence illumination, and images were acquired as detailed above. All images within a Z-stack were combined into a focused image using the EDF function in NIS Elements, and the pHrodo-Red channel was exported in monochrome. This experiment was replicated in 3-4 insects per treatment group for each species.

Visualization and quantification of hemocytes and pathogens in surveyed insects

Each dissected dorsal and ventral abdomen from an infected insect was imaged under bright-field and fluorescence illumination as described above. Each side of the abdomen was first imaged under low magnification to examine the distribution of hemocytes and GFP-*E. coli* over the entire length of the heart or the ventral nerve cord. Then, a region of the heart – and specifically, a periostial region where the ostia were clearly visible – was examined under high magnification to more clearly visualize the aggregation pattern of both hemocytes and GFP-*E. coli*. When an abdomen was too long to fit in a single frame at the lowest magnification, multiple images along the abdomen were acquired, and the images were stitched together using Adobe Photoshop CC 2019 (San Jose, CA, USA).

The aggregation pattern of hemocytes and pathogens was determined by examining the overlay of three fluorescence channels – red for hemocytes, green for GFP-*E. coli* and blue for cell nuclei – relative to the position of the heart, as identified in the Z-stacks by bright-field imaging and the cell nuclei fluorescence channel. The judgement of where immune responses occur was based primarily on the GFP-*E. coli* channel because hemocyte staining in insects collected in the wild is noisier and less efficient than in mosquitoes reared in our laboratory. For quantitative analysis of the distribution of GFP-*E. coli*, ImageJ was used to count the pixels that contained GFP-*E. coli* signal in EDF images of the entire dorsal and ventral abdomen (Figure 4 and Appendix Q-Y). These pixels were defined as the pixels with intensities above the threshold that distinguished GFP emitted by *E. coli* from background fluorescence. Quantitative analyses measured two different types of fluorescence distribution. To create

the graphs to the left of the fluorescence images in figure 4, images were collapsed along the insect's anterior-posterior axis such that the number of pixels within a horizontal row that had fluorescence intensity values above the threshold were counted, and the frequency of GFP-*E. coli* pixels was plotted along the width (laterally, from side to side) of the dorsal (blue line) and ventral (red line) abdomen, with the heart and ventral nerve cord on the horizontal midline of each graph. This informs on (i) the relative distribution of fluorescence in the dorsal and ventral sides, and (ii) whether fluorescence is concentrated on the heart (blue line with peak in the center) or is evenly distributed throughout the abdomen (blue line with no peak in the center). The frequency distribution of *E. coli* in the dorsal and ventral abdomen was compared by two-sample Kolmogorov-Smirnov test in the R software. To create the graphs to the right of the fluorescence images in figure 4, images were collapsed along the insect's left-right (lateral) axis such that the number of pixels within a vertical column that had fluorescence intensity values above the threshold were counted, and the frequency of GFP-*E. coli* was plotted along the length of the dorsal abdomen, with the anterior of the abdomen on the left and the posterior on the right. Together with the leftmost graphs showing heart-associated aggregation, the rightmost graphs in figure 4 inform on whether the GFP-*E. coli* does not aggregate, or aggregates (i) in foci at the periostial regions (vertical peaks with valleys), (ii) in both foci and also along the length of the heart (vertical peaks but no consistent valleys), or (iii) at the posterior of the heart (peaks only on the right). Finally, the pictures of the whole insects presented in figure 4 were either taken by the authors or acquired from the public domain.

CHAPTER VI

Conclusions and future directions

Substantial efforts have been made to characterize the insect immune system, but fewer studies have focused on the mechanics of hemolymph circulation (22, 48). The question of how the immune system interacts with the circulatory system in insects has gone largely ignored. This is surprising because in mammals, the immune and circulatory systems are intrinsically integrated, as exemplified by the immune functions of the spleen and lymph nodes (111). At the onset of this dissertation, we had gained an understanding of the mechanics of this interaction in *A. gambiae* mosquitoes (23, 112, 113), but the genetic mechanisms that drive periostial immune responses remained largely unknown. To fill this gap of knowledge, chapters II-IV of this dissertation determined several genetic factors in *A. gambiae* that drive immune responses on the heart, including pattern recognition receptors, immune signaling pathways and its associated regulators. This chapter integrates these findings with existing literature and discusses the genetic network that drive periostial hemocyte aggregation. Furthermore, chapter V shows that this integration between the immune and circulatory systems is not restricted to mosquitoes, but is evolutionarily conserved in all major lineages within class Insecta. Following this up, the current chapter proposes future directions to explore this integration of the insect's immune and circulatory systems.

The genetic mechanisms of periostial hemocyte aggregation

Pattern recognition receptors detect invading pathogens in the hemocoel and activate immune responses (245). Thioester-containing proteins (TEPs) are examples of such receptors that directly bind and opsonize malaria parasites and bacteria, which leads pathogen death via phagocytosis, melanization and lysis (63, 64, 69, 71, 129). Chapter II determined that TEP1, TEP3 and TEP4 positively regulate immune responses on the heart. Given the functions of TEP proteins, we hypothesize that TEP1, TEP3 and TEP4 opsonize pathogens and trigger the periostial hemocyte aggregation response.

After recognizing the pathogens, immune signaling pathways are activated (48). To determine the signaling pathways that activate periostial hemocyte aggregation, chapter III utilized RNAseq and identified that multiple components of the IMD and JNK pathways are highly expressed in periostial hemocytes during infection. RNAi-based knockdown showed that both the IMD and JNK pathways positively regulate the heart-associated immune response.

The RNAseq analysis from chapter III provided a large number of candidate genes that regulate the immune responses on the heart, including two transglutaminase genes *TGase1* and *TGase3*. Chapter IV investigated all three *TGase* genes in *A. gambiae* and determined that TGase1 and TGase2 are not involved in the heart-associated immunity, but TGase3 negatively regulates periostial hemocyte aggregation. In *Drosophila*, transglutaminase inhibits the IMD pathway by preventing the activity of the transcription factor (215, 216). Based on the positive role of the IMD pathway in periostial hemocyte

aggregation, as shown in chapter III, we hypothesize that TGase3 negatively regulates the periostial hemocyte aggregation response via inhibiting the IMD pathway.

In summary, chapters II-IV determined that periostial hemocyte aggregation in *A. gambiae* is positively driven by TEP1, TEP3, TEP4 and the IMD/JNK pathways, whereas it is negatively regulated by TGase3. A prior study also showed that members of the Nimrod family – Eater and Draper – positively regulate periostial hemocyte aggregation in *A. gambiae* (123). Both are transmembrane proteins that function as receptors, but Eater is involved in hemocyte adhesion and phagocytosis, whereas Draper degrades phagocytosed pathogens or apoptosis tissues (54, 125, 171, 172).

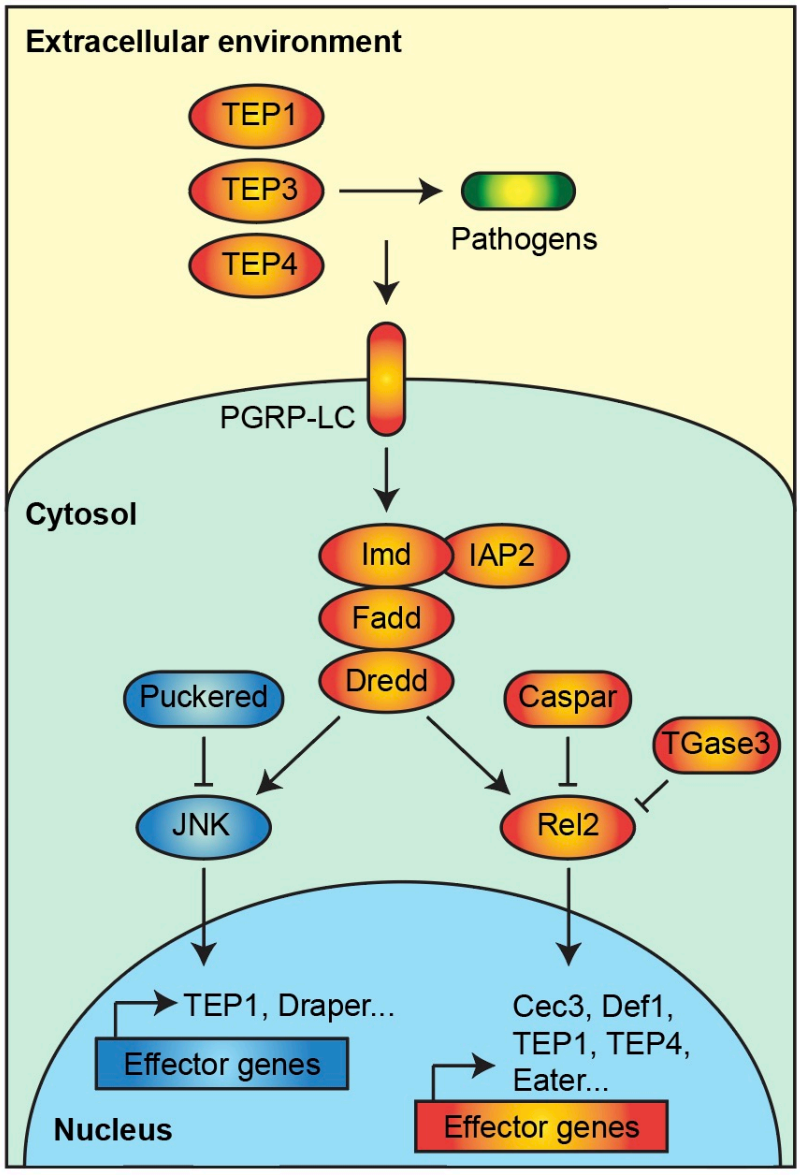

Figure 1 Schematic illustration shows the genetic mechanisms that drive the interaction between the immune and circulatory systems in *A. gambiae mosquitoes*. Invading pathogens are recognized and opsonized by TEP1, TEP3 and TEP4. The opsonized pathogens bind with PGRP-LC and trigger the signaling cascade in the IMD pathway. The transcription factor of the IMD pathway, Rel2, induces effector genes that further enhance the periostial hemocyte aggregation response. Within the IMD pathway, Caspar and TGase3 negatively regulate the periostial hemocyte aggregation response. The IMD pathway also bifurcates into the JNK pathway, and the activated JNK1/JNK3 phosphorylates transcription factors, which further induce effector genes and hemocyte adhesion and phagocytosis. The periostial hemocyte aggregation response is also inhibited by the negative regulator of the JNK pathway, Puckered. This illustration is modified from Hillyer, 2016 (48).

The research in this dissertation expanded what is known about the genetic factors that drive periostial hemocyte aggregation. Mechanistically, I hypothesize that the initiation of the periostial hemocyte aggregation response requires that the TEP proteins – TEP1, TEP3 and TEP4 – recognize and opsonize the pathogens (Figure 1). The opsonized pathogens are further recognized by the transmembrane receptor, PGRP-LC. PGRP-LC undergoes conformational changes and activates the downstream signaling cascade of the IMD pathway, which involves Imd, Fadd, Dredd, Iap2, Tak1/Tab2 and IKK complex. This eventually leads the transcription factor, Rel2, to disassociate from its inhibitor Caspar, translocate into the nucleus and bind with the promoter sequence of effector genes. However, TGase3 can cross-link Rel2 protein to prevent its nuclear translocation and adds amines to the DNA-binding sites, inhibiting their transcriptional activity. Despite TGase3 preventing Rel2 from over-activating the IMD pathway, infection still leads to successful translocation of Rel2 proteins to the nucleus, where they induce the production of effector molecules, such as TEP1, TEP4 and different antimicrobial peptides (15, 82, 143). TEP1 further activates its associated phagocytosis cascade that involves TEP1-TEP3-LRP1-CED6L, whereas TEP4 activates the TEP4-BINT2-CED2L-CED5L phagocytosis cascade (107). The two downstream molecules of these cascades, LRP1 and BINT2, are transmembrane proteins that both function in hemocyte adhesion (135, 136, 160), suggesting that they have roles in binding hemocytes to the heart. The IMD pathway is also positively regulated by another PGRP protein, PGRP-LE, and over-expression of PGRP-LE increases the expression of Eater, a hemocyte adhesion protein (54, 246). Given the positive roles of the IMD pathway and Eater in periostial hemocyte aggregation, I hypothesize that the IMD pathway activates Eater and further promotes

periostial hemocyte aggregation. The IMD pathway also bifurcates into the JNK pathway. JNK1 – and potentially JNK3 – phosphorylates the transcription factors, Jun and Fos, which form a dimer and activate effector genes, such as TEP1 and Draper (98, 99, 170). TEP1 then further induces the periostial immune response via the TEP1-TEP3-LRP1-CED6L mediated phagocytosis cascade (107, 127), whereas Draper degrades the pathogens phagocytosed by periostial hemocytes (123, 171, 172). The JNK pathway and its associated periostial hemocyte aggregation response is further negatively regulated by a phosphatase, puckered (puc), which dephosphorylates and deactivated JNK proteins (247).

The above genetic mechanisms of periostial hemocyte aggregation are centered around the IMD and JNK pathways and their associated effectors. However, various infections – bacteria, fungi and malaria parasites – all induce the heart-associated immune response (23, 112), suggesting that multiple conserved immune pathways may drive periostial hemocyte aggregation. To fully capture the genetic pathways that regulate this process, it would be worthwhile to investigate the roles of the innate immune pathways, TOLL and JAK/STAT, in periostial hemocyte aggregation. One such experiment would be to overexpress each pathway in uninfected mosquitoes by silencing their respective negative regulators, *cactus* and *socs/pias*, and evaluate whether the periostial hemocyte aggregation phenotype is enhanced. Evidence also suggests that neuropeptides and hormones may influence the periostial hemocyte aggregation response (133, 179). Therefore, a future research direction could be injecting mosquitoes with neuropeptides and juvenile hormone analogs and evaluating whether the phenotype of periostial hemocyte aggregation is altered.

This dissertation predominately focused on immune genes; however, genes belonging to the circulatory functions may also play a role in the interaction between the immune and circulatory systems. In *Drosophila*, silencing one component of the cardiac extracellular matrix (ECM) proteins – Pericardin – disrupts the formation of the heart and reduces the number of hemocytes attached to the heart (116). Therefore, factors belong to the heart and its associated structures may very well impact periostial hemocyte aggregation. In mosquitoes, the structure of the cardiac ECM has not been described; however, based on the *Drosophila* model, it keeps the heart from collapsing, regulates cardiac aging, and provides attachment for aggregating hemocytes (29, 248, 249). Therefore, it would be worthwhile to investigate the structure of the cardiac ECM in mosquitoes, which can be done via electron microscopy and different antibody-based fluorescence microscopy (250-252). Then, to identify the ligands on the heart that facilitate the aggregation of hemocytes, a proteomic approach could be used (29, 253). Comparing the proteomic profile of the isolated heart between infected and uninfected mosquitoes would uncover (i) the abundance proteins of the heart and its associated tissues (e.g. cardiac ECM) and (ii) which proteins increase their abundance during infection. Because hemocytes predominately aggregate on the heart but not on other tissues (34, 52, 127), it would also be worthwhile to identify cardiac-specific proteins. This can be achieved by employing a combination of liquid extraction surface analysis (LESA) with matrix-assisted laser desorption ionization mass spectrometry imaging (MALDI MSI) (254-256). This technology is innovative because it adds a spatial distribution on a proteomic profile, which, in this case, can distinguish proteins from the heart tissues against those from the surrounding dorsal tergum. These infection-induced, cardiac-

specific proteins could be the prime candidates that regulate periostial hemocyte aggregation and investigators can follow the same RNAi-based protocol from chapters II-IV and determine their involvement in this interaction between the immune and circulatory systems.

Overall, this dissertation identified several genetic factors that drive the interaction between the immune and circulatory systems of mosquitoes. With some of the future directions I propose above, more genetic factors will be identified. As many pathogens are able to enter the hemocoel, including malaria parasites, understanding these genetic factors would help us understand how mosquitoes kill malaria parasites in the hemocoel and this can contribute to novel vector control strategies.

The conserved integration between the insect immune and circulatory systems

Prior to the onset of this dissertation, hemocytes had been observed on or in the heart of insects from Diptera, Phasmatodea and Lepidoptera (115-117, 120, 121). This suggested that the heart-associated immune response might be conserved across insect evolution. Chapter V started with two notorious insect pests, *Aedes aegypti* mosquitoes and *Cimex lectularius* bed bugs, and found that infection induces the aggregation of hemocytes in both insects. Then, chapter V further examined 68 species of insects from 51 families spanning 16 insect orders and discovered that the heart-associated immune response is conserved in all major insect lineages. This means that the functional integration between the immune and circulatory systems is conserved across the class Insecta. This study is conceptually innovative because it provides a link between the

insect's immune and circulatory systems; both have always been studied separately in insects other than *A. gambiae*. However, much more work can be done following this.

Chapter V only focused on the integration between the immune and circulatory systems in the adult stage, but it remains largely unknown whether and how the two systems are integrated throughout developmental stages across class Insecta. Holometabolous insects have larval stages that are morphologically – and in many ways physiologically – different from the adult stage. Hemimetabolous insect, on the other hand, have immature stages, called nymphs, that are morphologically – and presumably physiologically – similar as the adult stage. Therefore, it would be interesting to determine whether the aggregation pattern of hemocytes and pathogens is different among developmental stages for holometabolous insects, but similar for hemimetabolous insects. For mosquitoes, at least, the immune and circulatory systems are integrated in larvae, but this integration occurs in a different pattern than that in adults (32, 113). This direction could also be expanded to study the strength of the immune system between the immature stages and the adult stage because larvae – in the case of mosquitoes – mount a stronger immune response than adults (114). This makes sense from an evolutionarily standpoint because the immature stages have to survive all the infections to reach adulthood and reproduce, passing down their genetic materials.

While chapter V can be expanded to the immature stages, further research should also seek the origin of this integration between the immune and circulatory systems. That is, chapter V only examined species in class Insecta, future research should expand this analysis to non-insect hexapods, other crustaceans, or even beyond. This experiment would determine whether the immune and circulatory systems are functionally integrated

in those species and potentially determine the origin of this interaction between the two systems. Indeed, hemocytes have been observed populating the endothelium of the hepatic arterioles of lobsters, the heart and arterial vessels of prawns and crabs, and in a lymphoid organ in shrimp and prawns (159, 240-243). All this evidence suggests that the integration between the immune and circulatory systems predates the origin of the insect lineage and may be conserved in the Pancrustacea or beyond.

Summary

This dissertation uncovered genetic factors that drive the immune responses on the heart of African malaria mosquitoes. These heart-associated hemocytes also sequester and phagocytose malaria parasites. Therefore, the genetic factors identified here could also have implications on limiting the malaria parasites in the mosquito hemocoel and contributing to the development of novel vector control strategies. Many immune genes and pathways are conserved among insects. For example, TEP proteins, Nimrod proteins and the JNK pathway are conserved among insects (150, 184-186). Some insects in the order of Hemiptera, like kissing bug and aphids, lack some components of the IMD pathway, but they still have a functional IMD-mediated immune response (187-190). This, together with the discovery that the heart-associated immune response is conserved in all the major insect lineages, suggests that the genetic factors we identified in *A. gambiae* also play a role in the heart-associated immune response in other insects. With the advances in genetic manipulation tools, we can use these genetic factors as targets to enhance or cripple the insect immune response so that we can

preserve beneficial insects, like honeybees, or make vectors species, like Asian tiger mosquitoes and sharpshooters, unable to carry mammalian and plant pathogens, respectively.

REFERENCES

1. WHO (2014) A global brief on vector-borne diseases. (World Health Organization).
2. WHO, World malaria report 2020: 20 years of global progress and challenges. (2020).
3. WHO, UNICEF, Global vector control response 2017-2030. (2017).
4. G. Benelli, J. C. Beier, Current vector control challenges in the fight against malaria. *Acta Trop* **174**, 91-96 (2017).
5. N. M. Ferguson, Challenges and opportunities in controlling mosquito-borne infections. *Nature* **559**, 490-497 (2018).
6. M. U. G. Kraemer *et al.*, Past and future spread of the arbovirus vectors *Aedes aegypti* and *Aedes albopictus*. *Nat Microbiol* **4**, 854-863 (2019).
7. E. S. Paixão, M. G. Teixeira, L. C. Rodrigues, Zika, chikungunya and dengue: the causes and threats of new and re-emerging arboviral diseases. *BMJ Glob Health* **3**, e000530 (2018).
8. L. P. Campbell *et al.*, Climate change influences on global distributions of dengue and chikungunya virus vectors. *Phil Trans R Soc B* **370**, 20140135 (2015).
9. M. U. Kraemer *et al.*, The global distribution of the arbovirus vectors *Aedes aegypti* and *Ae. albopictus*. *Elife* **4**, e08347 (2015).
10. W. R. Shaw, F. Catteruccia, Vector biology meets disease control: using basic research to fight vector-borne diseases. *Nat Microbiol* **4**, 20-34 (2019).
11. F. Aubry *et al.*, Enhanced Zika virus susceptibility of globally invasive. *Science* **370**, 991-996 (2020).
12. H. A. Flores, S. L. O'Neill, Controlling vector-borne diseases by releasing modified mosquitoes. *Nat Rev Microbiol* **16**, 508-518 (2018).
13. E. P. Caragata *et al.*, Prospects and pitfalls: next-generation tools to control mosquito-transmitted disease. *Annu Rev Microbiol* **74**, 455-475 (2020).
14. Y. Dong, M. L. Simões, G. Dimopoulos, Versatile transgenic multistage effector-gene combinations for *Plasmodium falciparum* suppression in *Anopheles*. *Sci Adv* **6**, eaay5898 (2020).
15. Y. Dong *et al.*, Engineered *Anopheles* immunity to *Plasmodium* infection. *PLoS Pathog* **7**, e1002458 (2011).
16. A. T. Isaacs *et al.*, Transgenic *Anopheles stephensi* coexpressing single-chain antibodies resist *Plasmodium falciparum* development. *Proc Natl Acad Sci U S A* **109**, E1922-1930 (2012).
17. N. Jupatanakul *et al.*, Engineered *Aedes aegypti* JAK/STAT pathway-mediated immunity to dengue virus. *PLoS Negl Trop Dis* **11**, e0005187 (2017).
18. A. W. Franz *et al.*, Engineering RNA interference-based resistance to dengue virus type 2 in genetically modified *Aedes aegypti*. *Proc Natl Acad Sci U S A* **103**, 4198-4203 (2006).
19. W. Kim *et al.*, Ectopic expression of a cecropin transgene in the human malaria vector mosquito *Anopheles gambiae* (Diptera: Culicidae): effects on susceptibility to *Plasmodium*. *J Med Entomol* **41**, 447-455 (2004).

20. V. Kokoza *et al.*, Engineering blood meal-activated systemic immunity in the yellow fever mosquito, *Aedes aegypti*. *Proc Natl Acad Sci U S A* **97**, 9144-9149 (2000).
21. L. C. Bartholomay, K. Michel, Mosquito immunobiology: the intersection of vector health and vector competence. *Annu Rev Entomol* **63**, 145-167 (2018).
22. J. F. Hillyer, G. Pass, The insect circulatory system: structure, function, and evolution. *Annu Rev Entomol* **65**, 121-143 (2020).
23. J. G. King, J. F. Hillyer, Infection-induced interaction between the mosquito circulatory and immune systems. *PLoS Pathog* **8**, e1003058 (2012).
24. C. S. Wirkner, M. Togel, G. Pass, "The arthropod circulatory system" in Arthropod biology and evolution, A. Minelli, G. Boxshall, G. Fusco, Eds. (Springer, Berlin, 2013), chap. 14, pp. 343-391.
25. K. Sláma, Mechanical aspects of heartbeat reversal in pupae of *Manduca sexta*. *J Insect Physiol* **49**, 645-657 (2003).
26. K. Slama, T. Miller, Physiology of heartbeat reversal in diapausing pupae of the tobacco hornworm, *Manduca sexta* (Lepidoptera : Sphingidae). *Eur J Entomol* **98**, 415-431 (2001).
27. L. Wasserthal, *Drosophila* flies combine periodic heartbeat reversal with a circulation in the anterior body mediated by a newly discovered anterior pair of ostial valves and 'venous' channels. *J Exp Biol* **210**, 3707-3719 (2007).
28. D. Dulcis, R. Levine, Glutamatergic innervation of the heart initiates retrograde contractions in adult *Drosophila melanogaster*. *J Neurosci* **25**, 271-280 (2005).
29. A. Sessions *et al.*, Extracellular matrix downregulation in the *Drosophila* heart preserves contractile function and improves lifespan. *Matrix Biol* **62**, 15-27 (2017).
30. J. D. Glenn, J. G. King, J. F. Hillyer, Structural mechanics of the mosquito heart and its function in bidirectional hemolymph transport. *J Exp Biol* **213**, 541-550 (2010).
31. J. W. Andereck, J. G. King, J. F. Hillyer, Contraction of the ventral abdomen potentiates extracardiac retrograde hemolymph propulsion in the mosquito hemocoel. *PLoS One* **5**, e12943 (2010).
32. G. P. League, O. C. Onuh, J. F. Hillyer, Comparative structural and functional analysis of the larval and adult dorsal vessel and its role in hemolymph circulation in the mosquito *Anopheles gambiae*. *J Exp Biol* **218**, 370-380 (2015).
33. L. T. Sigle, J. F. Hillyer, Structural and functional characterization of the contractile aorta and associated hemocytes of the mosquito *Anopheles gambiae*. *J Exp Biol* **221** (2018).
34. L. T. Sigle, J. F. Hillyer, Mosquito hemocytes associate with circulatory structures that support intracardiac retrograde hemolymph flow. *Front Physiol* **9**, 1187 (2018).
35. R. T. Chintapalli, J. F. Hillyer, Hemolymph circulation in insect flight appendages: physiology of the wing heart and circulatory flow in the wings of the mosquito *Anopheles gambiae*. *J Exp Biol* **219**, 3945-3951 (2016).
36. S. Boppana, J. F. Hillyer, Hemolymph circulation in insect sensory appendages: functional mechanics of antennal accessory pulsatile organs (auxiliary hearts) in the mosquito *Anopheles gambiae*. *J Exp Biol* **217**, 3006-3014 (2014).
37. T. Ichikawa, Mechanism of hemolymph circulation in the pupal leg of tenebrionid beetle *Zophobas atratus*. *Comp Biochem Physiol A Mol Integr Physiol* **153**, 174-180 (2009).

38. H. Krenn, G. Pass, Morphological diversity and phylogenetic analysis of wing circulatory organs in insects, part II. Holometabola. *Zoology* **98**, 147-164 (1994).
39. G. Pass, M. Togel, H. Krenn, A. Paululat, The circulatory organs of insect wings: Prime examples for the origin of evolutionary novelties. *Zoologischer Anzeiger* **256**, 82-95 (2015).
40. S. da Silva, R. da Silva, A. Lange, Effects of crustacean cardioactive peptide on the hearts of two Orthopteran insects, and the demonstration of a Frank-Starling-like effect. *Gen Comp Endocrinol* **171**, 218-224 (2011).
41. W. K. Lee, J. J. Socha, Direct visualization of hemolymph flow in the heart of a grasshopper (*Schistocerca americana*). *BMC Physiol* **9**, 2 (2009).
42. B. Gereben-Krenn, G. Pass, Circulatory organs of Diplura (Hexapoda): the basic design in Hexapoda? *Int J Insect Morphol Embryol* **28**, 71-79 (1999).
43. B. Gereben-Krenn, G. Pass, Circulatory organs of abdominal appendages in primitive insects (Hexapoda : Archaeognatha, Zygentoma and Ephemeroptera). *Acta Zool* **81**, 285-292 (2000).
44. G. Pass *et al.*, Phylogenetic relationships of the orders in Hexapoda: contributions from the circulatory organs for a morphological data matrix. *Arthropod Syst Phylo* **64**, 165-203 (2006).
45. M. Strand, The insect cellular immune response. *Insect Sci* **15**, 1-14 (2008).
46. J. F. Hillyer, "Mosquito Immunity" in Invertebrate Immunity, K. Söderhäll, Ed. (Springer US, Boston, MA, 2010), pp. 218-238.
47. C. M. Cirimotich, Y. Dong, L. S. Garver, S. Sim, G. Dimopoulos, Mosquito immune defenses against *Plasmodium* infection. *Dev Comp Immunol* **34**, 387-395 (2010).
48. J. F. Hillyer, Insect immunology and hematopoiesis. *Dev Comp Immunol* **58**, 102-118 (2016).
49. J. Hillyer, S. Schmidt, B. Christensen, Rapid phagocytosis and melanization of bacteria and *Plasmodium* sporozoites by hemocytes of the mosquito *Aedes aegypti*. *J Parasitol* **89**, 62-69 (2003).
50. J. Hillyer, S. Schmidt, B. Christensen, Hemocyte-mediated phagocytosis and melanization in the mosquito *Armigeres subalbatus* following immune challenge by bacteria. *Cell Tissue Res* **313**, 117-127 (2003).
51. J. Hillyer, M. Strand, Mosquito hemocyte-mediated immune responses. *Curr Opin Insect Sci.* **3**, 14-21 (2014).
52. J. G. King, J. F. Hillyer, Spatial and temporal in vivo analysis of circulating and sessile immune cells in mosquitoes: hemocyte mitosis following infection. *BMC Biol* **11**, 55 (2013).
53. R. Márkus *et al.*, Sessile hemocytes as a hematopoietic compartment in *Drosophila melanogaster*. *Proc Natl Acad Sci U S A* **106**, 4805-4809 (2009).
54. A. Bretscher *et al.*, The Nimrod transmembrane receptor Eater is required for hemocyte attachment to the sessile compartment in *Drosophila melanogaster*. *Biol Open* **4**, 355-363 (2015).
55. D. T. Babcock *et al.*, Circulating blood cells function as a surveillance system for damaged tissue in *Drosophila* larvae. *Proc Natl Acad Sci U S A* **105**, 10017-10022 (2008).

56. J. C. Castillo, A. E. Robertson, M. R. Strand, Characterization of hemocytes from the mosquitoes *Anopheles gambiae* and *Aedes aegypti*. *Insect Biochem Mol Biol* **36**, 891-903 (2006).
57. J. F. Hillyer, B. M. Christensen, Characterization of hemocytes from the yellow fever mosquito, *Aedes aegypti*. *Histochem Cell Biol* **117**, 431-440 (2002).
58. M. Severo *et al.*, Unbiased classification of mosquito blood cells by single-cell genomics and high-content imaging. *Proc Natl Acad Sci U S A* **115**, E7568-E7577 (2018).
59. H. Kwon, M. Mohammed, O. Franzén, J. Ankarklev, R. C. Smith, Single-cell analysis of mosquito hemocytes identifies signatures of immune cell subtypes and cell differentiation. *bioRxiv*, 2020.2007.2011.197939 (2021).
60. H. Kwon, R. Smith, Chemical depletion of phagocytic immune cells in *Anopheles gambiae* reveals dual roles of mosquito hemocytes in anti-*Plasmodium* immunity. *Proc Natl Acad Sci U S A* **116**, 14119-14128 (2019).
61. S. Das, Y. Dong, L. Garver, G. Dimopoulos, *Specificity of the innate immune system: a closer look at the mosquito pattern-recognition receptor repertoire* (Oxford University Press: New York, NY, USA, 2009).
62. R. Waterhouse *et al.*, Evolutionary dynamics of immune-related genes and pathways in disease-vector mosquitoes. *Science* **316**, 1738-1743 (2007).
63. S. Blandin *et al.*, Complement-like protein TEP1 is a determinant of vectorial capacity in the malaria vector *Anopheles gambiae*. *Cell* **116**, 661-670 (2004).
64. M. Fraiture *et al.*, Two mosquito LRR proteins function as complement control factors in the TEP1-mediated killing of *Plasmodium*. *Cell Host Microbe* **5**, 273-284 (2009).
65. T. Habtewold, M. Povelones, A. M. Blagborough, G. K. Christophides, Transmission blocking immunity in the malaria non-vector mosquito *Anopheles quadriannulatus* species A. *PLoS Pathog* **4**, e1000070 (2008).
66. S. Blandin, E. Marois, E. Levashina, Antimalarial responses in *Anopheles gambiae*: From a complement-like protein to a complement-like pathway. *Cell Host Microbe* **3**, 364-374 (2008).
67. C. Mitri *et al.*, An evolution-based screen for genetic differentiation between Anopheles sister taxa enriches for detection of functional immune factors. *PLoS Pathog* **11**, e1005306 (2015).
68. A. Molina-Cruz *et al.*, *Plasmodium* evasion of mosquito immunity and global malaria transmission: The lock-and-key theory. *Proc Natl Acad Sci U S A* **112**, 15178-15183 (2015).
69. M. Povelones, L. M. Upton, K. A. Sala, G. K. Christophides, Structure-function analysis of the *Anopheles gambiae* LRIM1/APL1C complex and its interaction with complement C3-like protein TEP1. *PLoS Pathog* **7**, e1002023 (2011).
70. H. Yassine, L. Kamareddine, S. Chamat, G. Christophides, M. Osta, A serine protease homolog negatively regulates TEP1 consumption in systemic infections of the malaria vector *Anopheles gambiae*. *J Innate Immun* **6**, 806-818 (2014).
71. M. Povelones, R. Waterhouse, F. Kafatos, G. Christophides, Leucine-rich repeat protein complex activates mosquito complement in defense against *Plasmodium* parasites. *Science* **324**, 258-261 (2009).

72. J. L. Ramirez, E. J. Muturi, L. B. Flor-Weiler, K. Vermillion, A. P. Rooney, Peptidoglycan recognition proteins (PGRPs) modulates mosquito resistance to fungal entomopathogens in a fungal-strain specific manner. *Front Cell Infect Microbiol* **9**, 465 (2019).
73. S. Wang, B. Beerntsen, Functional implications of the peptidoglycan recognition proteins in the immunity of the yellow fever mosquito, *Aedes aegypti*. *Insect Mol Biol* **24**, 293-310 (2015).
74. Y. Dong *et al.*, *Anopheles gambiae* immune responses to human and rodent *Plasmodium* parasite species. *PLoS Pathog* **2**, e52 (2006).
75. G. Volohonsky *et al.*, Transgenic expression of the anti-parasitic factor TEP1 in the malaria mosquito *Anopheles gambiae*. *PLoS Pathog* **13**, e1006113 (2017).
76. Y. Dong, M. L. Simões, E. Marois, G. Dimopoulos, CRISPR/Cas9 -mediated gene knockout of *Anopheles gambiae FREP1* suppresses malaria parasite infection. *PLoS Pathog* **14**, e1006898 (2018).
77. M. Simoes *et al.*, The *Anopheles* FBN9 immune factor mediates *Plasmodium* species-specific defense through transgenic fat body expression. *Dev Comp Immunol* **67**, 257-265 (2017).
78. A. Clayton, Y. Dong, G. Dimopoulos, The *Anopheles* innate immune system in the defense against malaria infection. *J Innate Immun* **6**, 169-181 (2014).
79. S. Meister *et al.*, Immune signaling pathways regulating bacterial and malaria parasite infection of the mosquito *Anopheles gambiae*. *Proc Natl Acad Sci U S A* **102**, 11420-11425 (2005).
80. L. S. Garver *et al.*, *Anopheles* Imd pathway factors and effectors in infection intensity-dependent anti-*Plasmodium* action. *PLoS Pathog* **8**, e1002737 (2012).
81. G. Carissimo *et al.*, Antiviral immunity of *Anopheles gambiae* is highly compartmentalized, with distinct roles for RNA interference and gut microbiota. *Proc Natl Acad Sci U S A* **112**, E176-E185 (2015).
82. L. S. Garver, Y. Dong, G. Dimopoulos, Caspar controls resistance to *Plasmodium falciparum* in diverse anopheline species. *PLoS Pathog* **5**, e1000335 (2009).
83. J. Ramirez, E. Muturi, A. Barletta, A. Rooney, The *Aedes aegypti* IMD pathway is a critical component of the mosquito antifungal immune response. *Dev Comp Immunol* **95**, 1-9 (2019).
84. C. Mitri *et al.*, Fine pathogen discrimination within the APL1 gene family protects *Anopheles gambiae* against human and rodent malaria species. *PLoS Pathog* **5**, e1000576 (2009).
85. T. Magalhaes, D. Leandro, C. Ayres, Knock-down of REL2, but not defensin A, augments *Aedes aegypti* susceptibility to *Bacillus subtilis* and *Escherichia coli*. *Acta trop* **113**, 167-173 (2010).
86. S. Zakovic, E. A. Levashina, NF-κB-like signaling pathway REL2 in immune defenses of the malaria vector *Anopheles gambiae*. *Front Cell Infect Microbiol* **7**, 258 (2017).
87. C. Frolet, M. Thoma, S. Blandin, J. Hoffmann, E. Levashina, Boosting NF-kappa B-dependent basal immunity of *Anopheles gambiae* aborts development of *Plasmodium berghei*. *Immunity* **25**, 677-685 (2006).
88. Z. Xi, J. L. Ramirez, G. Dimopoulos, The *Aedes aegypti* toll pathway controls dengue virus infection. *PLoS Pathog* **4**, e1000098 (2008).

89. G. Bian, S. Shin, H. Cheon, V. Kokoza, A. Raikhel, Transgenic alteration of Toll immune pathway in the female mosquito *Aedes aegypti*. *Proc Natl Acad Sci U S A* **102**, 13568-13573 (2005).
90. S. Sim, N. Jupatanakul, G. Dimopoulos, Mosquito immunity against arboviruses. *Viruses* **6**, 4479-4504 (2014).
91. Y. I. Angleró-Rodríguez *et al.*, *Aedes aegypti* molecular responses to Zika virus: modulation of infection by the Toll and Jak/Stat immune pathways and virus host factors. *Front Microbiol* **8** (2017).
92. A. R. McCrea, P. D. Jimenez Castro, R. M. Kaplan, M. Povelones, Activation of the Toll pathway in *Aedes aegypti* blocks the development of emerging third-stage larvae of drug-resistant *Dirofilaria immitis*. *Vet Parasitol* **282**, 109100 (2020).
93. V. Rhodes, M. Thomas, K. Michel, The interplay between dose and immune system activation determines fungal infection outcome in the African malaria mosquito, *Anopheles gambiae*. *Dev Comp Immunol* **85**, 125-133 (2018).
94. J. Ramirez, G. Dimopoulos, The Toll immune signaling pathway control conserved anti-dengue defenses across diverse *Ae. aegypti* strains and against multiple dengue virus serotypes. *Dev Comp Immunol* **34**, 625-629 (2010).
95. J. Souza-Neto, S. Sim, G. Dimopoulos, An evolutionary conserved function of the JAK-STAT pathway in anti-dengue defense. *Proc Natl Acad Sci U S A* **106**, 17841-17846 (2009).
96. P. Paradkar, L. Trinidad, R. Voysey, J. Duchemin, P. Walker, Secreted Vago restricts West Nile virus infection in *Culex* mosquito cells by activating the Jak-STAT pathway. *Proc Natl Acad Sci U S A* **109**, 18915-18920 (2012).
97. L. S. Garver, G. de Almeida Oliveira, C. Barillas-Mury, The JNK pathway is a key mediator of *Anopheles gambiae* antiplasmodial immunity. *PLoS Pathog* **9**, e1003622 (2013).
98. L. Souvannaseng *et al.*, Inhibition of JNK signaling in the Asian malaria vector *Anopheles stephensi* extends mosquito longevity and improves resistance to *Plasmodium falciparum* infection. *PLoS Pathog* **14**, e1007418 (2018).
99. M. J. Peirce *et al.*, JNK signaling regulates oviposition in the malaria vector *Anopheles gambiae*. *Sci Rep* **10**, 14344 (2020).
100. A. Chowdhury *et al.*, JNK pathway restricts DENV2, ZIKV and CHIKV infection by activating complement and apoptosis in mosquito salivary glands. *PLoS Pathog* **16**, e1008754 (2020).
101. U. Ramphul, L. Garver, A. Molina-Cruz, G. Canepa, C. Barillas-Mury, *Plasmodium falciparum* evades mosquito immunity by disrupting JNK-mediated apoptosis of invaded midgut cells. *Proc Natl Acad Sci U S A* **112**, 1273-1280 (2015).
102. W. Q. Liu *et al.*, The Ras/ERK signaling pathway couples antimicrobial peptides to mediate resistance to dengue virus in *Aedes* mosquitoes. *PLoS Negl Trop Dis* **14**, e0008660 (2020).
103. S. van Tol, G. Dimopoulos, "Chapter nine - influences of the mosquito microbiota on vector competence" in Advances in Insect Physiology, A. S. Raikhel, Ed. (Academic Press, 2016), vol. 51, pp. 243-291.
104. L. Gupta *et al.*, The STAT pathway mediates late-phase immunity against *Plasmodium* in the mosquito *Anopheles gambiae*. *Cell Host Microbe* **5**, 498-507 (2009).

105. S. Blandin, E. Levashina, Phagocytosis in mosquito immune responses. *Immunol Rev* **219**, 8-16 (2007).
106. A. E. Nazario-Toole, L. P. Wu, "Chapter two - phagocytosis in insect immunity" in Advances in Insect Physiology, P. Ligoxygakis, Ed. (Academic Press, 2017), vol. 52, pp. 35-82.
107. L. Moita *et al.*, In vivo identification of novel regulators and conserved pathways of phagocytosis in *A. gambiae*. *Immunity* **23**, 65-73 (2005).
108. F. Lombardo, Y. Ghani, F. C. Kafatos, G. K. Christophides, Comprehensive genetic dissection of the hemocyte immune response in the malaria mosquito *Anopheles gambiae*. *PLoS Pathog* **9**, e1003145 (2013).
109. J. Nakhleh, L. El Moussawi, M. A. Osta, "Chapter three - the melanization response in insect immunity" in Advances in Insect Physiology, P. Ligoxygakis, Ed. (Academic Press, 2017), vol. 52, pp. 83-109.
110. B. M. Christensen, J. Li, C. C. Chen, A. J. Nappi, Melanization immune responses in mosquito vectors. *Trends Parasitol* **21**, 192-199 (2005).
111. P. J. Delves, S. J. Martin, D. R. Burton, I. M. Roitt, *in Roitt's Essential Immunology* (Blackwell Publishing Ltd., West Sussex UK, 2011), vol. Chap. 7.
112. L. T. Sigle, J. F. Hillyer, Mosquito hemocytes preferentially aggregate and phagocytose pathogens in the periostial regions of the heart that experience the most hemolymph flow. *Dev Comp Immunol* **55**, 90-101 (2016).
113. G. P. League, J. F. Hillyer, Functional integration of the circulatory, immune, and respiratory systems in mosquito larvae: pathogen killing in the hemocyte-rich tracheal tufts. *BMC Biol* **14**, 78 (2016).
114. G. P. League, T. Y. Estévez-Lao, Y. Yan, V. A. Garcia-Lopez, J. F. Hillyer, *Anopheles gambiae* larvae mount stronger immune responses against bacterial infection than adults: evidence of adaptive decoupling in mosquitoes. *Parasit Vectors* **10**, 367 (2017).
115. S. Ghosh, A. Singh, S. Mandal, L. Mandal, Active hematopoietic hubs in *Drosophila* adults generate hemocytes and contribute to immune response. *Dev Cell* **33**, 478-488 (2015).
116. D. Cevik, M. Acker, C. Michalski, J. R. Jacobs, Pericardin, a *Drosophila* collagen, facilitates accumulation of hemocytes at the heart. *Dev Biol* **454**, 52-65 (2019).
117. L. Horn, J. Leips, M. Starz-Gaiano, Phagocytic ability declines with age in adult *Drosophila* hemocytes. *Aging Cell* **13**, 719-728 (2014).
118. M. Elrod-Erickson, S. Mishra, D. Schneider, Interactions between the cellular and humoral immune responses in *Drosophila*. *Curr Biol* **10**, 781-784 (2000).
119. P. Sanchez Bosch *et al.*, Adult *Drosophila* lack hematopoiesis but rely on a blood cell reservoir at the respiratory epithelia to relay infection signals to surrounding tissues. *Dev Cell* **51**, 787-803.e785 (2019).
120. R. da Silva, S. R. da Silva, A. B. Lange, The regulation of cardiac activity by nitric oxide (NO) in the Vietnamese stick insect, *Baculum extradentatum*. *Cell Signal* **24**, 1344-1350 (2012).
121. M. F. Pereira *et al.*, *Galleria mellonella* is an effective model to study *Actinobacillus pleuropneumoniae* infection. *Microbiology* **161**, 387-400 (2015).
122. Y. Bao *et al.*, An immune-induced Reeler protein is involved in the *Bombyx mori* melanization cascade. *Insect Biochem Mol Biol* **41**, 696-706 (2011).

123. L. T. Sigle, J. F. Hillyer, *Eater* and *draper* are involved in the periostial haemocyte immune response in the mosquito *Anopheles gambiae*. *Insect Mol Biol* **27**, 429-438 (2018).
124. E. Kurucz *et al.*, Nimrod, a putative phagocytosis receptor with EGF repeats in *Drosophila* plasmatocytes. *Curr Biol* **17**, 649-654 (2007).
125. C. Kocks *et al.*, Eater, a transmembrane protein mediating phagocytosis of bacterial pathogens in *Drosophila*. *Cell* **123**, 335-346 (2005).
126. T. Y. Estévez-Lao, J. F. Hillyer, Involvement of the *Anopheles gambiae* Nimrod gene family in mosquito immune responses. *Insect Biochem Mol Biol* **44**, 12-22 (2014).
127. Y. Yan, J. F. Hillyer, Complement-like proteins TEP1, TEP3 and TEP4 are positive regulators of periostial hemocyte aggregation in the mosquito *Anopheles gambiae*. *Insect Biochem Mol Biol* **107**, 1-9 (2019).
128. J. F. Hillyer, C. Barreau, K. D. Vernick, Efficiency of salivary gland invasion by malaria sporozoites is controlled by rapid sporozoite destruction in the mosquito haemocoel. *Int J Parasitol* **37**, 673-681 (2007).
129. E. A. Levashina *et al.*, Conserved role of a complement-like protein in phagocytosis revealed by dsRNA knockout in cultured cells of the mosquito, *Anopheles gambiae*. *Cell* **104**, 709-718 (2001).
130. S. A. Coggins, T. Y. Estévez-Lao, J. F. Hillyer, Increased survivorship following bacterial infection by the mosquito *Aedes aegypti* as compared to *Anopheles gambiae* correlates with increased transcriptional induction of antimicrobial peptides. *Dev Comp Immunol* **37**, 390-401 (2012).
131. K. J. Livak, T. D. Schmittgen, Analysis of relative gene expression data using real-time quantitative PCR and the $2^{-\Delta\Delta C^T}$ method. *Methods* **25**, 402-408 (2001).
132. K. Michel, A. Budd, S. Pinto, T. J. Gibson, F. C. Kafatos, *Anopheles gambiae* SRPN2 facilitates midgut invasion by the malaria parasite *Plasmodium berghei*. *EMBO Rep* **6**, 891-897 (2005).
133. S. Hernández-Martínez *et al.*, Allatotropin: A pleiotropic neuropeptide that elicits mosquito immune responses. *PLoS One* **12**, e0175759 (2017).
134. E. F. Stone *et al.*, The circadian clock protein timeless regulates phagocytosis of bacteria in *Drosophila*. *PLoS Pathog* **8**, e1002445 (2012).
135. L. F. Moita, G. Vriend, V. Mahairaki, C. Louis, F. C. Kafatos, Integrins of *Anopheles gambiae* and a putative role of a new beta integrin, BINT2, in phagocytosis of *E. coli*. *Insect Biochem Mol Biol* **36**, 282-290 (2006).
136. E. Mantuano, M. Jo, S. L. Gonias, W. M. Campana, Low density lipoprotein receptor-related protein (LRP1) regulates Rac1 and RhoA reciprocally to control Schwann cell adhesion and migration. *J Biol Chem* **285**, 14259-14266 (2010).
137. M. S. Severo, E. A. Levashina, Mosquito defenses against *Plasmodium* parasites. *Curr Opin Insect Sci* **3**, 30-36 (2014).
138. R. C. Smith, J. Vega-Rodríguez, M. Jacobs-Lorena, The *Plasmodium* bottleneck: malaria parasite losses in the mosquito vector. *Mem Inst Oswaldo Cruz* **109**, 644-661 (2014).
139. S. Wang, M. Jacobs-Lorena, Genetic approaches to interfere with malaria transmission by vector mosquitoes. *Trends Biotechnol* **31**, 185-193 (2013).

140. Y. Yan, J. Hillyer, The immune and circulatory systems are functionally integrated across insect evolution. *Science Advances* **6** (2020).
141. M. Gendrin *et al.*, The peptidoglycan recognition proteins PGRPLA and PGRPLB regulate *Anopheles* immunity to bacteria and affect infection by *Plasmodium*. *J Innate Immun* **9**, 333-342 (2017).
142. H. Myllymäki, S. Valanne, M. Rämet, The *Drosophila* imd signaling pathway. *J Immunol* **192**, 3455-3462 (2014).
143. C. Luna *et al.*, Expression of immune responsive genes in cell lines from two different Anopheline species. *Insect Mol Biol* **15**, 721-729 (2006).
144. M. Boutros, H. Agaisse, N. Perrimon, Sequential activation of signaling pathways during innate immune responses in *Drosophila*. *Dev Cell* **3**, 711-722 (2002).
145. A. T. Tate, A. L. Graham, Dissecting the contributions of time and microbe density to variation in immune gene expression. *Proc Biol Sci* **284** (2017).
146. N. Silverman *et al.*, Immune activation of NF-kappaB and JNK requires *Drosophila* TAK1. *J Biol Chem* **278**, 48928-48934 (2003).
147. Z. H. Zhuang *et al.*, *Drosophila* TAB2 is required for the immune activation of JNK and NF-kappaB. *Cell Signal* **18**, 964-970 (2006).
148. J. I. Etchegaray *et al.*, Draper acts through the JNK pathway to control synchronous engulfment of dying germline cells by follicular epithelial cells. *Development* **139**, 4029-4039 (2012).
149. H. Weavers, I. R. Evans, P. Martin, W. Wood, Corpse engulfment generates a molecular memory that primes the macrophage inflammatory response. *Cell* **165**, 1658-1671 (2016).
150. A. A. Horton *et al.*, The mitogen-activated protein kinome from *Anopheles gambiae*: identification, phylogeny and functional characterization of the ERK, JNK and p38 MAP kinases. *BMC Genomics* **12**, 574 (2011).
151. G. Dimopoulos *et al.*, Genome expression analysis of *Anopheles gambiae*: responses to injury, bacterial challenge, and malaria infection. *Proc Natl Acad Sci U S A* **99**, 8814-8819 (2002).
152. S. B. Pinto *et al.*, Discovery of *Plasmodium* modulators by genome-wide analysis of circulating hemocytes in *Anopheles gambiae*. *Proc Natl Acad Sci U S A* **106**, 21270-21275 (2009).
153. L. A. Baton, A. Robertson, E. Warr, M. R. Strand, G. Dimopoulos, Genome-wide transcriptomic profiling of *Anopheles gambiae* hemocytes reveals pathogen-specific signatures upon bacterial challenge and *Plasmodium berghei* infection. *BMC Genomics* **10**, 257 (2009).
154. T. Thomas *et al.*, Hemocytome: deep sequencing analysis of mosquito blood cells in Indian malarial vector *Anopheles stephensi*. *Gene* **585**, 177-190 (2016).
155. L. C. Bartholomay *et al.*, Description of the transcriptomes of immune response-activated hemocytes from the mosquito vectors *Aedes aegypti* and *Armigeres subalbatus*. *Infect Immun* **72**, 4114-4126 (2004).
156. Y. J. Choi, J. F. Fuchs, G. F. Mayhew, H. E. Yu, B. M. Christensen, Tissue-enriched expression profiles in *Aedes aegypti* identify hemocyte-specific transcriptome responses to infection. *Insect Biochem Mol Biol* **42**, 729-738 (2012).
157. G. Raddi *et al.*, Mosquito cellular immunity at single-cell resolution. *Science* **369**, 1128-1132 (2020).

158. A. B. Leitão, É. Sucena, *Drosophila* sessile hemocyte clusters are true hematopoietic tissues that regulate larval blood cell differentiation. *Elife* **4** (2015).
159. K. Koiwai, H. Kondo, I. Hirono, The immune functions of sessile hemocytes in three organs of kuruma shrimp *Marsupenaeus japonicus* differ from those of circulating hemocytes. *Fish Shellfish Immunol* **78**, 109-113 (2018).
160. V. K. Rabiej *et al.*, Low density lipoprotein receptor-related protein 1 mediated endocytosis of β1-integrin influences cell adhesion and cell migration. *Exp Cell Res* **340**, 102-115 (2016).
161. S. Meister *et al.*, *Anopheles gambiae* PGRPLC-mediated defense against bacteria modulates infections with malaria parasites. *PLoS Pathog* **5**, e1000542 (2009).
162. M. B. Khan, J. W. Liew, C. S. Leong, Y. L. Lau, Role of NF-kβ factor Rel2 during *Plasmodium falciparum* and bacterial infection in *Anopheles dirus*. *Parasit Vectors* **9**, 525 (2016).
163. A. S. Dekmak, X. Yang, H. Zu Dohna, N. Buchon, M. A. Osta, The route of infection influences the contribution of key immunity genes to antibacterial defense in *Anopheles gambiae*. *J Innate Immun* **13**, 107-126 (2021).
164. Z. Kambris *et al.*, *Wolbachia* stimulates immune gene expression and inhibits *plasmodium* development in *Anopheles gambiae*. *PLoS Pathog* **6**, e1001143 (2010).
165. A. K. Schnitger, F. C. Kafatos, M. A. Osta, The melanization reaction is not required for survival of *Anopheles gambiae* mosquitoes after bacterial infections. *J Biol Chem* **282**, 21884-21888 (2007).
166. S. Nsango *et al.*, AP-1/Fos-TGase2 axis mediates wounding-induced *Plasmodium falciparum* killing in *Anopheles gambiae*. *J Biol Chem* **288**, 16145-16154 (2013).
167. M. J. Williams, M. L. Wiklund, S. Wikman, D. Hultmark, Rac1 signalling in the *Drosophila* larval cellular immune response. *J Cell Sci* **119**, 2015-2024 (2006).
168. C. J. Zettervall *et al.*, A directed screen for genes involved in *Drosophila* blood cell activation. *Proc Natl Acad Sci U S A* **101**, 14192-14197 (2004).
169. L. Ma *et al.*, JNK pathway plays a key role in the immune system of the pea aphid and is regulated by microRNA-184. *PLoS Pathog* **16**, e1008627 (2020).
170. J. M. Macdonald, J. Doherty, R. Hackett, M. R. Freeman, The c-Jun kinase signaling cascade promotes glial engulfment activity through activation of draper and phagocytic function. *Cell Death Differ* **20**, 1140-1148 (2013).
171. J. Manaka *et al.*, Draper-mediated and phosphatidylserine-independent phagocytosis of apoptotic cells by *Drosophila* hemocytes/macrophages. *J Biol Chem* **279**, 48466-48476 (2004).
172. I. R. Evans, F. S. Rodrigues, E. L. Armitage, W. Wood, Draper/CED-1 mediates an ancient damage response to control inflammatory blood cell migration in vivo. *Curr Biol* **25**, 1606-1612 (2015).
173. K. Nagaosa *et al.*, Integrin βv-mediated phagocytosis of apoptotic cells in *Drosophila* embryos. *J Biol Chem* **286**, 25770-25777 (2011).
174. P. N. Paradkar, J. B. Duchemin, R. Voysey, P. J. Walker, Dicer-2-dependent activation of *Culex* Vago occurs via the TRAF-Rel2 signaling pathway. *PLoS Negl Trop Dis* **8**, e2823 (2014).
175. S. Chakrabarti *et al.*, Remote control of intestinal stem cell activity by haemocytes in *Drosophila*. *PLoS Genet* **12**, e1006089 (2016).

176. H. Agaisse, U. M. Petersen, M. Boutros, B. Mathey-Prevot, N. Perrimon, Signaling role of hemocytes in *Drosophila* JAK/STAT-dependent response to septic injury. *Dev Cell* **5**, 441-450 (2003).
177. P. Qiu, P. C. Pan, S. Govind, A role for the *Drosophila* Toll/Cactus pathway in larval hematopoiesis. *Development* **125**, 1909-1920 (1998).
178. H. Chiu *et al.*, dUbc9 negatively regulates the Toll-NF-kappa B pathways in larval hematopoiesis and drosomycin activation in *Drosophila*. *Dev Biol* **288**, 60-72 (2005).
179. I. H. Kim *et al.*, A mosquito juvenile hormone binding protein (mJHBP) regulates the activation of innate immune defenses and hemocyte development. *PLoS Pathog* **16**, e1008288 (2020).
180. M. Destalminil-Letourneau, I. Morin-Poulard, Y. Tian, N. Vanzo, M. Crozatier, The vascular niche controls *Drosophila* hematopoiesis via fibroblast growth factor signaling. *Elife* **10** (2021).
181. M. Dragojlovic-Munther, J. A. Martinez-Agosto, Extracellular matrix-modulated Heartless signaling in *Drosophila* blood progenitors regulates their differentiation via a Ras/ETS/FOG pathway and target of rapamycin function. *Dev Biol* **384**, 313-330 (2013).
182. J. Iklé, J. A. Elwell, A. L. Bryantsev, R. M. Cripps, Cardiac expression of the *Drosophila Transglutaminase* (CG7356) gene is directly controlled by myocyte enhancer factor-2. *Dev Dyn* **237**, 2090-2099 (2008).
183. M. Schmid *et al.*, Insect hemolymph coagulation: Kinetics of classically and non-classically secreted clotting factors. *Insect Biochem Mol Biol* **109**, 63-71 (2019).
184. S. Blandin, E. A. Levashina, Thioester-containing proteins and insect immunity. *Mol Immunol* **40**, 903-908 (2004).
185. R. Bou Aoun *et al.*, Analysis of thioester-containing proteins during the innate immune response of *Drosophila melanogaster*. *J Innate Immun* **3**, 52-64 (2011).
186. K. Somogyi *et al.*, Evolution of genes and repeats in the Nimrod superfamily. *Mol Biol Evol* **25**, 2337-2347 (2008).
187. Y. Nishide *et al.*, Functional crosstalk across IMD and Toll pathways: insight into the evolution of incomplete immune cascades. *Proc Biol Sci* **286**, 20182207 (2019).
188. N. Salcedo-Porras, A. Guarneri, P. L. Oliveira, C. Lowenberger, *Rhodnius prolixus*: Identification of missing components of the IMD immune signaling pathway and functional characterization of its role in eliminating bacteria. *PLoS One* **14**, e0214794 (2019).
189. R. D. Mesquita *et al.*, Genome of *Rhodnius prolixus*, an insect vector of Chagas disease, reveals unique adaptations to hematophagy and parasite infection. *Proc Natl Acad Sci U S A* **112**, 14936-14941 (2015).
190. N. M. Gerardo *et al.*, Immunity and other defenses in pea aphids, *Acyrthosiphon pisum*. *Genome Biol* **11**, R21 (2010).
191. A. Dobin *et al.*, STAR: ultrafast universal RNA-seq aligner. *Bioinformatics* **29**, 15-21 (2013).
192. G. I. Giraldo-Calderón *et al.*, VectorBase: an updated bioinformatics resource for invertebrate vectors and other organisms related with human diseases. *Nucleic Acids Res* **43**, D707-713 (2015).

193. M. I. Love, W. Huber, S. Anders, Moderated estimation of fold change and dispersion for RNA-seq data with DESeq2. *Genome Biol* **15**, 550 (2014).
194. L. Lorand, R. Graham, Transglutaminases: crosslinking enzymes with pleiotropic functions. *Nat Rev Mol Cell Biol* **4**, 140-156 (2003).
195. R. Eckert *et al.*, Transglutaminase regulation of cell function. *Physiol Rev* **94**, 383-417 (2014).
196. I. Aloisi, G. Cai, D. Serafini-Fracassini, S. Del Duca, Transglutaminase as polyamine mediator in plant growth and differentiation. *Amino Acids* **48**, 2467-2478 (2016).
197. T. Shibata, S. Kawabata, Pluripotency and a secretion mechanism of *Drosophila* transglutaminase. *J Biochem* **163**, 165-176 (2018).
198. A. Dziedziech, S. Shivankar, U. Theopold, *Drosophila melanogaster* responses against entomopathogenic nematodes: focus on hemolymph clots. *Insects* **11**, 62 (2020).
199. T. Osaki, S. Kawabata, Structure and function of coagulogen, a clottable protein in horseshoe crabs. *Cell Mol Life Sci* **61**, 1257-1265 (2004).
200. Y. Matsuda *et al.*, An arthropod cuticular chitin-binding protein endows injured sites with transglutaminase-dependent mesh. *J Biol Chem* **282**, 37316-37324 (2007).
201. R. Wang, Z. Liang, M. Hal, K. Söderhall, A transglutaminase involved in the coagulation system of the freshwater crayfish, *Pacifastacus leniusculus*. Tissue localisation and cDNA cloning. *Fish Shellfish Immunol* **11**, 623-637 (2001).
202. M. Hall, R. Wang, R. van Antwerpen, L. Sottrup-Jensen, K. Soderhall, The crayfish plasma clotting protein: A vitellogenin-related protein responsible for clot formation in crustacean blood. *Proc Natl Acad Sci* **96**, 1965-1970 (1999).
203. M. Maningas, H. Kondo, I. Hirono, T. Saito-Taki, T. Aoki, Essential function of transglutaminase and clotting protein in shrimp immunity. *Mol Immunol* **45**, 1269-1275 (2008).
204. C. Chang, H. Chang, K. Liu, W. Cheng, The known two types of transglutaminases regulate immune and stress responses in white shrimp, *Litopenaeus vannamei*. *Dev Comp Immunol* **59**, 164-176 (2016).
205. Y. Zhu *et al.*, Role of transglutaminase in immune defense against bacterial pathogens via regulation of antimicrobial peptides. *Dev Comp Immunol* **55**, 39-50 (2016).
206. X. Zhao, L. Liu, W. Zhou, Q. Cai, Q. Huang, Roles of selenoprotein T and transglutaminase in active immunization against entomopathogenic fungi in the termite *Reticulitermes chinensis*. *J Insect Physiol* **125** (2020).
207. L. Liu, G. Li, P. Sun, C. Lei, Q. Huang, Experimental verification and molecular basis of active immunization against fungal pathogens in termites. *Sci Rep* **5** (2015).
208. H. Silveira *et al.*, CpG-containing oligodeoxynucleotides increases resistance of *Anopheles* mosquitoes to *Plasmodium* infection. *Insect Biochem Mol Biol* **42**, 758-765 (2012).
209. D. Rogers *et al.*, Transglutaminase-mediated semen coagulation controls sperm storage in the malaria mosquito. *PLoS Biol* **7** (2009).
210. B. V. Le *et al.*, Characterization of *Anopheles gambiae* transglutaminase 3 (AgTG3) and its native substrate Plugin. *J Biol Chem* **288**, 4844-4853 (2013).

211. B. Le *et al.*, Dihydroisoxazole inhibitors of *Anopheles gambiae* seminal transglutaminase AgTG3. *Malar J* **13** (2014).
212. M. M. A. Whitten, C. J. Coates, Re-evaluation of insect melanogenesis research: Views from the dark side. *Pigment Cell Melanoma Res* **30**, 386-401 (2017).
213. J. F. Hillyer, B. M. Christensen, Mosquito phenoloxidase and defensin colocalize in melanization innate immune responses. *J Histochem Cytochem* **53**, 689-698 (2005).
214. S. Hernández-Martínez, H. Lanz-Mendoza, J. Martínez-Barnetche, M. H. Rodríguez, Antimicrobial properties of *Anopheles albimanus* pericardial cells. *Cell Tissue Res* **351**, 127-137 (2013).
215. T. Shibata *et al.*, Transglutaminase-catalyzed protein-protein cross-linking suppresses the activity of the NF-κB–like transcription factor Relish. *Sci Signal* **6**, ra61-ra61 (2013).
216. K. Maki, T. Shibata, S. Kawabata, Transglutaminase-catalyzed incorporation of polyamines masks the DNA-binding region of the transcription factor Relish. *J Biol Chem* **292**, 6369-6380 (2017).
217. A. M. Belkin *et al.*, Transglutaminase-mediated oligomerization of the fibrin(ogen) alphaC domains promotes integrin-dependent cell adhesion and signaling. *Blood* **105**, 3561-3568 (2005).
218. V. Nelea, Y. Nakano, M. T. Kaartinen, Size distribution and molecular associations of plasma fibronectin and fibronectin crosslinked by transglutaminase 2. *Protein J* **27**, 223-233 (2008).
219. T. A. Spurlin, K. Bhadriraju, K. H. Chung, A. Tona, A. L. Plant, The treatment of collagen fibrils by tissue transglutaminase to promote vascular smooth muscle cell contractile signaling. *Biomaterials* **30**, 5486-5496 (2009).
220. D. Y. Chau, R. J. Collighan, E. A. Verderio, V. L. Addy, M. Griffin, The cellular response to transglutaminase-cross-linked collagen. *Biomaterials* **26**, 6518-6529 (2005).
221. J. Forsprecher, Z. Wang, V. Nelea, M. T. Kaartinen, Enhanced osteoblast adhesion on transglutaminase 2-crosslinked fibronectin. *Amino Acids* **36**, 747-753 (2009).
222. X. Lin, K. Soderhall, I. Soderhall, Transglutaminase activity in the hematopoietic tissue of a crustacean, *Pacifastacus leniusculus*, importance in hemocyte homeostasis. *BMC Immunol* **9** (2008).
223. K. Junkunlo, K. Soderhall, I. Soderhall, Clotting protein - An extracellular matrix (ECM) protein involved in crustacean hematopoiesis. *Dev Comp Immunol* **78**, 132-140 (2018).
224. R. Sirikharin, K. Junkunlo, K. Söderhäll, I. Söderhäll, Role of astakine1 in regulating transglutaminase activity. *Dev Comp Immunol* **76**, 77-82 (2017).
225. B. Misof *et al.*, Phylogenomics resolves the timing and pattern of insect evolution. *Science* **346**, 763-767 (2014).
226. E. M. Hystad, H. Salmela, G. V. Amdam, D. Munch, Hemocyte-mediated phagocytosis differs between honey bee (*Apis mellifera*) worker castes. *PLoS One* **12**, e0184108 (2017).

227. R. G. Chiang, J. A. Chiang, K. G. Davey, Morphology of the dorsal vessel in the abdomen of the blood-feeding insect *Rhodnius prolixus*. *J Morphol* **204**, 9-23 (1990).
228. T. A. Woolley, The circulatory system of the box elder bug *Leptocoris trivittatus* (Say). *Am Midl Nat* **46**, 634-639 (1951).
229. W. L. Nutting, A comparative anatomical study of the heart and accessory structures of the orthopteroid insects. *J Morphol* **89**, 501-597 (1951).
230. T. Gopel, C. S. Wirkner, Morphological description, character conceptualization and the reconstruction of ancestral states exemplified by the evolution of arthropod hearts. *PLoS One* **13**, e0201702 (2018).
231. I. Matetovici, J. Van Den Abbeele, Thioester-containing proteins in the tsetse fly (*Glossina*) and their response to trypanosome infection. *Insect Mol Biol* **27**, 414-428 (2018).
232. J. F. Hillyer, Insect heart rhythmicity is modulated by evolutionarily conserved neuropeptides and neurotransmitters. *Curr Opin Insect Sci* **29**, 41-48 (2018).
233. K. E. Broderick *et al.*, The nitric oxide scavenger cobinamide profoundly improves survival in a *Drosophila melanogaster* model of bacterial sepsis. *FASEB J* **20**, 1865-1873 (2006).
234. T. Y. Estevez-Lao, L. T. Sigle, S. N. Gomez, J. F. Hillyer, Nitric oxide produced by periostial hemocytes modulates the bacterial infection induced reduction of the mosquito heart rate. *J Exp Biol* **223**, jeb225821 (2020).
235. S. Smiljic, V. Nestorovic, S. Savic, Modulatory role of nitric oxide in cardiac performance. *Med Pregl* **67**, 345-352 (2014).
236. C. Bogdan, Nitric oxide synthase in innate and adaptive immunity: an update. *Trends Immunol* **36**, 161-178 (2015).
237. D. A. Legg, M. D. Sutton, G. D. Edgecombe, Arthropod fossil data increase congruence of morphological and molecular phylogenies. *Nat Commun* **4**, 2485 (2013).
238. J. F. Harrison, Handling and use of oxygen by Pancrustaceans: conserved patterns and the evolution of respiratory structures. *Integr Comp Biol* **55**, 802-815 (2015).
239. J. F. Hillyer, Integrated immune and cardiovascular function in Pancrustacea: lessons from the insects. *Integr Comp Biol* **55**, 843-855 (2015).
240. J. R. Factor, M. Naar, The digestive system of the lobster, *Homarus americanus*: II. Terminal hepatic arterioles of the digestive gland. *J Morphol* **206**, 283-291 (1990).
241. P. T. Johnson, Bacterial infection in the blue crab, *Callinectes sapidus*: course of infection and histopathology. *J Invertebr Pathol* **28**, 25-36 (1976).
242. E. Sagristà, M. Durfort, Ultrastructural study of hemocytes and phagocytes associated with hemolymphatic vessels in the hepatopancreas of *Palaemonetes zariquieyi* (Crustacea, Decapoda). *J Morphol* **206**, 173-180 (1990).
243. Rusaini, L. Owens, Insight into the lymphoid organ of penaeid prawns: a review. *Fish Shellfish Immunol* **29**, 367-377 (2010).
244. E. R. Eaton, K. Kaufman, *Kaufman Field Guide to Insects of North America* (Houghton Mifflin Company, 2007), pp. 392.

245. X. Wang, Y. Zhang, R. Zhang, J. Zhang, The diversity of pattern recognition receptors (PRRs) involved with insect defense against pathogens. *Curr Opin Insect Sci* **33**, 105-110 (2019).
246. C. O. Wong *et al.*, Lysosomal degradation is required for sustained phagocytosis of bacteria by macrophages. *Cell Host Microbe* **21**, 719-730.e716 (2017).
247. E. Martín-Blanco *et al.*, *puckered* encodes a phosphatase that mediates a feedback loop regulating JNK activity during dorsal closure in *Drosophila*. *Genes Dev* **12**, 557-570 (1998).
248. B. Rotstein, A. Paululat, On the morphology of the *Drosophila* heart. *J Cardiovasc Dev Dis* **3** (2016).
249. M. Drechsler, A. C. Schmidt, H. Meyer, A. Paululat, The conserved ADAMTS-like protein lonely heart mediates matrix formation and cardiac tissue integrity. *PLoS Genet* **9**, e1003616 (2013).
250. W. Ramos-Lewis, K. S. LaFever, A. Page-McCaw, A scar-like lesion is apparent in basement membrane after wound repair *in vivo*. *Matrix Biol* **74**, 101-120 (2018).
251. C. Lehmacher, B. Abeln, A. Paululat, The ultrastructure of *Drosophila* heart cells. *Arthropod Struct Dev* **41**, 459-474 (2012).
252. J. Na *et al.*, A *Drosophila* model of high sugar diet-induced cardiomyopathy. *PLoS Genet* **9**, e1003175 (2013).
253. A. Cammarato *et al.*, A mighty small heart: the cardiac proteome of adult *Drosophila melanogaster*. *PLoS One* **6**, e18497 (2011).
254. E. C. Randall, A. M. Race, H. J. Cooper, J. Bunch, MALDI imaging of liquid extraction surface analysis sampled tissue. *Anal Chem* **88**, 8433-8440 (2016).
255. C. Harkin *et al.*, On-tissue chemical derivatization in mass spectrometry imaging. *Mass Spectrom Rev* (2021).
256. J. G. Swales *et al.*, Spatial quantitation of drugs in tissues using liquid extraction surface analysis mass spectrometry imaging. *Sci Rep* **6**, 37648 (2016).

Appendix A

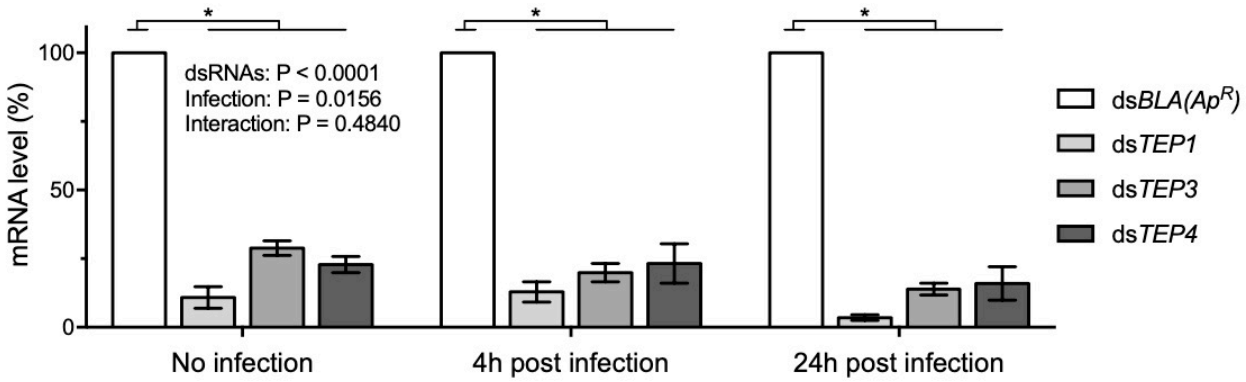

A. *TEP1*, *TEP3* and *TEP4* expression is significantly knocked down by RNAi. Columns show the average mRNA levels in dsBLA(ApR)-, dsTEP1-, dsTEP3- and dsTEP4-injected mosquitoes that were not infected or had been infected with E. coli for 4 h or 24 h. Whiskers mark the S.E.M. Data were analyzed by two-way ANOVA, followed by Dunnett's post-hoc test. Asterisks indicate $P < 0.05$.

B. Information of primers used in chapter II.

Gene	VectorBase ID[a]	Application	Sequence (forward and reverse)[b]	Amplicon (bp)[c,d]	
				Transcript	Genomic
RPS7	AGAP010592	qPCR	GACGGATCCCAGCTGATAAA	132	281
		qPCR	GTTCTCTGGGAATTCGAACG		
TEP1	AGAP010815	qPCR	GACGTCCAAATACGGATCTCA	184	NA
		qPCR	CTTTCAGGCATCACCCGTAT		
TEP3	AGAP010816	qPCR	CCCATTTAAGGATGTGGAGGT	127	NA
		qPCR	GCGGTGAAATGCTACCCTAA		
TEP4	AGAP010812	qPCR	ATTGACCACCGTTCAGCCAT	238	301
		qPCR	TAGGAACGCCACTGGAACAC		
BLA(Ap^R)	(Bacterial gene)	RNAi	TAATACGACTCACTATAGGGCCGAGCGCAGAAGTGGT	214	214
		RNAi	TAATACGACTCACTATAGGGAACCGGAGCTGAATGAA		
TEP1	AGAP010815	RNAi	TAATACGACTCACTATAGGGCTGAAAGCGCTGACCAA	358	358
		RNAi	TAATACGACTCACTATAGGGTATGTAGCTGGCACAGACC		
TEP3	AGAP010816	RNAi	TAATACGACTCACTATAGGGCAAGGAAACGGACGCAA	170	170
		RNAi	TAATACGACTCACTATAGGGAATGTCTAGTTGCATGT		
TEP4	AGAP010812	RNAi	TAATACGACTCACTATAGGGTAAAACGCTCGCCACCG	447	447
		RNAi	TAATACGACTCACTATAGGGCCCAAAAGCGCTCCGTA		

a Vectorbase IDs were obtained from the AgamP4 assembly in www.vectorbase.org (exception: *BLA(Ap^R)*).
b Underlined sequences are specific to the T7 RNA polymerase promoter sites needed for dsRNA synthesis.
c Amplicon sizes are based on the sequences in Vectorbase. For dsRNA primers, amplicon lengths include the T7 promoter sequence tags.
d "NA" indicates the primer span an exon-intron junction, thus unable to amplify from genomic DNA.

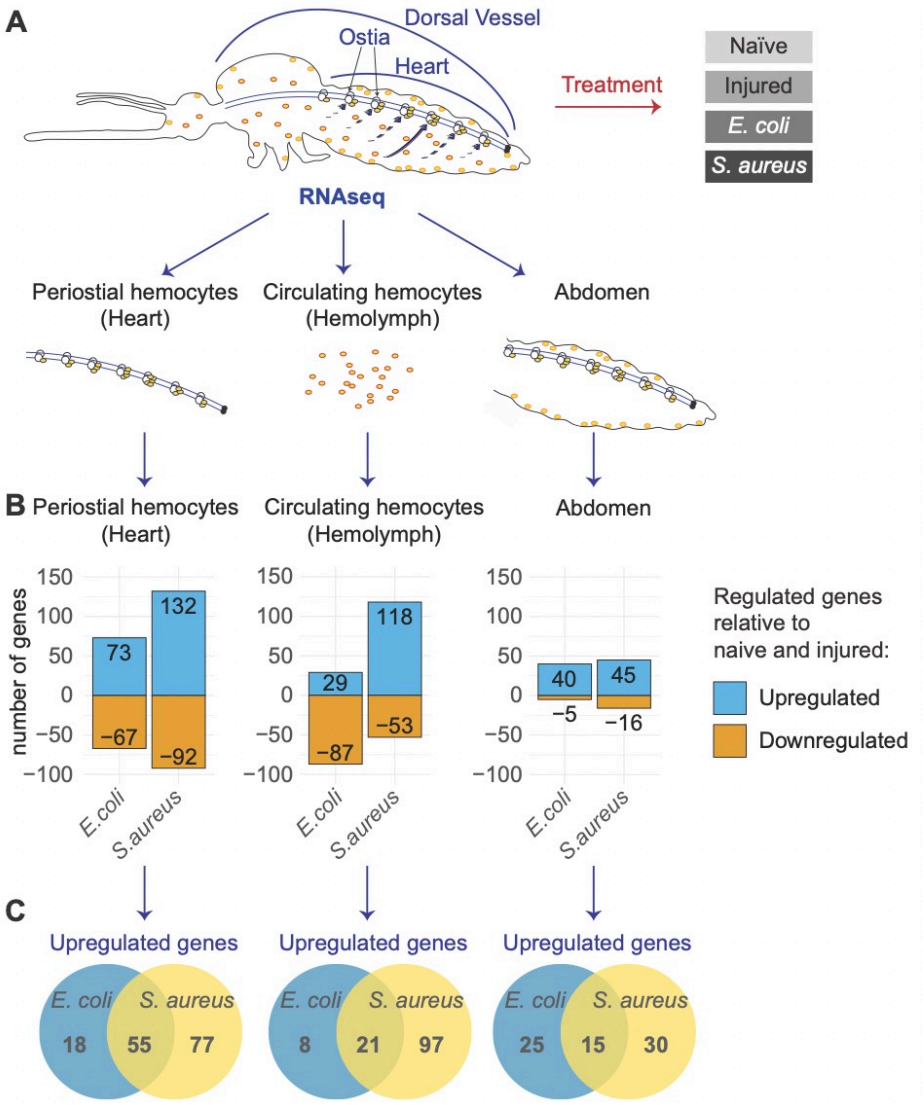

C. Infection upregulates more genes in periostial hemocytes than in circulating hemocytes or abdomen.
(*A*) The heart with periostial hemocytes, the circulating hemocytes and the abdomen of mosquitoes that were uninfected, injured, or infected with GFP-*E. coli* or *S. aureus* were sequenced by RNAseq. (*B*) Bar plot shows the number of genes significantly upregulated or downregulated at 4 hr after GFP-*E. coli* or *S. aureus* infection in the periostial hemocytes (left), the circulating hemocytes (middle), and the entire abdomen (right). (*C*) Venn diagram shows that 55, 21 and 15 genes are significantly upregulated in the periostial hemocytes, the circulating hemocytes and the abdomen, respectively, during both GFP-*E. coli* and *S. aureus* infections.

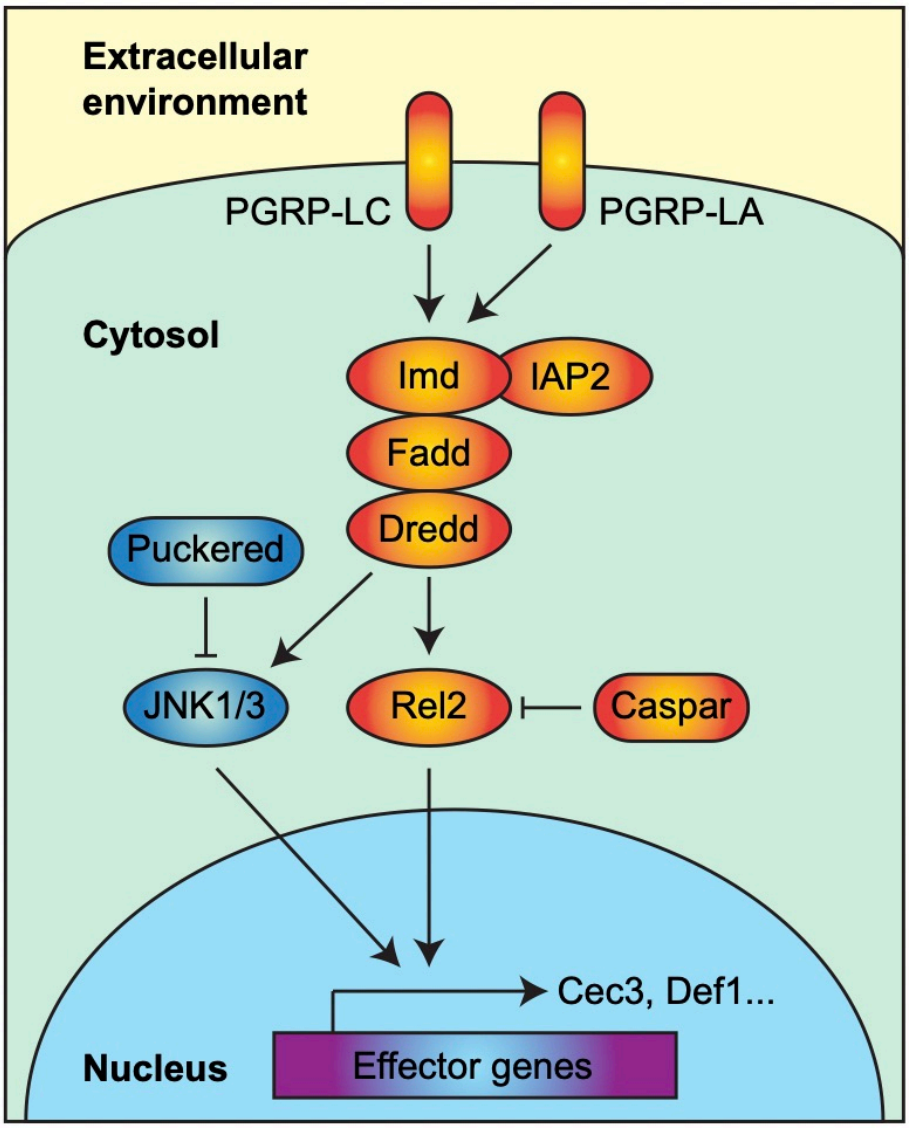

D. Schematic illustration of the IMD and JNK pathways expressed in periostial hemocytes.
Invading pathogens bind with PGRP-LC and trigger the signaling cascade in the IMD pathway that includes IAP2, Imd, Fadd, Dredd, etc. This leads to the transcription factor, Rel2, to disassociate with the inhibitor protein, Caspar, and translocate into the nucleus and induce effect genes, such as Cec3 and Def1. The IMD pathway also bifurcates into the JNK pathway, and the activated JNK1/JNK3 phosphorylates transcription factors, which further induce effector genes. The JNK pathway is negatively regulated by Puckered. This illustration is modified from Hillyer, 2016 (48).

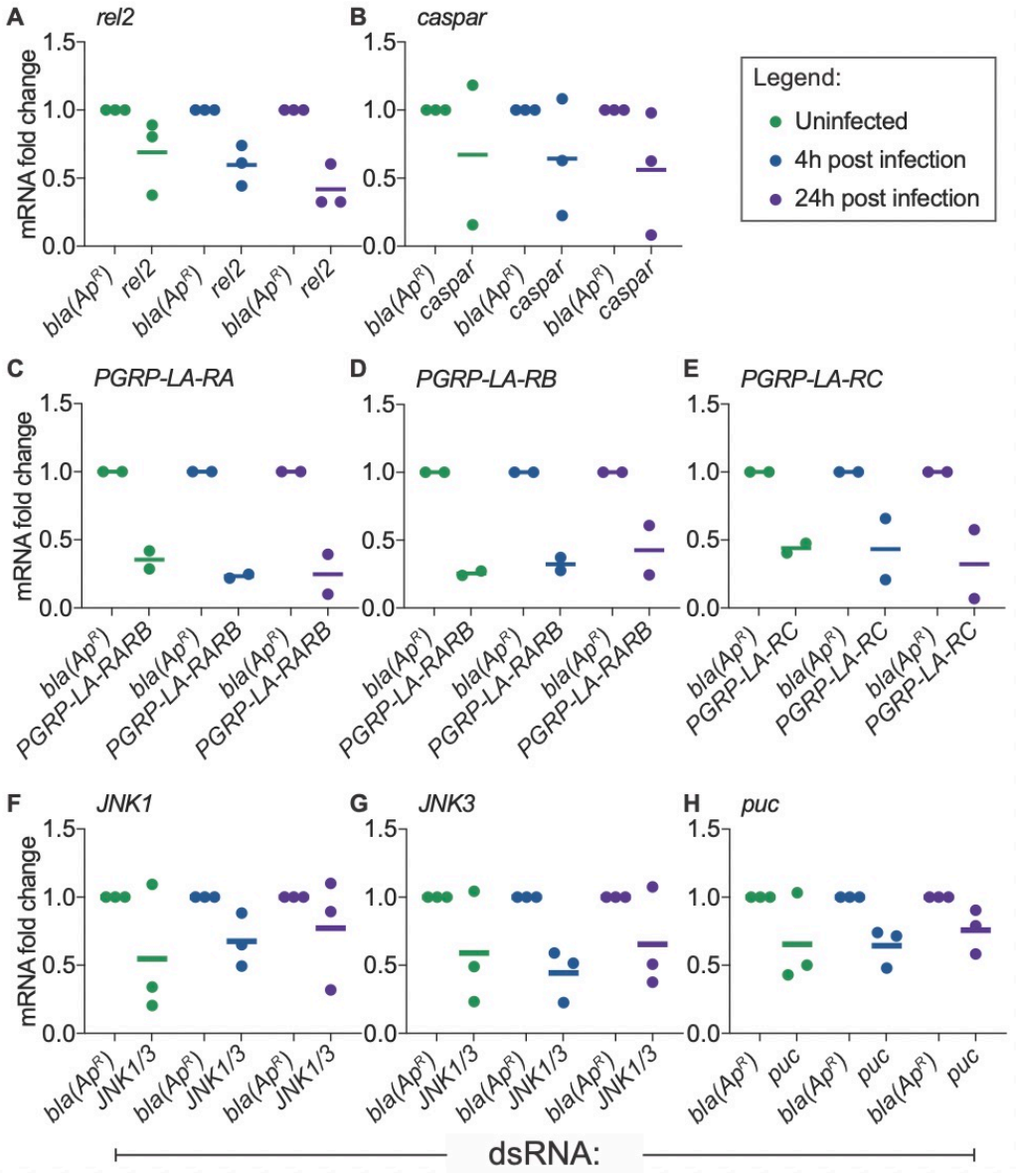

E. Efficiency of RNA interference-mediated gene silencing of *rel2*, *caspar*, *PGRP-LA*, *JNK1*, *JNK3* and *puc*.
mRNA abundance of *rel2* (A), *caspar* (B), *PGRP-LA-RA* (C), *PGRP-LA-RB* (D), *PGRP-LA-RC* (E), *JNK1* (F), *JNK3* (G) and *puc* (H) in mosquitoes injected ds*bla(Ap^R)* or dsRNA for the gene being assayed. mRNA abundance was measured mosquitoes that were not infected or had been infected with GFP-*E. coli* for 4 or 24 hr. Horizontal lines indicate the average mRNA abundance, and each circle represents an independent trial. Data are relative to mRNA abundance in the ds*bla(Ap^R)* group of that specific trial.

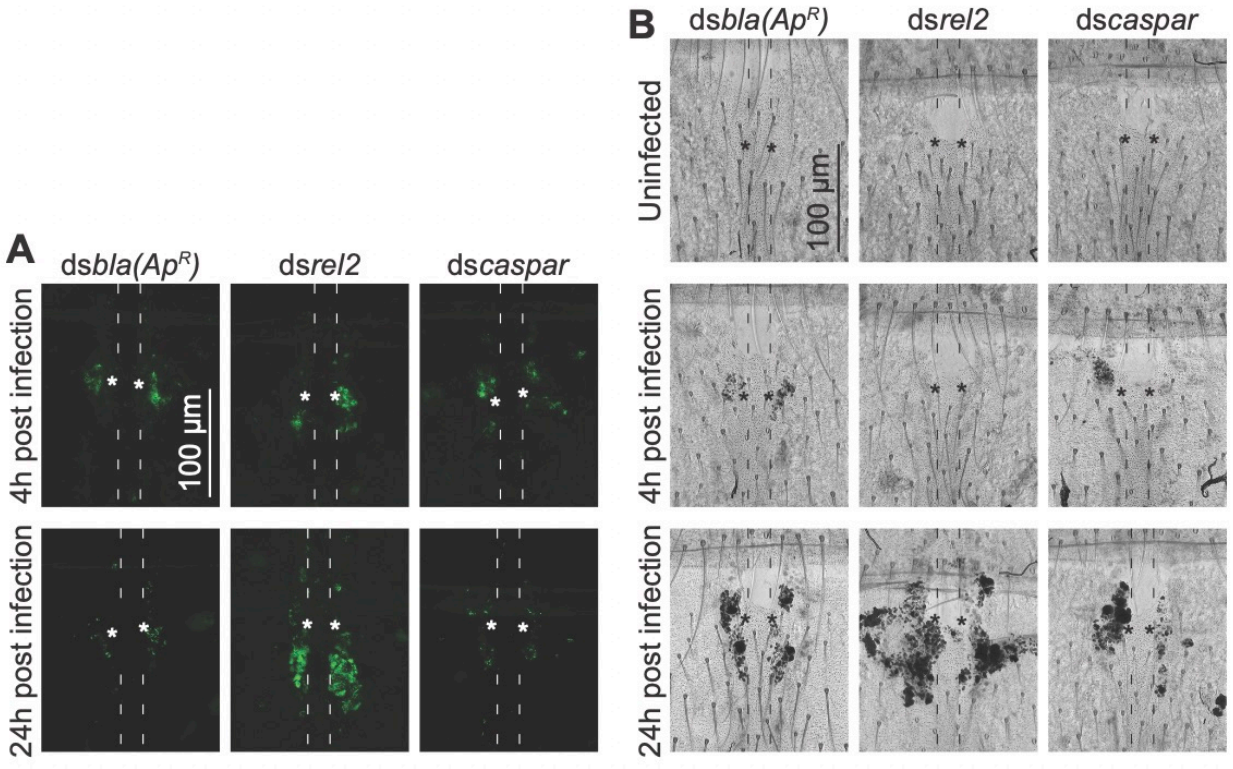

F. The IMD pathway regulates GFP-*E. coli* and melanin accumulation at periostial regions.
(*A*) Fluorescence images show the accumulation of GFP-*E. coli* around a single pair of ostia (asterisks) on a segment of the heart (outlined by dotted lines) of ds*bla(Ap^R)*-, ds*rel2*- and ds*caspar*-injected mosquitoes that had been infected with GFP-*E. coli* for 4 or 24 hr. (*B*) Bright field images show the accumulation melanin around a single pair of ostia (asterisks) on a segment of the heart (outlined by dotted lines) of ds*bla(Ap^R)*-, ds*rel2*- and ds*caspar*-injected mosquitoes that were not infected or had been infected with GFP-*E. coli* for 4 or 24 hr.

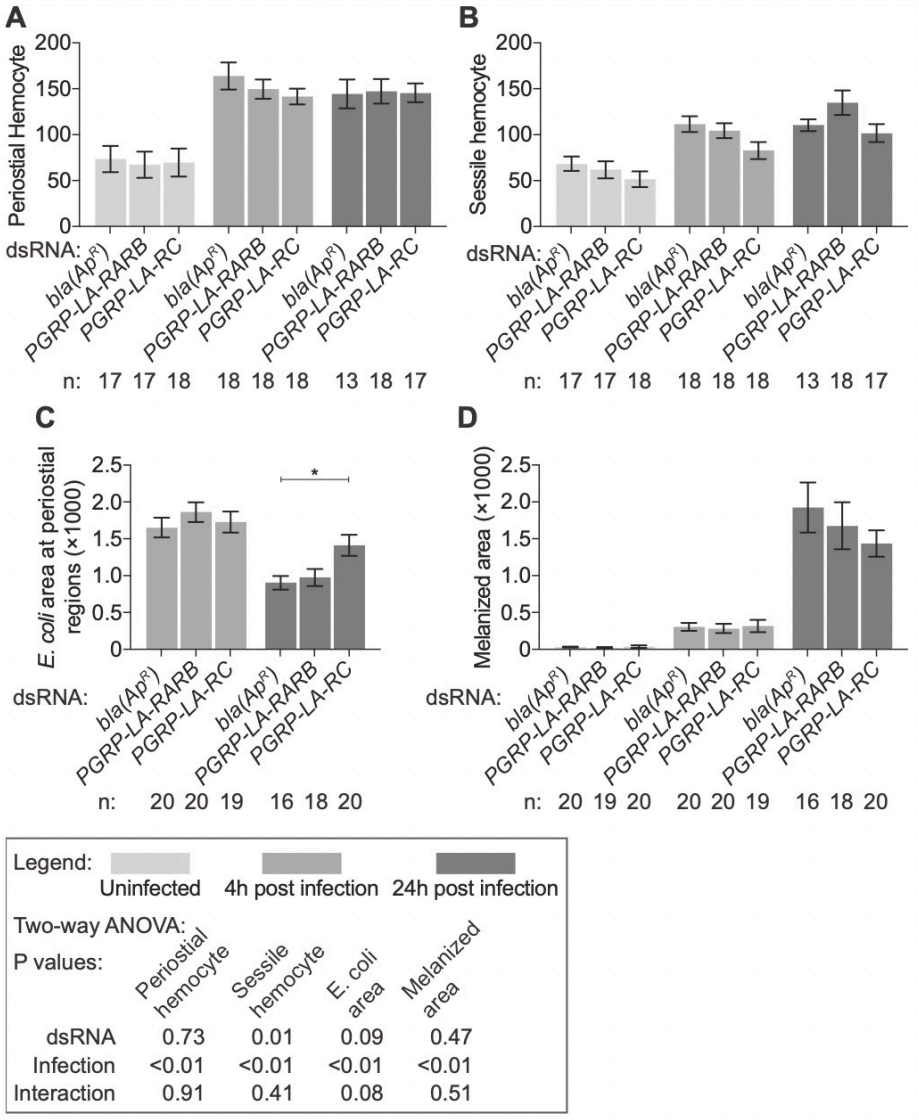

G. The RC splice form of PGRP-LA regulates phagocytosis by periostial hemocytes.

(*A*-*D*) Graphs showing for ds*bla(Ap^R)*-, ds*PGRP-LA-RARB*- and ds*PGRP-LA-RC*-injected mosquitoes that were not infected or had been infected with GFP-*E. coli* for 4 or 24 hr: (*A*) average number of periostial hemocytes; (*B*) average number of sessile hemocytes outside of periostial regions; (*C*) pixel area of GFP-*E. coli* in the periostial regions; and (*D*) pixel area of melanin in the periostial regions. The data were analyzed by two-way ANOVA, followed by Dunnett's multiple comparison test. The ds*bla(Ap^R)*-injected mosquitoes were used as the reference group. Whiskers show S.E.M. and the asterisks indicates $P < 0.05$.

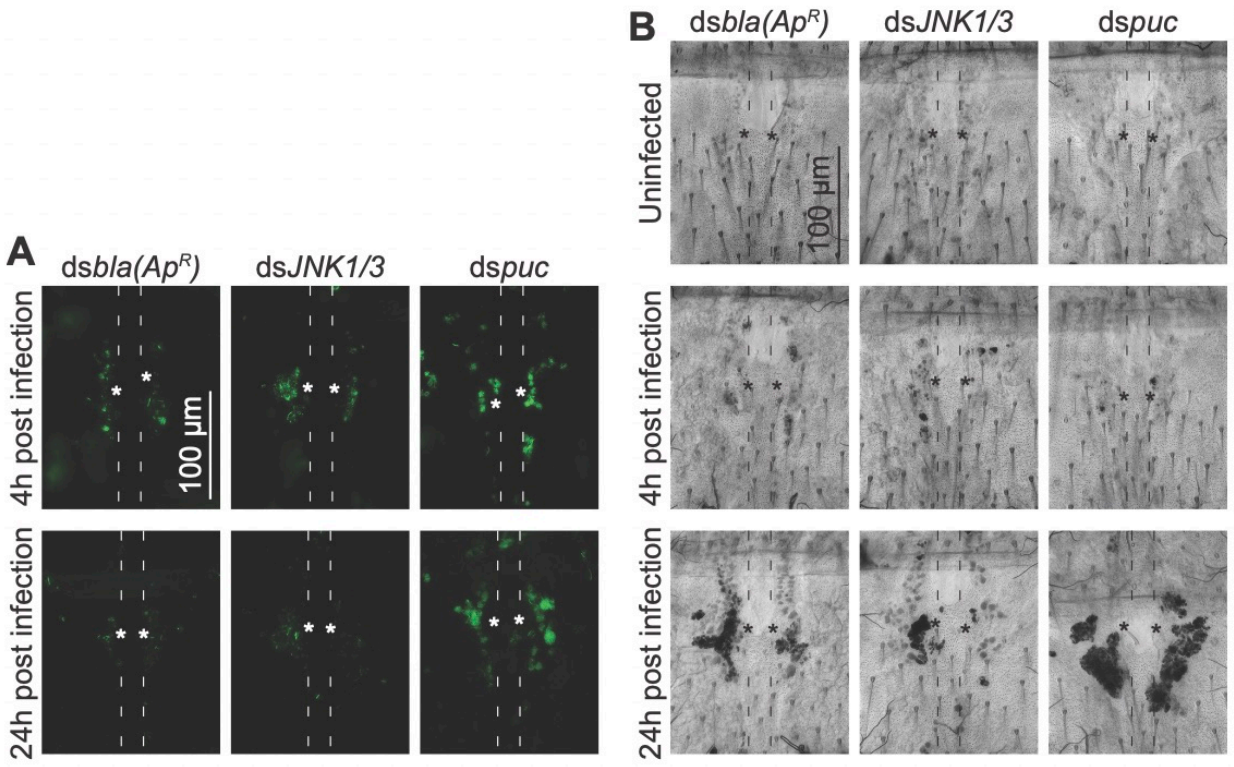

H. The JNK pathway regulates GFP-*E. coli* and melanin accumulation at periostial regions.
(*A*) Fluorescence images show the accumulation of GFP-*E. coli* around a single pair of ostia (asterisks) on a segment of the heart (outlined by dotted lines) of ds*bla(Ap^R)*-, ds*JNK1/3*- and ds*puc*-injected mosquitoes that had been infected with GFP-*E. coli* for 4 or 24 hr. (*B*) Bright field images show the accumulation melanin around a single pair of ostia (asterisks) on a segment of the heart (outlined by dotted lines) of ds*bla(Ap^R)*-, ds*JNK1/3*- and ds*puc*-injected mosquitoes that were not infected or had been infected with GFP-*E. coli* for 4 or 24 hr.

I. Upregulated genes in the heart with periostial hemocytes at 4 hr following both GFP-*E. coli* and *S. aureus* infection.

Gene ID	Gene name	Gene description
AGAP000694	*CEC3*	cecropin anti-microbial peptide
AGAP000786		
AGAP001160		
AGAP001212	*PGRPLB*	peptidoglycan recognition protein (long)
AGAP001508		
AGAP001563		glycerol kinase
AGAP001597		
AGAP001610		
AGAP001634		
AGAP001648	*CLIPB17*	CLIP-domain serine protease
AGAP001828		
AGAP002064		
AGAP002065		alpha-tocopherol transfer protein
AGAP002291		ebony
AGAP002323		
AGAP002331	*ESP*	sodium-independent sulfate anion transporter
AGAP002359		carbonic anhydrase
AGAP002536		
AGAP002883		
AGAP003488		nucleotide exchange factor SIL1
AGAP004170		
AGAP004181		Fibroblast growth factor
AGAP004826		
AGAP005205	*PGRPLA*	peptidoglycan recognition protein (long)
AGAP005610		
AGAP005839		MFS transporter, FLVCR family
AGAP006426		cyanogenic beta-glucosidase
AGAP006670		gamma-glutamyl hydrolase
AGAP006671		
AGAP006674		chymotrypsin-like protease (Precursor)
AGAP006745		
AGAP006747	*REL2*	NF-kappaB Relish-like transcription factor
AGAP007659		
AGAP008279	*D7L2*	D7 long form salivary protein
AGAP008851		E3 ubiquitin-protein ligase mind-bomb
AGAP009091	*DDC*	aromatic-L-amino-acid decarboxylase
AGAP009099	*TGase3*	Transglutaminase
AGAP009100	*TGase1*	Protein-glutamine gamma-glutamyltransferase E
AGAP009145		
AGAP009213	*SRPN16*	serine protease inhibitor (serpin) 16
AGAP009214	*CLIPB11*	CLIP-domain serine protease
AGAP009460	*JNK3*	c-Jun N-terminal kinase
AGAP009985		4-nitrophenylphosphatase
AGAP010197		SPRY domain-containing SOCS box protein 1
AGAP010398		Flavin-containing monooxygenase FMO GS-OX-like 1
AGAP010934		
AGAP011294	*DEF1*	defensin anti-microbial peptide
AGAP011326	*IAP2*	inhibitor of apoptosis 2
AGAP011588		
AGAP011654		membrane dipeptidase
AGAP011764		
AGAP011992		lysosomal acid lipase
AGAP012166		
AGAP013506	*UPD3A*	JAK/STAT pathway cytokine unpaired 3 variant A
AGAP028615	*NAT5*	nutrient amino acid transporter 5

J. Upregulated genes in circulating hemocytes at 4 hr following both GFP-*E. coli* and *S. aureus* infection.

Gene ID	Gene name	Gene description
AGAP000899		
AGAP001212	*PGRPLB*	peptidoglycan recognition protein (long)
AGAP001430		
AGAP001508		
AGAP002291		ebony
AGAP004115		cystinosin
AGAP005610		
AGAP005639	*ABCB2*	ATP-binding cassette transporter (ABC transporter) family B member 2
AGAP007651		growth arrest and DNA-damage-inducible protein
AGAP009091	*DDC*	aromatic-L-amino-acid decarboxylase
AGAP010349		
AGAP010387		alanine-glyoxylate aminotransferase
AGAP010571		
AGAP010855		solute carrier family 45, member 1/2/4
AGAP011326	*IAP2*	inhibitor of apoptosis 2
AGAP011391		
AGAP011588		
AGAP011589		
AGAP012565		
AGAP013285	*IR7u*	ionotropic receptor IR7u
AGAP028615	*NAT5*	nutrient amino acid transporter 5

K. Upregulated genes in the abdomen at 4 hr following both GFP-*E. coli* and *S. aureus* infection.

Gene ID	Gene name	Gene description
AGAP001212	*PGRPLB*	peptidoglycan recognition protein (long)
AGAP001508		
AGAP001610		
AGAP001648	*CLIPB17*	CLIP-domain serine protease
AGAP002291		ebony
AGAP006670		gamma-glutamyl hydrolase
AGAP006745		
AGAP007651		growth arrest and DNA-damage-inducible protein
AGAP007659		
AGAP009145		
AGAP010398		Flavin-containing monooxygenase FMO GS-OX-like 1
AGAP010934		
AGAP011294	*DEF1*	defensin anti-microbial peptide
AGAP011326	*IAP2*	inhibitor of apoptosis 2
AGAP013348		

L. Gene names, gene IDs, and primers used in chapter III.

Application	Gene	dsRNA	VectorBase ID[a]	Sequence (forward and reverse)[b]
qPCR	*Rps7*		AGAP010592	GACGGATCCCAGCTGATAAA
qPCR				GTTCTCTGGGAATTCGAACG
qPCR	*Rps17*		AGAP004887	GACGAAACCACTGCGTAACA
qPCR				TGCTCCAGTGCTGAAACATC
qPCR	*rel2*		AGAP006747	TTCGCTGCTCGACTTTCACT
qPCR				CCAACCGAAGGCAGCAAATC
qPCR	*caspar*		AGAP006473	TCGTAGCCAATGCGAAGTGT
qPCR				TCGTTCGTTCTCTTCACGCA
qPCR	*PGRP-LA-RA*		AGAP005205	GGCAATGGCGGAAATACGAC
qPCR				GGTTCCGCTGAAGGTAGTCC
qPCR	*PGRP-LA-RB*		AGAP005205	GGTACGTTTGACGCGGATC
qPCR				GTCCGCGGTTCTGATTGTT
qPCR	*PGRP-LA-RC*		AGAP005205	GCAATGGCGGAAATACGAC
qPCR				ATGCCCGGCGAAGTATATG
qPCR	*JNK1*[c]		AGAP029555[c]	TGTTTCCGACCGACTCGAA
qPCR				CGTCCACGCTGTGATCGTA
qPCR	*JNK3*		AGAP009460	ACAGTCTTAAGCATCCCGGC
qPCR				GCGGCAAAACACACTCCTTT
qPCR	*puckered*		AGAP004353	ATTCAACGGAGGTCGATTTG
qPCR				AACTTTCTAGCCCCCATCGT
RNAi	*bla(Ap^R)*	ds*bla(Ap^R)*	(Bacterial gene)	TAATACGACTCACTATAGGGCCGAGCGCAGAAGTGGT
RNAi				TAATACGACTCACTATAGGGAACCGGAGCTGAATGAA
RNAi	*rel2*	ds*rel2*	AGAP006747	TAATACGACTCACTATACGGAGAAGTCGAAGAAAACG
RNAi				TAATACGACTCACTATACACAGGCACACCTGATTGAG
RNAi	*caspar*	ds*caspar*	AGAP006473	TAATACGACTCACTATAGGGACAGAAGGCCGCTTT
RNAi				TAATACGACTCACTATAGGGAGTGGTGGTGCAGAGTT
RNAi	*PGRP-LA*	ds*PGRP-LA-RARB*	AGAP005205	TAATACGACTCACTATAGGGAGATACTGTTCGACACCA
RNAi				TAATACGACTCACTATAGGGCTGGCTGTGGTAGGTTT
RNAi	*PGRP-LA*	ds*PGRP-LA-RC*	AGAP005205	TAATACGACTCACTATAGGGCACATGGTCATCGATC
RNAi				TAATACGACTCACTATAGGGATCGATTTTGGGTATTC
RNAi	*JNK1/JNK3*	ds*JNK1/3*[d]	AGAP0290555 /AGAP009460	TAATACGACTCACTATAGGGGTCACGCCTTCTACACCGTC
RNAi				TAATACGACTCACTATAGGGCAGCCCAAAGTCGAGGATT
RNAi	*puc*	ds*puc*	AGAP004353	TAATACGACTCACTATAGGGTGAAACATAAATCGCCCTGC
RNAi				TAATACGACTCACTATAGGGGACAGACCCTTGTAGCGCAT

a Vectorbase IDs are obtained from the AgamP4 assembly in www.vectorbase.org (exception: *bla(Ap^R)*).
b Underlined sequences are specific to the T7 RNA polymerase promoter sites needed for dsRNA synthesis.
c The previous gene ID of JNK1 is AGAP009461.
d ds*JNK1/3* targets the expression of both *JNK1* and *JNK3*.

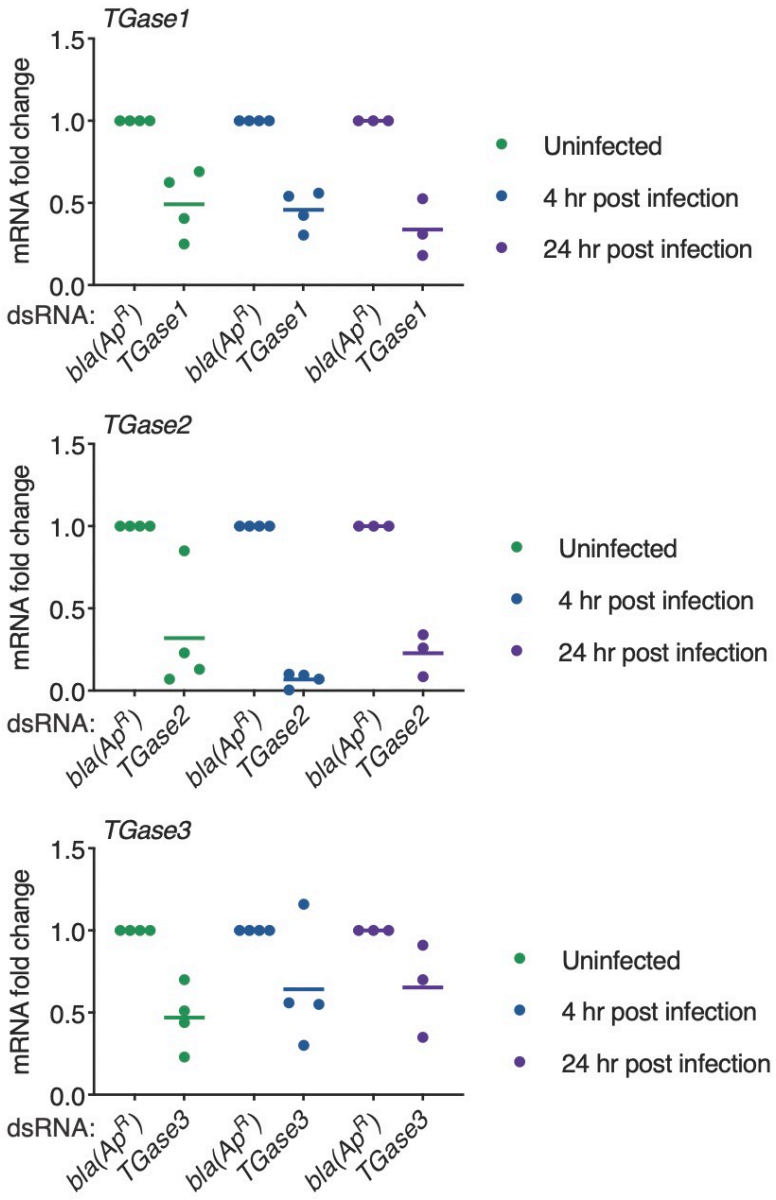

M. RNAi-based knockdown efficiency of *TGase1*, *TGase2* and *TGase3*.
Graphs show the relative mRNA abundance in mosquitoes treated with ds*bla(Ap^R)*-, ds*TGase1*-, ds*TGase2*- and ds*TGase3* that were uninfected or had been infected with GFP-*E. coli* for 4 or 24 hr. Each circle represents an independent trial, and each value is the average mRNA abundance across 2-4 technical replicates within the trial. The horizontal line marks the average. Data are presented relative to mRNA abundance in the ds*bla(Ap^R)* group of that specific trial.

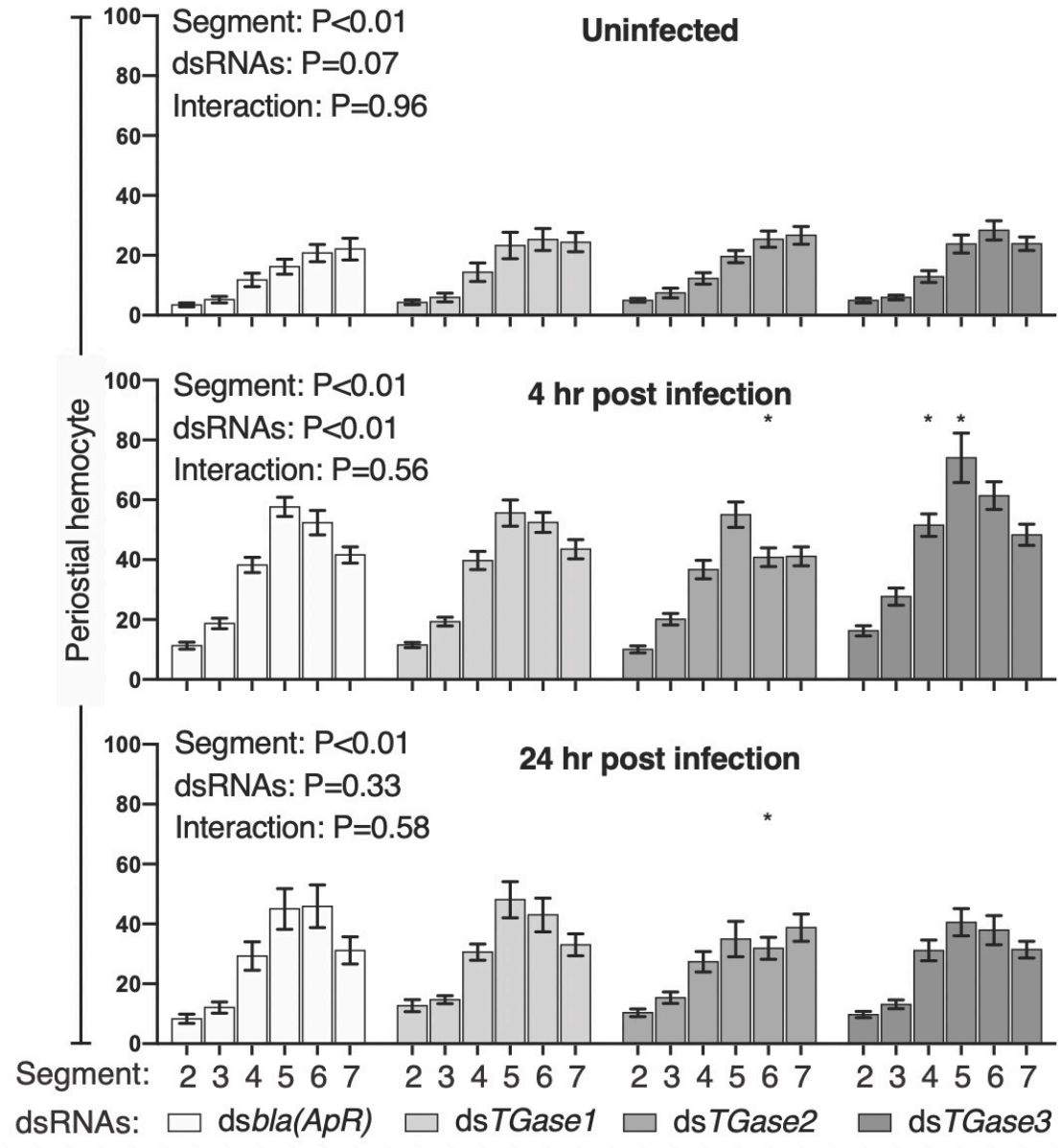

N. RNAi-based knockdown of transglutaminase genes does not alter the spatial distribution of periostial hemocytes.

Graph shows the average number of periostial hemocytes in each periostial region of abdominal segments 2-7 in ds*bla(Ap^R)*-, ds*TGase1*-, ds*TGase2*- and ds*TGase3*-injected mosquitoes that were not infected or had been infected with GFP-*E. coli* for 4 or 24 hr. Data were analyzed by two-way ANOVA followed by Dunnett's post-hoc test, using ds*bla(Ap^R)* mosquitoes as the reference. Column heights mark the means, whiskers show the S.E.M., and asterisks indicate $P < 0.05$.

O. Gene names, gene IDs, and primers used in chapter IV.

Gene	VectorBase ID[a]	Application	Sequence (forward and reverse)[b]	Amplicon (bp)[c]	
				Transcript	Genomic
RPS7	AGAP010592	qPCR	GACGGATCCCAGCTGATAAA	132	281
		qPCR	GTTCTCTGGGAATTCGAACG		
RPS17	AGAP004887	qPCR	GACGAAACCACTGCGTAACA	153	264
		qPCR	TGCTCCAGTGCTGAAACATC		
TGase1	AGAP009100	qPCR	CTGCACAAGGGACTGTTCCA	191	259
		qPCR	AACGCCAAAAAGCCATCCAC		
TGase2	AGAP009098	qPCR	CGGTGGACGCTGACTATCAA	225	297
		qPCR	GTACTGGCCGAGCTTCCATT		
TGase3	AGAP009099	qPCR	TACAGCAGCCAGCGGTTTAG	236	236
		qPCR	ATATCGCGCCCAGTGTAGTC		
BLA(Ap^R)	(Bacterial gene)	RNAi	TAATACGACTCACTATAGGGCCGAGCGCAGAAGTGGT	214	214
		RNAi	TAATACGACTCACTATAGGGAACCGGAGCTGAATGAA		
TGase1	AGAP009100	RNAi	TAATACGACTCACTATAGGGCATTCCGGTTAATCAGT	361	433
		RNAi	TAATACGACTCACTATAGGGCGTAGTCGATTGTAAGA		
TGase2	AGAP009098	RNAi	TAATACGACTCACTATAGGGTCAGAGCTGTCTAACAAA	490	490
		RNAi	TAATACGACTCACTATAGGCGTACCGCTCAACTCC		
TGase3	AGAP009099	RNAi	TAATACGACTCACTATAGGGAAAACCTTCCACACGTC	501	501
		RNAi	TAATACGACTCACTATAGGGTTGAACAGCACAAACAA		

a Vectorbase IDs were obtained from the AgamP4 assembly in www.vectorbase.org (exception: *BLA(Ap^R)*).
b Underlined sequences are specific to the T7 RNA polymerase promoter sites needed for dsRNA synthesis.
c Amplicon sizes are based on the sequences in Vectorbase. For dsRNA primers, amplicon lengths include the T7 promoter sequence tags.

Appendix P

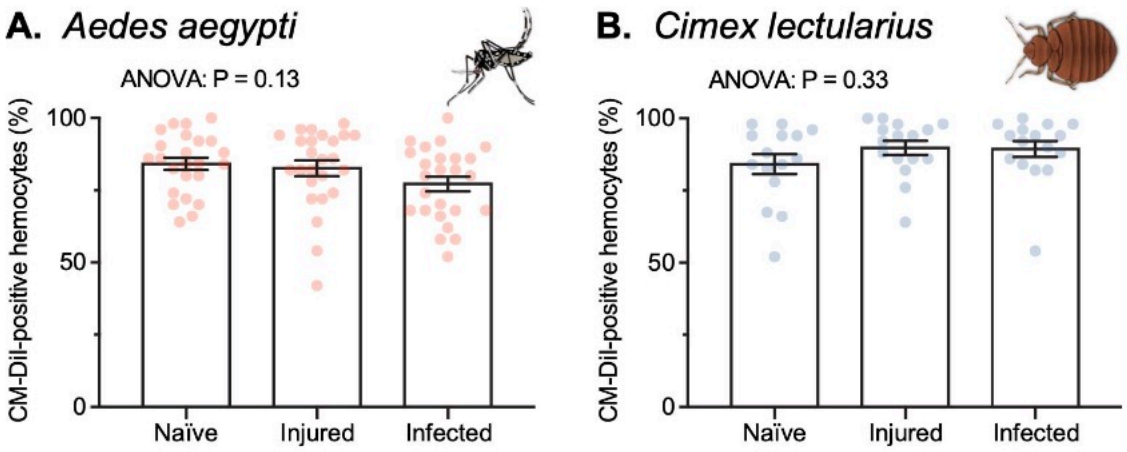

P. The efficiency of Vybrant CM-DiI staining of hemocytes in *Aedes aegypti* and *Cimex lectularius*.
Quantitative analysis of *in vivo* CM-DiI staining in perfused hemocytes from naïve, injured (LB) and *E. coli*-infected *Ae. aegypti* (A) and *C. lectularius* (B). Column heights mark the mean and the whiskers denote the standard error of the mean. Each circle represents the percentage of hemocytes that are positively stained by CM-DiI in an individual insect. The vast majority of hemocytes stain with CM-DiI.

Appendix Q

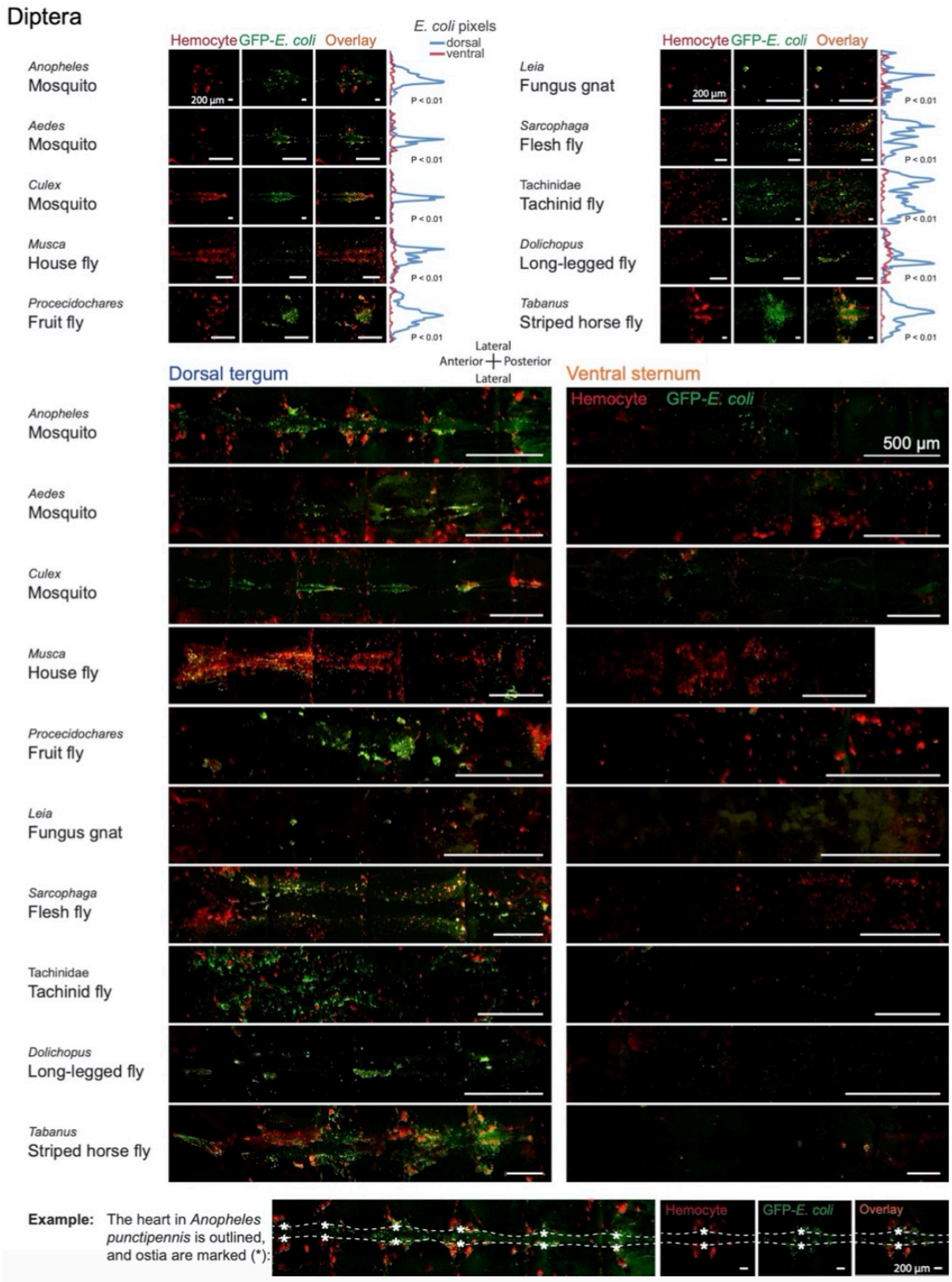
Diptera
Hemocyte GFP-E. coli Overlay
E. coli pixels
dorsal
ventral
Anopheles Mosquito
Aedes Mosquito
Culex Mosquito
Musca House fly
Procecidochares Fruit fly
Leia Fungus gnat
Sarcophaga Flesh fly
Tachinidae Tachinid fly
Dolichopus Long-legged fly
Tabanus Striped horse fly
200 µm
P < 0.01
Lateral
Anterior Posterior
Lateral
Dorsal tergum
Ventral sternum
Hemocyte GFP-E. coli
500 µm
Example: The heart in Anopheles punctipennis is outlined, and ostia are marked (*):
Hemocyte
GFP-E. coli
Overlay
200 µm

Q. The aggregation of hemocytes and pathogens on the heart of members of the order Diptera.
Fluorescence microscopy images show one region of the heart (top section of the figure) and the entire dorsal and ventral abdomen (bottom section of the figure) in each insect. Graphs show quantification of GFP-*E. coli* pixel frequency along the width of the entire dorsal (blue line) and ventral (red line) abdomen. Hemocytes (red) and GFP-*E. coli* (green) distinctively aggregate and co-localize (overlay) on the heart – but not the surrounding tergum – and are largely absent in the ventral sternum.

Appendix R

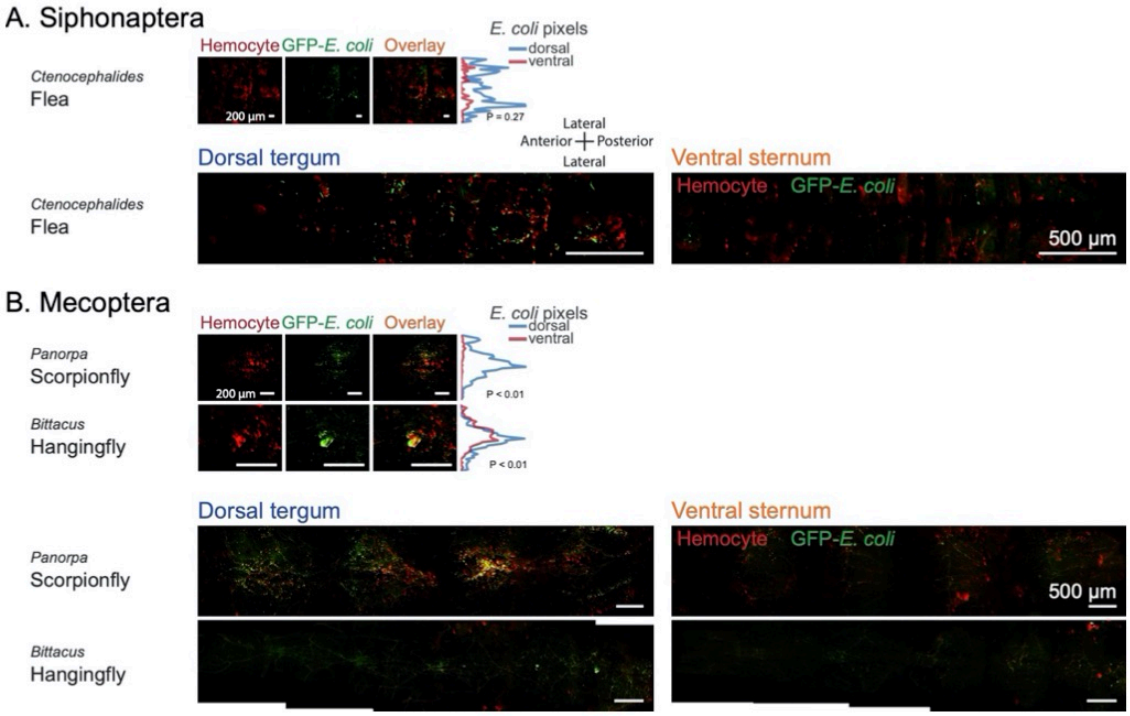

R. The aggregation of hemocytes and pathogens on the heart of members of the orders Siphonaptera (A) and Mecoptera (B).
Fluorescence microscopy images show one region of the heart (top section of each panel) and the entire dorsal and ventral abdomen (bottom section of each panel) in each insect. Graphs show quantification of GFP-*E. coli* pixel frequency along the width of the entire dorsal (blue line) and ventral (red line) abdomen. In Siphonaptera, hemocytes (red) and GFP-*E. coli* (green) do not aggregate or co-localize (overlay) on the heart. In Mecoptera, hemocytes and GFP-*E. coli* distinctively aggregate and co-localize on the heart – but not the surrounding tergum – and are largely absent in the ventral sternum.

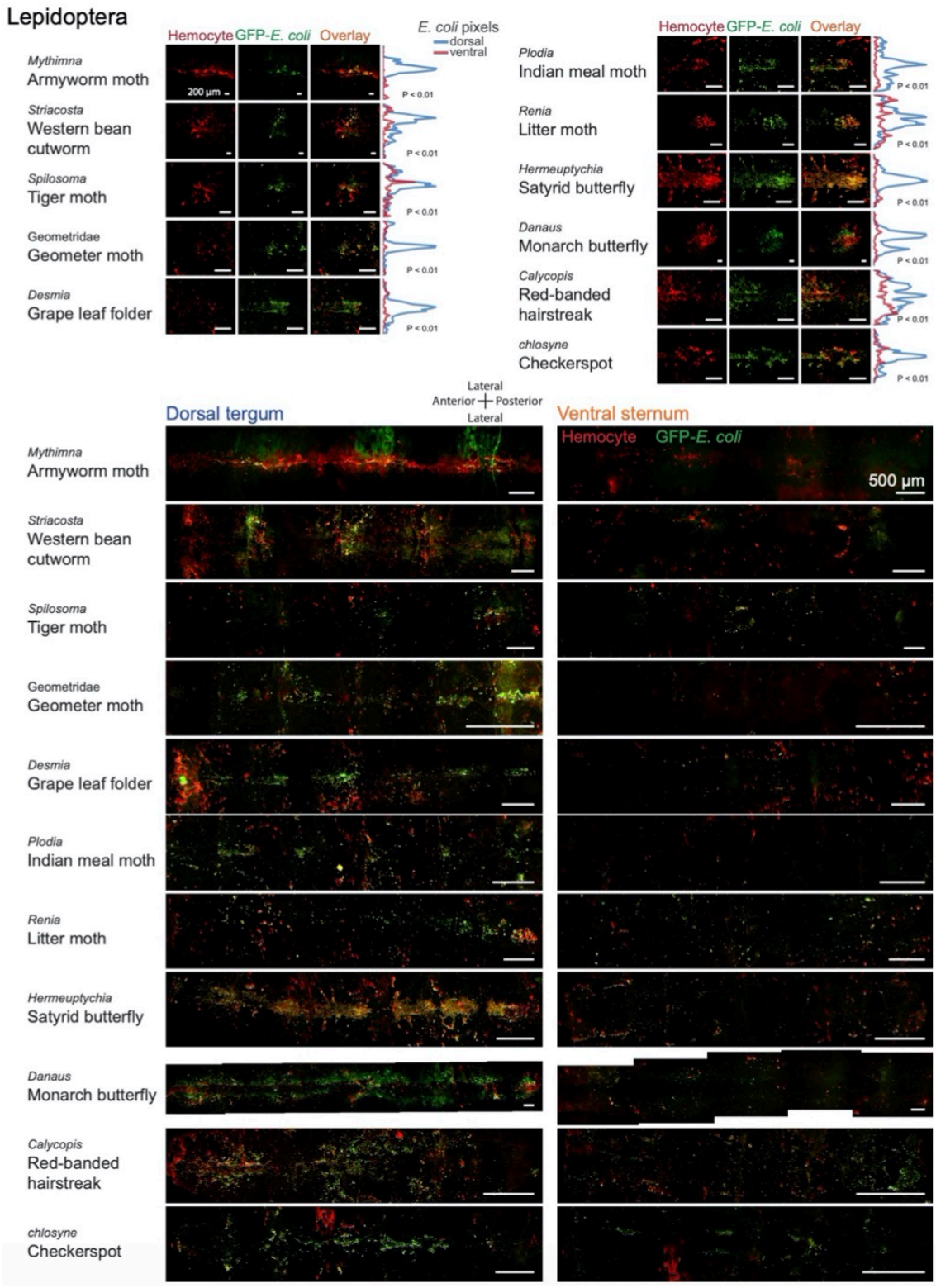
Lepidoptera
Hemocyte GFP-E. coli Overlay
E. coli pixels
dorsal
ventral
Mythimna
Armyworm moth
200 µm
Striacosta
Western bean cutworm
Spilosoma
Tiger moth
Geometridae
Geometer moth
Desmia
Grape leaf folder
P < 0.01
Plodia
Indian meal moth
Renia
Litter moth
Hermeuptychia
Satyrid butterfly
Danaus
Monarch butterfly
Calycopis
Red-banded hairstreak
chlosyne
Checkerspot
Lateral
Anterior Posterior
Lateral
Dorsal tergum
Ventral sternum
Hemocyte GFP-E. coli
500 µm

S. The aggregation of hemocytes and pathogens on the heart of members of the order Lepidoptera.
Fluorescence microscopy images show one region of the heart (top section of the figure) and the entire dorsal and ventral abdomen (bottom section of the figure) in each insect. Graphs show quantification of GFP-*E. coli* pixel frequency along the width of the entire dorsal (blue line) and ventral (red line) abdomen. Hemocytes (red) and GFP-*E. coli* (green) distinctively aggregate and co-localize (overlay) on the heart – but not the surrounding tergum – and are largely absent in the ventral sternum.

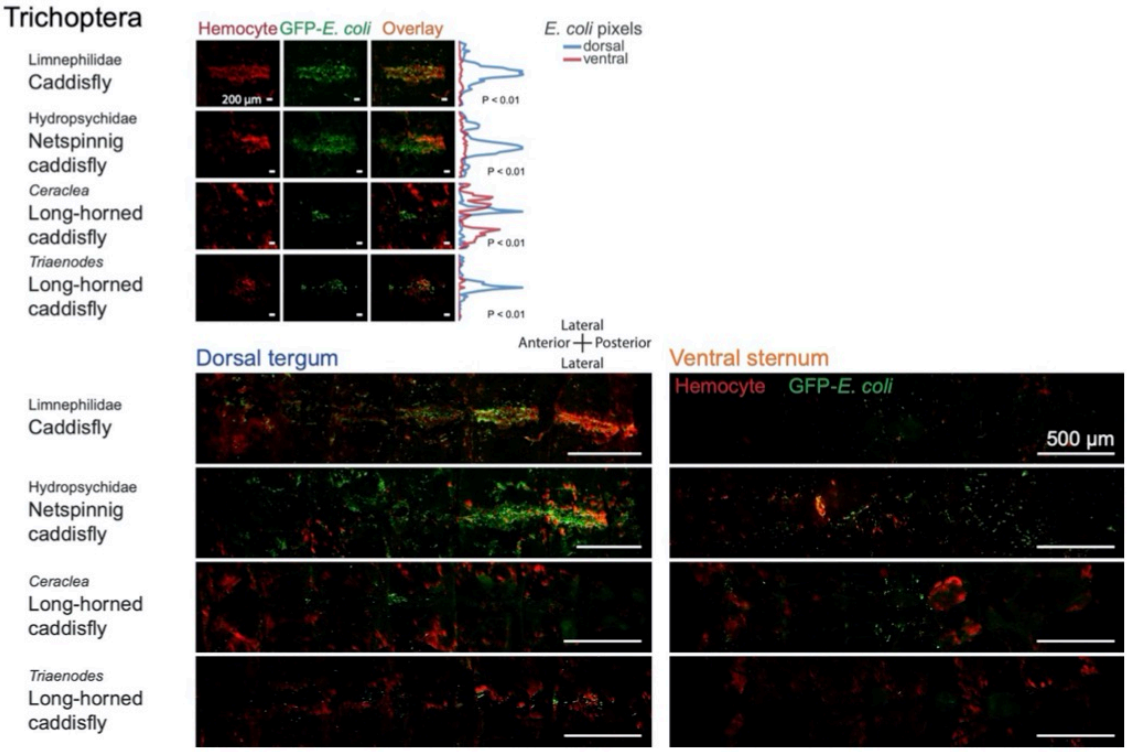

T. The aggregation of hemocytes and pathogens on the heart of members of the order Trichoptera.
Fluorescence microscopy images show one region of the heart (top section of the figure) and the entire dorsal and ventral abdomen (bottom section of the figure) in each insect. Graphs show quantification of GFP-*E. coli* pixel frequency along the width of the entire dorsal (blue line) and ventral (red line) abdomen. Hemocytes (red) and GFP-*E. coli* (green) distinctively aggregate and co-localize (overlay) on the heart – but not the surrounding tergum – and are largely absent in the ventral sternum.

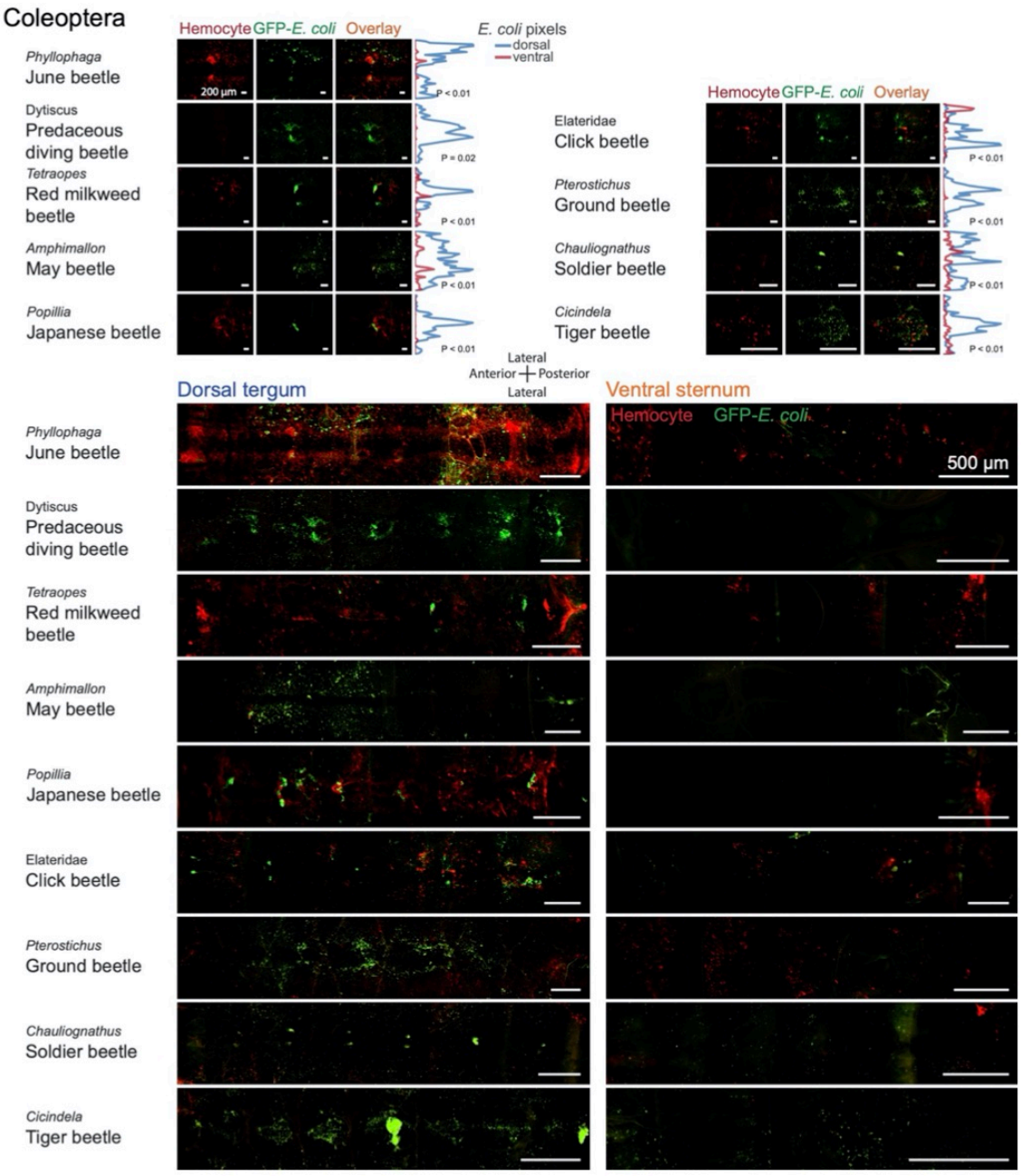

U. The aggregation of hemocytes and pathogens on the heart of members of the order Coleoptera.
Fluorescence microscopy images show one region of the heart (top section of the figure) and the entire dorsal and ventral abdomen (bottom section of the figure) in each insect. Graphs show quantification of GFP-*E. coli* pixel frequency along the width of the entire

dorsal (blue line) and ventral (red line) abdomen. Hemocytes (red) and GFP-*E. coli* (green) distinctively aggregate and co-localize (overlay) on the heart – but not the surrounding tergum – and are largely absent in the ventral sternum.

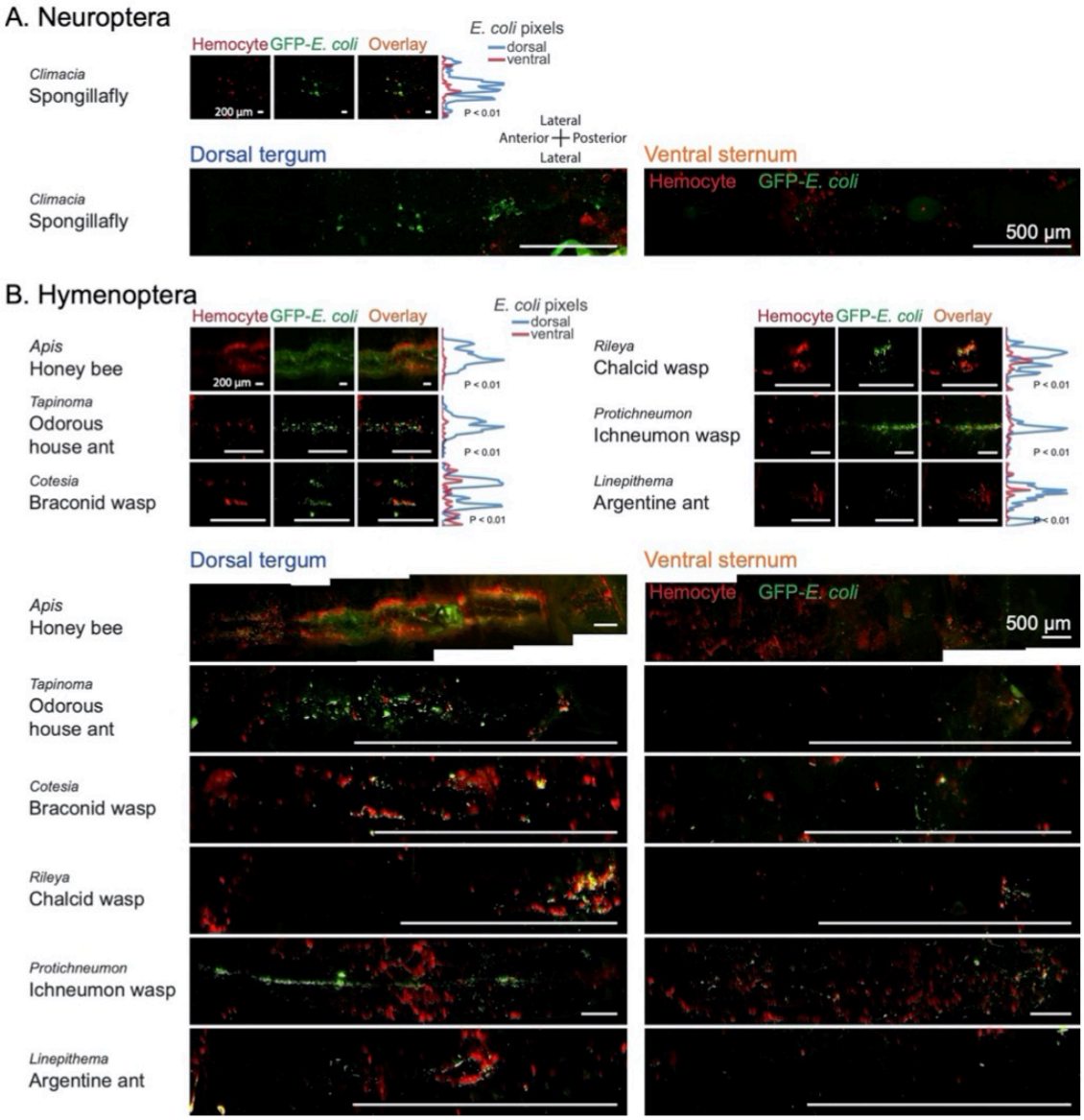

V. The aggregation of hemocytes and pathogens on the heart of members of the orders Neuroptera (A) and Hymenoptera (B).
Fluorescence microscopy images show one region of the heart (top section of each panel) and the entire dorsal and ventral abdomen (bottom section of each panel) in each insect. Graphs show quantification of GFP-*E. coli* pixel frequency along the width of the entire dorsal (blue line) and ventral (red line) abdomen. In both Neuroptera and Hymenoptera, hemocytes (red) and GFP-*E. coli* (green) distinctively aggregate and co-localize (overlay) on the heart – but not the surrounding tergum – and are largely absent in the ventral sternum.

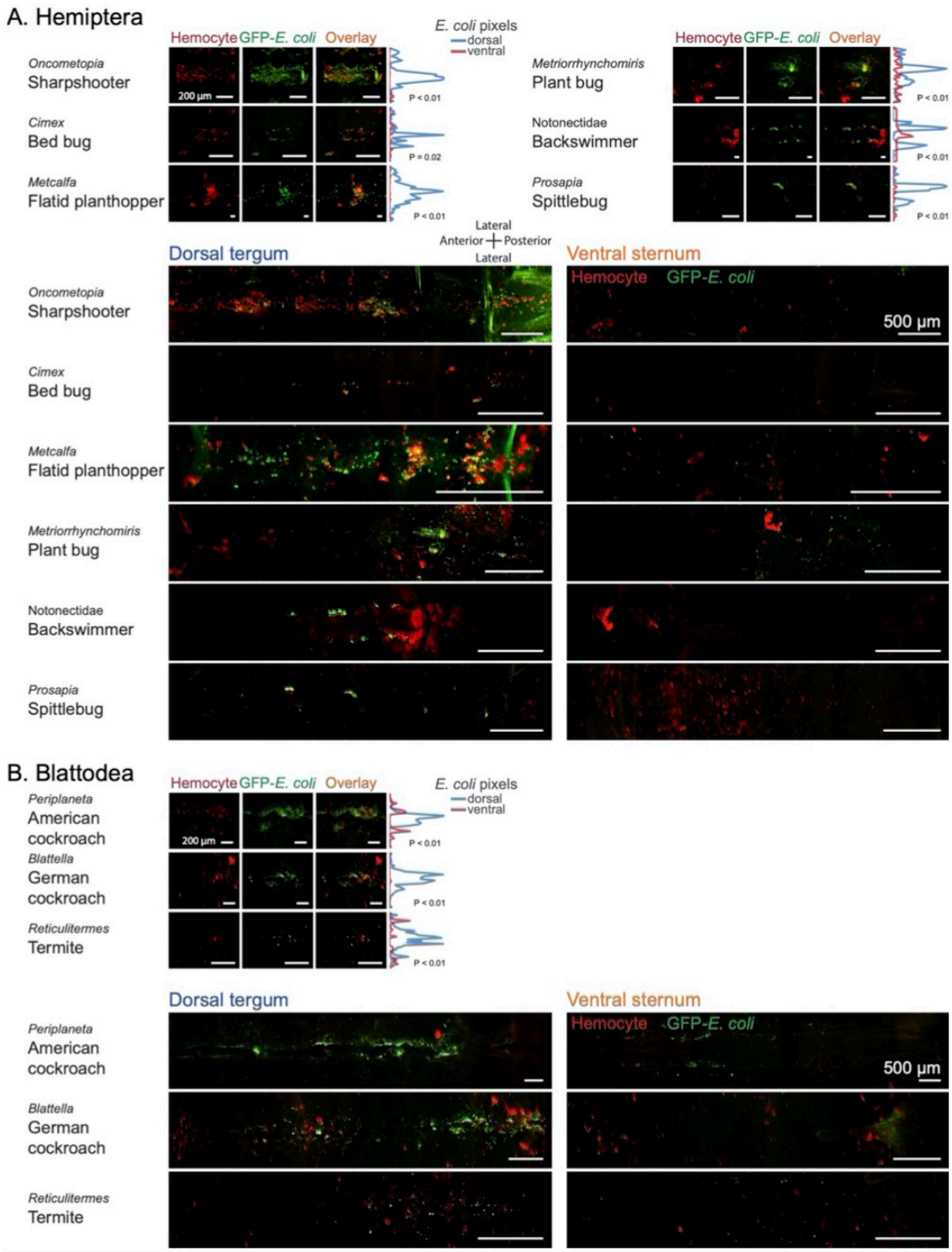
A. Hemiptera
Hemocyte GFP-E. coli Overlay
E. coli pixels
dorsal
ventral
Oncometopia
Sharpshooter
Cimex
Bed bug
Metcalfa
Flatid planthopper
Metriorrhynchomiris
Plant bug
Notonectidae
Backswimmer
Prosapia
Spittlebug
200 µm
P < 0.01
P = 0.02
Lateral
Anterior Posterior
Lateral
Dorsal tergum
Ventral sternum
Hemocyte GFP-E. coli
500 µm
B. Blattodea
Periplaneta
American
cockroach
Blattella
German
cockroach
Reticulitermes
Termite

W. The aggregation of hemocytes and pathogens on the heart of members of the orders Hemiptera (A) and Blattodea (B).
Fluorescence microscopy images show one region of the heart (top section of each panel) and the entire dorsal and ventral abdomen (bottom section of each panel) in each insect. Graphs show quantification of GFP-*E. coli* pixel frequency along the width of the entire dorsal (blue line) and ventral (red line) abdomen. In both Hemiptera and Blattodea, hemocytes (red) and GFP-*E. coli* (green) distinctively aggregate and co-localize (overlay) on the heart – but not the surrounding tergum – and are largely absent in the ventral sternum.

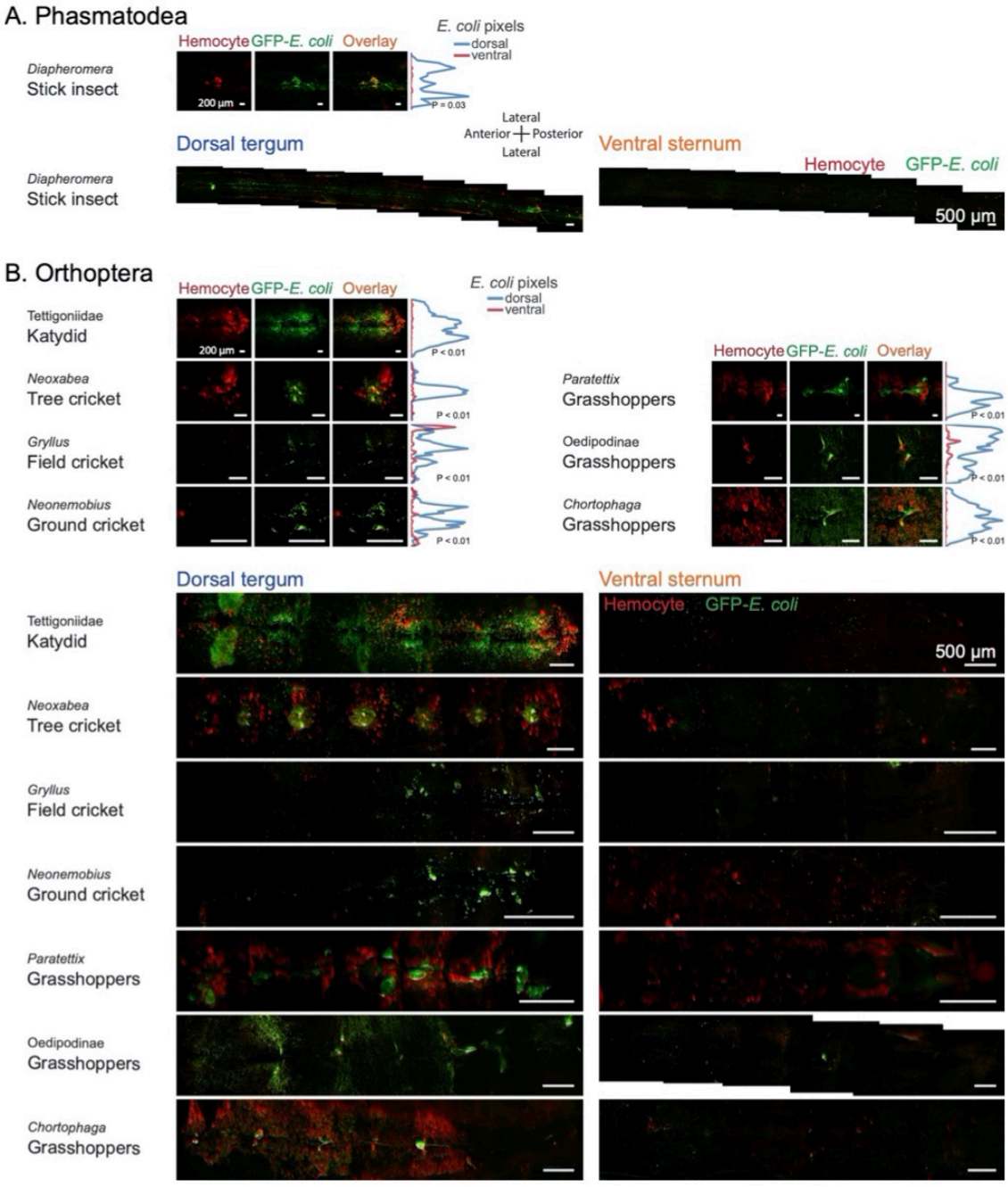

X. The aggregation of hemocytes and pathogens on the heart of members of the orders Phasmatodea (A) and Orthoptera (B).
Fluorescence microscopy images show one region of the heart (top section of each panel) and the entire dorsal and ventral abdomen (bottom section of each panel) in each insect.

Graphs show quantification of GFP-*E. coli* pixel frequency along the width of the entire dorsal (blue line) and ventral (red line) abdomen. In both Phasmatodea and Orthoptera, hemocytes (red) and GFP-*E. coli* (green) distinctively aggregate and co-localize (overlay) on the heart – but not the surrounding tergum – and are largely absent in the ventral sternum.

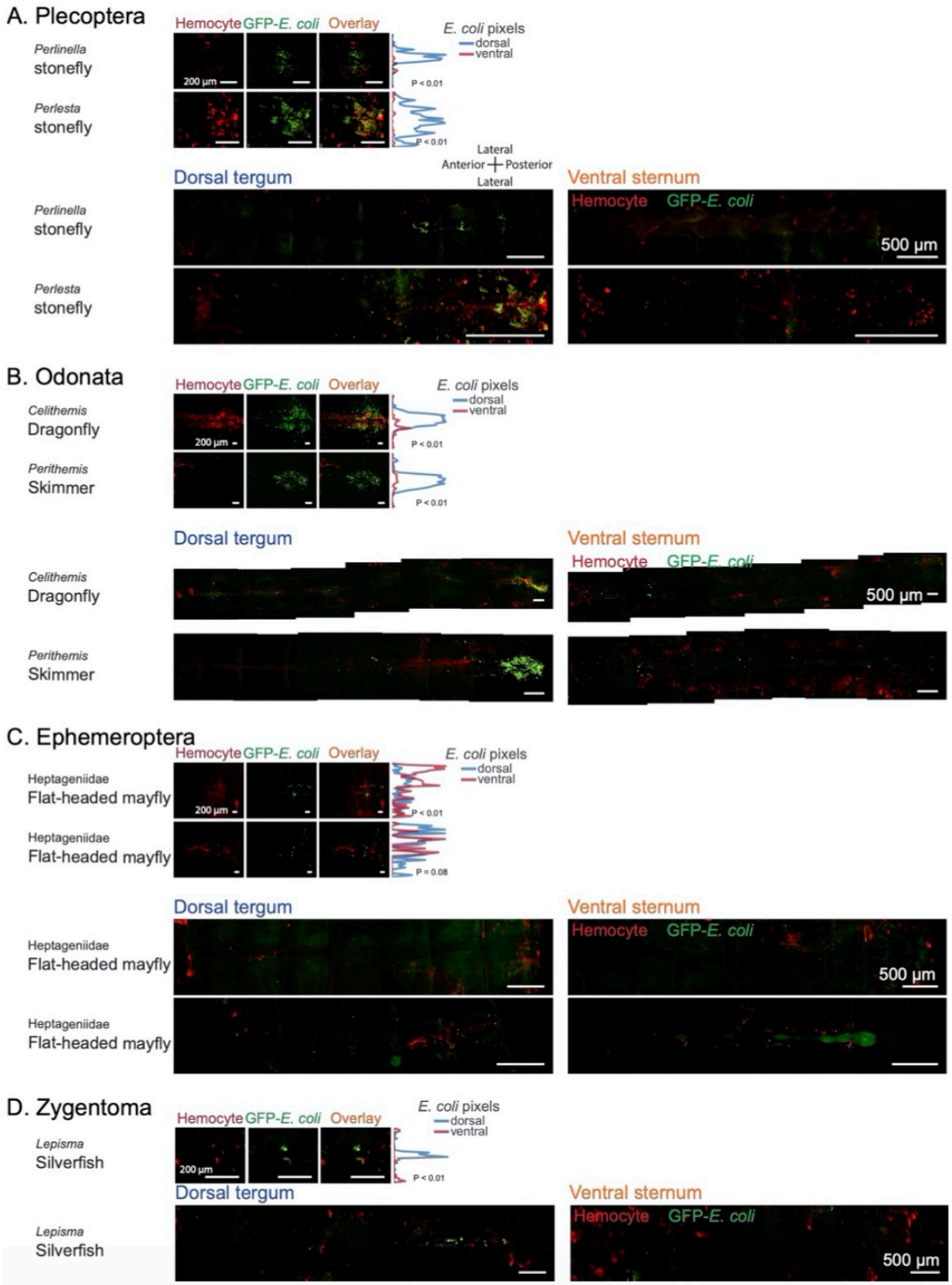
A. Plecoptera
Hemocyte GFP-E. coli Overlay
E. coli pixels
dorsal
ventral
Perlinella
stonefly
200 µm
P < 0.01
Perlesta
stonefly
P < 0.01
Lateral
Anterior Posterior
Lateral
Dorsal tergum
Ventral sternum
Perlinella
stonefly
Hemocyte GFP-E. coli
500 µm
Perlesta
stonefly
B. Odonata
Hemocyte GFP-E. coli Overlay
E. coli pixels
dorsal
ventral
Celithemis
Dragonfly
200 µm
P < 0.01
Perithemis
Skimmer
P < 0.01
Dorsal tergum
Ventral sternum
Celithemis
Dragonfly
Hemocyte GFP-E. coli
500 µm
Perithemis
Skimmer
C. Ephemeroptera
Hemocyte GFP-E. coli Overlay
E. coli pixels
dorsal
ventral
Heptageniidae
Flat-headed mayfly
200 µm
P < 0.01
Heptageniidae
Flat-headed mayfly
P = 0.08
Dorsal tergum
Ventral sternum
Heptageniidae
Flat-headed mayfly
Hemocyte GFP-E. coli
500 µm
Heptageniidae
Flat-headed mayfly
D. Zygentoma
Hemocyte GFP-E. coli Overlay
E. coli pixels
dorsal
ventral
Lepisma
Silverfish
200 µm
P < 0.01
Dorsal tergum
Ventral sternum
Lepisma
Silverfish
Hemocyte GFP-E. coli
500 µm

Y. The aggregation of hemocytes and pathogens on the heart of members of the orders Plecoptera (A), Odonata (B), Ephemeroptera (C) and Zygentoma (D). Fluorescence microscopy images show one region of the heart (top section of each panel) and the entire dorsal and ventral abdomen (bottom section of each panel) in each insect. Graphs show quantification of GFP-*E. coli* pixel frequency along the width of the entire dorsal (blue line) and ventral (red line) abdomen. In Plecoptera, Odonata and Zygentoma, hemocytes (red) and GFP-*E. coli* (green) distinctively aggregate and co-localize (overlay) on the posterior end of the heart – but not the surrounding tergum – and are largely absent in the ventral sternum. In Ephemeroptera, hemocytes and GFP-*E. coli* do not aggregate or co-localize on the heart.

Appendix Z

Z. Detailed information on the insects used in chapter V.
(See the next three pages)

Common name	Order	Family	Species	Location collected	Date of collection	Collection method	Collector[a]	Volume Injected (nL)	Number of *E. coli* injected	Incubation after infection
Mosquito	Diptera	Culicidae	*Culex sp.*	Cheekwood Garden, Nashville, TN	5/17/2019	scooping	YY	207	80523	1 hour
Mosquito	Diptera	Culicidae	*Aedes albopictus*	Vanderbilt University Campus, Nashville, TN	7/21/2019	sweep net	YY, LJ	90	22246	1 hour
Mosquito	Diptera	Culicidae	*Anopheles punctipennis*	Mulberry way, Nashville, TN	8/15/2019	trap	YY	104	67068	1 hour
House fly	Diptera	Muscidae	*Musca domestica*	Belle Forest Cave, Bellevue, TN	5/12/2018	sweep net	YY, JS	235	142061	1 hour
Fruit fly	Diptera	Tephritidae	*Procecidochares sp.*	Willow Pond, Nashville, TN	5/25/2019	sweep net	YY, LJ, JC, DG	414	318780	4 hours
Fungus gnat	Diptera	Mycetophilidae	*Leia bivittata*	Hidden Lake Trail, Harpeth River State Park, Nashville, TN	6/9/2018	sweep net	YY, LJ, JS, PR, MT	173	129720	1 hour
Flesh fly	Diptera	Sarcophagidae	*Sarcophaga sp.*	Gossett Tract, Harpeth River State Park, Kingston Springs, TN	5/18/2019	sweep net	YY, SW, MT, MGG	1104	473616	4 hours
Tachinid fly	Diptera	Tachinidae	unidentified	North Judson, IN (emerged from monarch caterpillar)	8/4/2019	by hand	SW	1201	1006103	1 hour
Long-legged fly	Diptera	Dolichopodidae	*Dolichopus sp.*	Hidden Lake Trail, Harpeth River State Park, Nashville, TN	6/9/2018	sweep net	YY, LJ, JS, PR, MT	676	508502	1 hour
Striped horse fly	Diptera	Tabanidae	*Tabanus sp.*	Leopold, IN	7/28/2019	sweep net	YY	2001	1538769	1 hour
Cat flea	Siphonaptera	Pulicidae	*Ctenocephalides felis*	Bellevue, Nashville, TN	7/13/2019	trap	LJ	69	18768	1 hour
Scorpionfly	Mecoptera	Panorpidae	*Panorpa sp.*	Gossett Tract, Harpeth River State Park, Kingston Springs, TN	5/18/2019	sweep net	YY, SW, MT, MGG	2484	1967328	4 hours
Hangingfly	Mecoptera	Bittacidae	*Bittacus sp.*	Willow Pond, Nashville, TN	7/7/2018	sweep net	YY, LJ	1546	1545600	1 hour
Armyworm moth	Lepidoptera	Noctuidae	*Mythimna sp.*	Mulberry way, Nashville, TN	6/18/2019	light trap	YY	14490	3941280	4 hours
Western bean cutworm	Lepidoptera	Noctuidae	*Striacosta albicosta*	Cornfield, IN	7/11/2019	sweep net	SW	10557	2079729	1 hour
Tiger moth	Lepidoptera	Erebidae	*Spilosoma sp.*	Willow Pond, Nashville, TN	5/25/2019	sweep net	YY, LJ, JC, DG	5589	4303530	4 hours
Geometer moth	Lepidoptera	Geometridae	unidentified	Deer Trail, Long Hunter State Park, Hermitage, TN	4/28/2019	sweep net	YY, LJ, PR, EH, MW	759	745338	4 hours
Grape leaf folder	Lepidoptera	Crambidae	*Desmia sp.*	Willow Pond, Nashville, TN	7/7/2018	sweep net	YY, LJ	2491	2680208	1 hour
Indian meal moth	Lepidoptera	Pyralidae	*Plodia interpunctella*	Purdue University, West Lafayette, IN	5/6/2019	lab colony	SW	552	395232	1 hour
Litter moth	Lepidoptera	Erebidae	*Renia sp.*	Gossett Tract, Harpeth River State Park, Kingston Springs, TN	5/18/2019	sweep net	YY, SW, MT, MGG	2484	1967328	4 hours
Satyrid butterfly	Lepidoptera	Nymphalidae	*Hermeuptychia sp.*	Willow Pond, Nashville, TN	7/1/2018	sweep net	YY, LJ	2491	3437442	1 hour
Monarch butterfly	Lepidoptera	Nymphalidae	*Danaus plexippus*	Leopold, IN	7/28/2019	sweep net	YY	45512	33769904	1 hour
Red-banded hairstreak	Lepidoptera	Lycaenidae	*Calycopis sp.*	Willow Pond, Nashville, TN	7/1/2018	sweep net	YY, LJ	1270	1752048	1 hour
Checkerspot	Lepidoptera	Nymphalidae	*Chlosyne sp.*	Willow Pond, Nashville, TN	7/1/2018	sweep net	YY, LJ	1608	2218626	1 hour
Northern caddisfly	Trichoptera	Limnephilidae	unidentified	Mulberry way, Nashville, TN	7/28/2019	light trap	YY	276	212244	1 hour
Net-spinning caddisfly	Trichoptera	Hydropsychidae	unidentified	Mulberry way, Nashville, TN	7/31/2019	light trap	YY	1297	901554	1 hour
Long-horned caddisfly	Trichoptera	Leptoceridae	*Ceraclea sp.*	Mulberry way, Nashville, TN	7/29/2019	light trap	YY	173	127995	1 hour

Long-horned caddisfly	Trichoptera	Leptoceridae	*Triaenodes sp.*	Mulberry way, Nashville, TN	7/10/2019	light trap	YY	235	66157	1 hour
June beetle	Coleoptera	Scarabaeidae	*Phyllophaga sp.*	Mulberry way, Nashville, TN	6/18/2019	light trap	YY	11730	3190560	4 hours
Predaceous diving beetle	Coleoptera	Dytiscus	unidentified	West Lafayette, IN	7/15/2019	light trap	SW	4913	4116926	1 hour
Red milkweed beetle	Coleoptera	Cerambycidae	*Tetraopes sp.*	West Lafayette, IN	7/21/2019	sweep net	SW	8280	6375600	1 hour
May beetle	Coleoptera	Scarabaeidae	*Amphimallon sp.*	Bellevue, Nashville, TN	4/21/2019	light trap	JH	9522	9998100	1 hour
Japanese beetle	Coleoptera	Scarabaeidae	*Popillia japonica*	Vanderbilt University Campus, Nashville, TN	6/17/2019	sweep net	YY	6486	252954	4 hours
Click beetle	Coleoptera	Elateridae	unidentified	Mulberry way, Nashville, TN	6/18/2019	light trap	YY	5106	3497610	4 hours
Ground beetle	Coleoptera	Carabidae	*Pterostichus sp.*	Bellevue, Nashville, TN	6/8/2019	trap	LJ	15870	11934240	1 hour
Soldier beetle	Coleoptera	Cantharidae	*Chauliognathus marginatus*	Hidden Lake Trail, Harpeth River State Park, Nashville, TN	6/2/2018	sweep net	YY, LJ, JC, JS	3243	1563126	1 hour
Tiger beetle	Coleoptera	Carabidae	*Cicindela sexguttata*	Hidden Lake Trail, Harpeth River State Park, Nashville, TN	6/9/2018	sweep net	YY, LJ, JS, PR, MT	5382	3998826	1 hour
Spongillafly	Neuroptera	Sisyridae	*Climacia sp.*	Mulberry way, Nashville, TN	7/9/2019	light trap	YY	173	132825	1 hour
Honeybee	Hymenoptera	Apidae	*Apis mellifera*	Vanderbilt University Campus, Nashville, TN	5/23/2018	sweep net	LJ	18561	13549530	1 hour
Odorous house ant	Hymenoptera	Formicidae	*Tapinoma sessile*	Purdue University, West Lafayette, IN	5/6/2019	lab colony	GB	40	37360	4 hours
Braconid wasp	Hymenoptera	Braconidae	*Cotesia sp.*	Nolensville pike, TN (emerged from hornworm caterpillar)	7/18/2019	by hand	PR	46	9062	1 hour
Chalcid wasp	Hymenoptera	Eurytomidae	*Riley asp.*	Willow Pond, Nashville, TN	5/25/2019	sweep net	YY, LJ, JC, DG	27	20790	4 hours
Ichneumon wasp	Hymenoptera	Ichneumonidae	*Protichneumon grandis*	Willow Pond, Nashville, TN	7/7/2018	sweep net	YY, LJ	4009	3700215	1 hour
Argentine ant	Hymenoptera	Formicidae	*Linepithema humile*	Purdue University, West Lafayette, IN	5/6/2019	lab colony	GB	40	37360	4 hours
Bed bug	Hemiptera	Cimicidae	*Cimex lectularius*	Purdue University, West Lafayette, IN	5/6/2019	lab colony	GB	276	186576	4 hours
Sharpshooter	Hemiptera	Cicadellidae	*Oncometopia sp.*	Mulberry way, Nashville, TN, USA	5/24/2018	sweep net	YY	3588	2619240	1 hour
Flatid planthopper	Hemiptera	Flatidae	*Metcalfa sp.*	Mulberry way, Nashville, TN	8/4/2019	light trap	YY	725	607131	1 hour
Plant bug	Hemiptera	Miridae	*Metriorrhynchomiris sp.*	Gossett Tract, Harpeth River State Park, Kingston Springs, TN	5/18/2019	sweep net	YY, SW, MT, MGG	828	355212	4 hours
Backswimmer	Hemiptera	Notonectidae	unidentified	West Lafayette, IN	6/29/2019	light trap	SW	1380	1188180	4 hours
Spittlebug	Hemiptera	Cercopidae	*Prosapia bicincta*	Willow Pond, Nashville, TN	7/7/2018	sweep net	YY, LJ	2760	2969760	1 hour
American cockroach	Blattodea	Blattidae	*Periplaneta americana*	Purdue University, West Lafayette, IN	5/6/2019	lab colony	GB	43263	29245788	4 hours
German cockroach	Blattodea	Ectobiidae	*Blattella germanica*	Purdue University, West Lafayette, IN	5/6/2019	lab colony	GB	5590	3778840	4 hours
Termite	Blattodea	Rhinotermitidae	*Reticulitermes flavipes*	Purdue University, West Lafayette, IN	5/6/2019	lab colony	GB	69	66171	4 hours
Walking stick	Phasmatodea	Diapheromeridae	*Diapheromera femorata*	Bellevue, Nashville, TN	8/21/2019	sweep net	MGG	15870	6824100	1 hour
Katydid	Orthoptera	Tettigoniidae	unidentified	Mulberry way, Nashville, TN	7/30/2019	light trap	YY	20100	10311300	1 hour
Tree cricket	Orthoptera	Gryllidae	*Neoxabea sp.*	Mulberry way, Nashville, TN	7/21/2019	sweep net	YY	4830	1197840	1 hour

Field cricket	Orthoptera	Gryllidae	*Gryllus sp.*	Deer Trail, Long Hunter State Park, TN	4/28/2019	sweep net	YY, LJ, PR, EH, MW	15000	14520000	4 hours
Ground cricket	Orthoptera	Gryllidae	*Neonemobius sp.*	Willow Pond, Nashville, TN	7/7/2018	sweep net	YY, LJ	3126	3344499	1 hour
Grasshopper	Orthoptera	Tetrigidae	*Paratettix sp.*	Willow Pond, Nashville, TN	5/25/2019	sweep net	YY, LJ, JC, DG	3933	3028410	4 hours
Grasshopper	Orthoptera	Acrididae	unidentified	Deer Trail, Long Hunter State Park, TN	4/28/2019	sweep net	YY, LJ, PR, EH, MW	30000	29460000	4 hours
Grasshopper	Orthoptera	Acrididae	*Chortophaga sp.*	Hidden Lake Trail, Harpeth River State Park, Nashville, TN	6/9/2018	sweep net	YY, LJ, JS, PR, MT	17733	13175619	1 hour
Stonefly	Plecoptera	Perlidae	*Perlinella sp.*	Hidden Lake Trail, Harpeth River State Park, Nashville, TN	6/9/2018	sweep net	YY, LJ, JS, PR, MT	3795	2819685	1 hour
Stonefly	Plecoptera	Perlidae	*Perlesta sp.*	Bellevue, Nashville, TN	7/19/2019	light trap	LJ	759	53130	1 hour
Dragonfly	Odonata	Libellulidae	*Celithemis elisa*	Leopold, IN	7/28/2019	sweep net	YY	6141	4722429	1 hour
Skimmer	Odonata	Libellulidae	*Perithemis tenera*	Willow Pond, Nashville, TN	7/7/2018	sweep net	YY, LJ	4140	1349640	1 hour
Mayfly	Ephemeroptera	Heptageniidae	*Leucrocuta sp.*	Mulberry way, Nashville, TN	7/31/2019	light trap	YY	311	215798	1 hour
Flat-headed mayfly	Ephemeroptera	Heptageniidae	unidentified	Mulberry way, Nashville, TN	6/24/2019	light trap	YY	200	106200	4 hours
Silverfish	Zygentoma	Lepismatidae	*Lepisma saccharina*	Mulberry way, Nashville, TN	3/21/2019	trap	YY	1497	330903	1 hour

[a] YY = Yan Yan; LJ = Luisa Jabbur; JC = Justin Critchlow; DG = Destane Garrett; JS = Jacob Steenwyk; PR = Parker Rundstrom; MT = Michael Tackenberg; SW = Scott Williams; MGG = Manuel Giannoni Guzman; EH = Emily Hudson; MW = Matt Wilkins; JH = Julián Hillyer; GB = Grzegorz Buczkowski.